UNIVERSITY OF THESSALY
SCHOOL OF ENGINEERING
DEPARTMENT OF CIVIL ENGINEERING

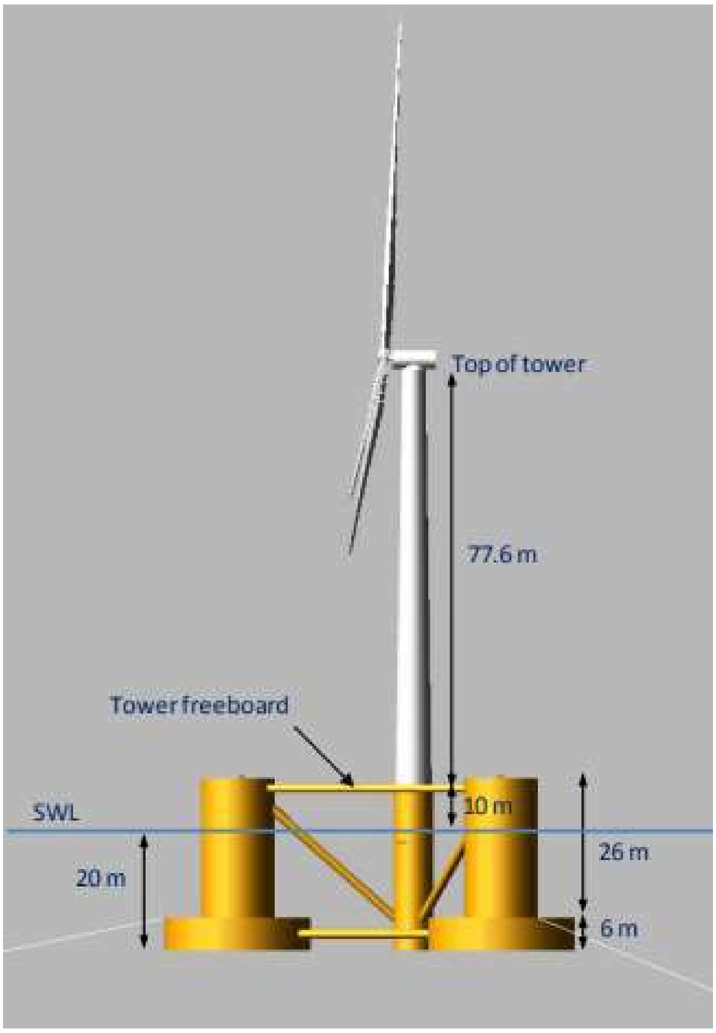

DYNAMIC RESPONSE OF A FLOATING OFFSHORE WIND TURBINE SUBJECT TO STEEP SURFACE WATER WAVES

ATHANASIA TSINOUDI

MASTER'S THESIS IN MASTER'S PROGRAM: ANALYSIS AND DESIGN OF ENERGY INFRASTRUCTURE CONSTRUCTION

VOLOS, GREECE, 2024

UNIVERSITY OF THESSALY
SCHOOL OF ENGINEERING
DEPARTMENT OF CIVIL ENGINEERING

DYNAMIC RESPONSE OF A FLOATING OFFSHORE WIND TURBINE SUBJECT TO STEEP SURFACE WATER WAVES

ATHANASIA TSINOUDI
MASTER'S THESIS IN MASTER'S PROGRAM: ANALYSIS AND DESIGN OF ENERGY INFRASTRUCTURE CONSTRUCTION

VOLOS, GREECE 2024

The approval of the diploma thesis by the Department of Civil Engineering of the Polytechnic School of the University of Thessaly does not imply acceptance of the views of the author (Law 5343/32 no. 202 par. 2).

Approved by the Members of the Three-Member Examination Committee:

First Examiner	Dr. Vanessa Katsardi
(Supervisor)	Assistant Professor, Department of Civil Engineering, University of Thessaly
Second Examiner	Dr. Euripidis Mistakidis
	Professor, Department of Civil Engineering, University of Thessaly
Third Examiner	Dr. Theofanis Grammenos
	Associate Professor, Department of Civil Engineering, University of Thessaly

DYNAMIC RESPONSE OF A FLOATING OFFSHORE WIND TURBINE SUBJECT TO STEEP SURFACE WATER WAVES

Athanasia Tsinoudi

University of Thessaly, Department of Civil Engineering, 2024

Supervisor Professor: **Vanessa Katsardi**

Abstract

In order to address the energy and climate crisis, industrial and research interest is turning to renewable energy sources. In fact, the exploitation of a country's energy potential with the main aim of its self-reliance in the energy sector, is estimated to be the main issue and engineering will be called upon to provide effective solutions. In the context of these efforts, this work examines a type of construction suitable for the Greek seas, the floating semi-submersible offshore wind turbine, and wave loads effect on it. The study uses the OC4 model, a semi-submersible floating offshore wind system model created for the US-based DeepCwind project to generate data for offshore wind turbine modeling tools verification (Robertson et al, 2014). The aim is to achieve domain-realistic results using classical wave theories (Airy, 2^{nd} order Stokes, 5th-order Stokes, and 18th-order Fourier wave theories, as well as Linear Random Wave Theory (LRWT)) but also the most advanced fully nonlinear model of HOS wave theory. Both wave field and its interaction with floating structure simulation are investigated.

Key words: *intermediate and shallow waters wave theories, floating offshore wind turbine, semisubmersible, floating structure simulation, wave – structure interaction, non-linear waves.*

DYNAMIC RESPONSE OF A FLOATING OFFSHORE WIND TURBINE SUBJECT TO STEEP SURFACE WATER WAVES

Αθανασία Τσινούδη

Πανεπιστήμιο Θεσσαλίας, Τμήμα Πολιτικών Μηχανικών, 2024

Επιβλέπουσα Καθηγήτρια: **Βασιλική Κατσαρδή**

Περίληψη

Προκειμένου να αντιμετωπιστεί η ενεργειακή και κλιματική κρίση, το βιομηχανικό και ερευνητικό ενδιαφέρον στρέφεται στις ανανεώσιμες πηγές ενέργειας. Μάλιστα η εκμετάλλευση του ενεργειακού δυναμικού των χωρών με κύριο σκοπό την αυτοδυναμία τους στον τομέα της ενέργειας, εκτιμάται πως θα αποτελεί το κύριο ζήτημα και η μηχανική θα κληθεί να δώσει αποτελεσματικές λύσεις. Στο πλαίσιο των προσπαθειών αυτών η παρούσα εργασία μελετά έναν κατάλληλο για τις ελληνικές θάλασσες τύπο κατασκευής, της πλωτής ημιβυθισμένης θαλάσσιας ανεμογεννήτριας, και την επίδραση των κυματικών φορτίων σε αυτή. Η μελέτη χρησιμοποιεί το μοντέλο OC4, ένα μοντέλο ημι-βυθιζόμενου πλωτού υπεράκτιου αιολικού συστήματος που αναπτύχθηκε για το πρότζεκτ DeepCwind, πρότζεκτ που εδρεύει στις ΗΠΑ με στόχο τη δημιουργία δεδομένων για χρήση στην επικύρωση εργαλείων μοντελοποίησης πλωτών υπεράκτιων ανεμογεννητριών (Robertson et al, 2014). Στόχος είναι επίτευξη ρεαλιστικών για την περιοχή αποτελεσμάτων χρησιμοποιώντας κλασικές μεθόδους κυματικών θεωριών (θεωρίες κυματισμού Airy, Stokes 2ης τάξης, Stokes 5ης τάξης και Fourier 18ης τάξης, καθώς και η Θεωρία Τυχαίων Γραμμικών Κυματισμών (LRWT)) αλλά και το πιο προηγμένο πλήρως μη γραμμικό μοντέλο της κυματικής θεωρία HOS. Διερευνάται τόσο το κυματικό πεδίο όσο και η αλληλεπίδρασή του με προσομοίωμα της πλωτής κατασκευής.

Λέξεις Κλειδιά: *θεωρίες κυμάτων ενδιάμεσων και ρηχών υδάτων, πλωτή υπεράκτια ανεμογεννήτρια, ημιβυθιζόμενη, προσομοίωση πλωτής υπεράκτιας κατασκευής, αλληλεπίδραση κύματος – κατασκευής, μη γραμμικά κύματα.*

Aberge

Afin de faire face à la crise énergétique et climatique, l'intérêt de l'industrie et de la recherche se tourne vers les sources d'énergie renouvelables. En fait, l'exploitation du potentiel énergétique des pays, dans le but principal de leur autonomie dans le secteur énergétique, est considérée comme le principal problème et l'ingénierie sera appelée à apporter des solutions efficaces. Dans le contexte de ces efforts, ce travail examine un type de construction adapté aux mers grecques, l'éolienne marine flottante semi-submergée, et l'effet des charges des vagues sur elle. L'étude utilise le modèle OC4, un modèle de système éolien offshore flottant semi-submersible développé pour le projet américain DeepCwind, afin de générer des données destinées à valider les outils de modélisation d'éoliennes offshore flottantes (Robertson et al, 2014). L'objectif est d'obtenir des résultats réalistes dans le domaine en utilisant les théories des ondes classiques (théories d'Airy, de Stokes du 2e ordre, de Stokes du 5e ordre et de Fourier du 18e ordre, ainsi que la théorie des ondes aléatoires linéaires (LRWT)) mais aussi les théories les plus avancées. modèle non linéaire de la théorie des ondes HOS. Le champ de vagues et son interaction avec la simulation de structures flottantes sont étudiés.

Mots clés : théories des vagues en eaux intermédiaires et peu profondes, éolienne offshore flottante, semi-submersible, simulation de structures flottantes, interaction vague – structure, vagues non linéaires.

Acknowledgements

I would like to thank my supervisor, Vanessa Katsardi, for the guidance and care she provided during the studies and our enlightening discourses.

Also, I am grateful to all professors of the examination board for their interest and comments on the research carried out. A very special thanks to Dr. Euripidis Mistakidis for the prolonged support and his valuable help, useful comments, and suggestions.

Finally, I owe a big thank you to my family who contributed both practically and mentally to the completion of my work.

Athanasia Tsinoudi

Table of Contents

Table of Figures

1. INTRODUCTION

State-of-the-art: In the contemporary context of a shift in community attention from non-renewable energy sources to renewable, the offshore structures field and marine hydraulics sector are strongly attracting global political and industrial interest. As energy-related constructions have inconceivable environmental and economic cost, design research has made significant progress in recent years. Nevertheless, the level of knowledge that has been acquired today on the wave-offshore structure interaction is in its early stage. It is therefore necessary to identify accurately the design wave and to develop more extensively the available statistical tools and to gather valid data on the results of studies with accuracy, and to ensure the safety and proper operation of such constructions.

To deal with the climate crisis, "smart" and "green" offshore facilities with wave energy devices are now being built in the Mediterranean, while the power generated by offshore wind farms has increased more than 13 times in the last decade. These developments impose the need for an in-depth understanding of not only the design wave height but the entire wave directional field and its interaction with marine structures. The engineer's response to these challenges cannot be limited to a point size design but must also study the development of the phenomenon in space and time. Indeed, the so-called blue energy represents an inexhaustible and renewable source of energy including the enormous potential of marine energy (both wind and wave energy). It is therefore expected in the modern era, while the climate crisis is a dominant challenge, that blue energy attracts global interest.

Literature: Previous research has reached to a mathematical description of the energy and kinematics of the particles, by establishing equations that describe wave characteristics, including wavelength, period, amplitude, phase, group velocities and accelerations, but also by creating numerical models to approximate the values related to the kinematic behavior of the waves, mainly in deep water. However, the mechanism of development and propagation of random waves in shallow water is still not well understood. Their description with analytical solutions (linear and second order) has proven to be insufficient. More specifically, the simplest way of describing a random wave field is the superposition of the wave frequency components. Waves are the dominant load on ships and marine structures, rendering understanding the behavior and response of marine structures under extreme wave loading crucial. Extreme waves occur when all individual wave components are in phase at a specific point in space and time (focused wave). This mechanism in the real sea is extremely complex due to directionality, non-linearity and rapid energy transfers between wave components. In fact, it becomes more complex when the depth is finite by including changes in the geometry of the bottom. Thus, the possibility of the formation of walls of water in shallow depths is increased, as waves tend to acquire the same direction due to refraction, creating a critical wave field because it affects the structures, exerting on them additional huge instantaneous loads (slamming/impact waves) ([1], [2], [3]).

Therefore, the mechanisms that need further investigation regarding the wave field are the estimation of the directionality but also its effect on the wave field formation, the adequacy of normal energy distribution at different frequencies such as the JONSWAP distribution and the understanding of the mechanism associated with extreme waves, in particular their very shape, their breaking point and the underlying non-linear interactions of the wave frequency components ([4], [5]).

Scope of Work: The present research aspires to contribute to the abovementioned field by investigating these questions of the science of wave mechanics, and specifically the wave - structure interaction, a subject that is called to help solve construction issues in marine structures and therefore problems related to dealing with the climate crisis. The benefits of understanding the wave mechanisms are crucial considering concerns related to interaction of waves with any element, such as the shoreline e.g. [6], or an offshore structure e.g. [7], as in the present work. The study will highlight the importance of understanding the proper design of offshore structures. Environmental protection through the development of blue energy also helps economic development because it is linked to the reduction of the use of fossil fuels, which release large amounts of polluting substances, while strengthening the autonomy and energy self-sufficiency of a country. Finally, the study aspires to strengthen Greece's participation in the promising and rapidly growing sector of marine and ocean technology.

All the mechanisms described above, including the generation and propagation of the waves, the wave theories and equations, linearity, and non-linearity, will be discussed at the first theoretical part of the present study, before the reader is led to the presentation of the practical part of this work, that of the offshore platform simulation and then, of the wave-structure interaction results. Specifically, in this research, the simulation of the floating semi-submersible platform OC4 will be carried out using the MARC MSC software, which will be subjected to wave loads as obtained from the literature. After setting up the model, a solution is carried out under the influence of these wave loads with the aim to examine the horizontal displacement of the platform.

Why a floating structure: The reason for choosing floating over rigid offshore construction is a combination of advantages related to geographical location, environmental conditions, design quality and cost considerations. These advantages are:

- Offshore wind farms provide the possibility of utilizing higher power wind turbines. This can be achieved as the open sea is characterized by environmental conditions of higher wind speeds. It is understood that obstacles on the shore render the winds weaker, while on the offshore the potential is much stronger, more stable, and less turbulent.
- Floating wind turbines have the advantage of being easy to move and transport since they are easily assembled and disassembled, independent of the bottom

layer. So, since there isn't as much impact on the bottom as a grounded structure has, they have a significantly smaller environmental footprint.

- An additional important issue regarding wind turbines is the visual and acoustic disturbance that wind farms often cause to residents near residential areas on the shore. Offshore wind farms away from the coastline present less of this problem.
- The most suitable installation for the Greek area is that of the offshore floating wind turbines, as the Aegean offers the appropriate sea conditions with the presence of strong winds. It is noted that the waves do not exceed 8 meters. Therefore, the waves would be relatively unlikely to cause any problem to the wind turbine construction, reducing installation and maintenance costs. Finally, the installation of floating platforms is considered cost-effective as the bottom of the Greek seas is characterized by great depths and extremely uneven geomorphology, which makes it difficult to establish the wind turbines with rigid foundations [8].
- On the contrary, a grounded construction, although considerably more economical, is used for depths of only up to 25m while its cost is increased for transport and installation.

The organization of the work into chapters is presented below.

Chapters:

CHAPTER 2: presents the basic terminology related to waves, characteristic measurements, and offshore structure design.

CHAPTER 3: information regarding categories of different offshore structures is with the aim of understanding the suitability of the floating offshore structure chosen for this work.

CHAPTER 4: describes the basic wave theories used for wave modelling both for steady and random waves.

CHAPTER 5: presents the main geometrical and structural characteristics of the floating offshore platform OC4 that will be used for the simulation. The MARC MSC software that will be used for the simulation and its capabilities are also described.

CHAPTER 6: investigates the wave loading applied on the platform, *obtained from the literature and introduces the significance of Morison's equation in the simulation.*

CHAPTER 7: discusses the results arising regarding wave – structure interaction. The response of the structure is investigating as it is the main purpose of this work.

CHAPTER 8: summarizes the undertaken work and highlights the resulting conclusions.

CHAPTER 9: provides suggestions for future study using the results taken from the present work.

2. BASIC TERMINOLOGY

This chapter presents the basic concepts related to wave mechanics and the understanding of their generation, evolution, and propagation, as well as the main equations that describe their kinematics and their interactions. It is important for the reader to get to know the above elements in depth before proceeding to the study of the effect of waves on the offshore structures, which is characterized by complexity due to the multiplicity of different factors that the researcher is called to consider.

2.1 Characteristic computational measurements

- **wave amplitude**: Maximum height displacement of a particle, from its equilibrium point to the crest or to the trough, during wave propagation (m)
- **wave period**: The duration for two successive crests (or troughs) to take place in the amplitude-time diagram (sec)
- **wavelength**: The distance from crest to crest (or trough to trough), the duration for two successive crests (troughs) to take place in the amplitude-distance diagram (m)
- **wave height:** Trough to crest distance (m)
- **wave crest**: Top (highest) point of the wave
- **wave trough**: Bottom (lowest) point of the wave
- **wave steepness**: wave height/wavelength (H/λ)

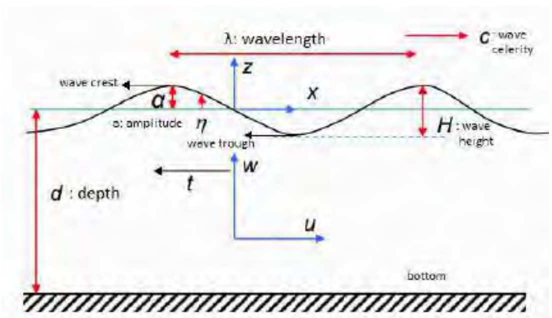

Figure 1: Wave parts

Design wave: Offshore structure design depends on the estimation of the design wave resulting from the wave load calculation generated by waves and currents. The design wave refers to a large wave with a long return period, which occurs rarely. The return period is taken depending on the structure and can be estimated at rates of 1 per 100, 1.000, even 10.000 years.

To calculate the design wave, either dispersion of wave records in the frequency domain or *stochastic analysis* of the wave records is performed. The stochastic approach is a statistical method where the components of the waves are analyzed in relation to the time domain. As stochastic quantity is defined a quantity that follows random evolution, which is expressed by probability distributions or probabilistic models. Such a quantity is the elevation of the sea, η, and it results from a number of waves N which are ranked in descending order in relation to the height corresponding to them, Hi. The Hi sizes result from the zero up-crossing method. This method includes the determination of the mean water level. After the mean water level is determined, wave records are marked every time the water surface goes through this level in an upward direction [9].By this method, individual waves are identified between the up crossings and the individual wave height, Hi and wave period, Tj [9].To perform the statistical analysis, the rank order of the waves is first determined.

The probability of exceeding a value H (probability of exceedance) follows the Rayleigh distribution and is calculated as follows:

$$P(H_i \geq H) = e^{-(\frac{H}{H_{rms}})^2} \qquad \textit{Equation 1}$$

where $H_{rms} = \sqrt{\frac{\Sigma {H_i}^2}{N}}$ is the root mean square value of the wave height. The mean wave height is defined as $\overline{H}$:

$$\overline{H} = H_{100} = \frac{\sqrt{\pi}}{2} H_{rms} \quad \textit{Equation 2}$$

The significant wave height is calculated as the mean value of the upper 33% of wave heights of the recordings:

$$H_S = H_{33} = \sqrt{2}H_{rms} \text{ with probablility of exceedance } \mathrm{P}(H > H_{33}) = 0.135$$

The maximum height value H_{max} for N number of H values, is calculated as follows:

$$H_{max} = H_{rms}\sqrt{ln\,(N)} \quad \textit{Equation 3}$$

Where: $N = \frac{T_L}{T_Z}$

- T_L : the recording duration
- T_Z : average wave period

There are regulations that approximate the design height in marine structures as $H_{max} = 2H_S$ [9]. The spectrum analysis of the wave recordings in the frequency domain is held after choosing a spectrum model (e.g. JONSWAP, Pierson-Moskowitz). Through the chosen spectrum, the design height is calculated, which is the maximum wave height. The wave load which will act on the structure in the simulation of the present work, were obtained from spectrum analysis of wave recordings using the JONSWAP spectrum.

JONSWAP SPECTRUM (Tp, γ, Akp) where:

- **Tp**: peak period (eg (Tp = 1.4, γ = 5.5, Akp = 0.17, values for Atlantic or Aegean winds for 7-8 Beaufort)
- **c:** parameter that determines how narrow or wide the spectrum is. The higher the value of γ is the spectrum range becomes narrower.
- **A*kp**: wave steepness. Defines how non-linear and therefore abrupt the wave is. (A: wavelength, kp: wave number)

More details on the calculation of wave load can be found in Chapter 6: WAVE LOADING.

Significant Wave Height (Hs): We define as significant wave height, the height that we perceive as a wave height when the phenomenon unfolds in front of us, is the sensation that the human eye perceives. Its mathematical determination is estimated at the average of one third of the largest waves.

Probability of Exceedance: The characteristic shape of large waves is close to that of the freak wave and therefore in any relevant research it is necessary to calculate the probability of exceedance (Hcrest / Hs). In the diagram of the curve resulting from the calculation of this probability, the points observed outside the curve refer to the freak waves, which do not follow the curve as much as we extend it using the available data. Therefore, identifying such a wave requires a huge amount of data. In the instance of New Year's Event, for example, a sufficient amount of data would be a sample of 100.000.000 waves.

Directionality/ Statistics: Determining the directionality of the waves is a difficult task as the wave propagation evolves depending on the day and the prevailing wind conditions. This stochasticity of the wind is transferred to the sea through the shear, while the dispersion follows a normal Gauss distribution. The danger is increased the more directional the wave becomes, with the most extreme the phenomenon of unidirectional wave leading to wave slamming. This phenomenon occurs in both horizontal and vertical direction and is characterized by the abrupt fluid-construction interaction **(Prestige oil tanker, 2002**)[12]. However, regarding the air gap loading, the risk increases with the number of directions.

2.2 Wave transformation: mechanism description

The various changes at the bottom of the sea, the obstacles encountered by the waves and wave currents, modify the parameters of the waves, causing the phenomena described below, the transformations of the waves.

A wave is affected by the seabed as it approaches the shore, passing through a series of processes. These processes, including refraction, diffraction, shoaling, bottom friction, and wave-breaking are described below. The wave breaking process takes place in deep water with high steepness. In general, the interaction of wave particles with potential constructions or strong shoreline fluctuations is important to assess as they cause the diffraction effect. If the waves encounter a submerged reef or structure, they will overtop the reef. These transformations are related to offshore and port constructions. When the waves meet a steep structure, reflection will take place and if the waves encounter a permeable structure, partial transmission is observed. Below, the detailed mechanisms and processes are described.

Shoaling: The phenomenon during which waves evolve perpendicularly to the depth contour lines with a constant period, while the seabed follows a slope (decrease in depth) resulting in a change in the wave height H (increase) and the wavelength λ, is referred as shoaling. The phenomenon is characterized by hydrodynamic instability [13] and the shoaling coefficient can be calculated, considering a small slope, variant or constant at the bottom, without energy losses due to breaking waves or energy increase by wind load and ignoring the phenomenon of reflection, as follows:

$$K_s = \sqrt{\frac{K_C}{2nc}} \quad \textit{Equation 4}$$

Where $n = \frac{1}{2}\left[1 + \frac{2kd}{\sinh(2kd)}\right]$

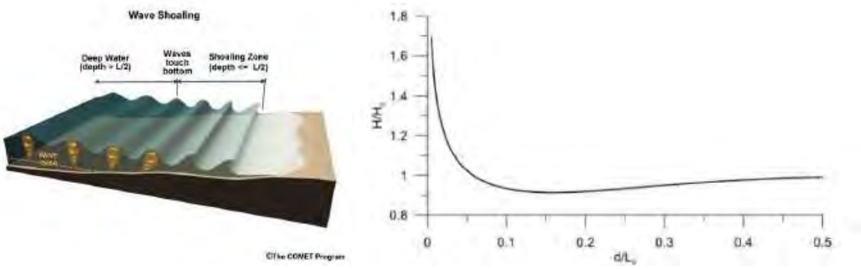

Figure 2: Wave shoaling[10], Shoaling coefficient Ks=H/Ho against the ratio d/Lo[13]

Refraction: The depth of the sea bottom affects the wave speed c, by such way that when waves travel diagonally (lateral incidence of waves) across the depth contour lines, the wave part in deep water moves faster than the wave part which propagates in shallower water depths. This process leads the wave to turn parallel to the contour lines, and the shift in the direction of motion is called refraction.

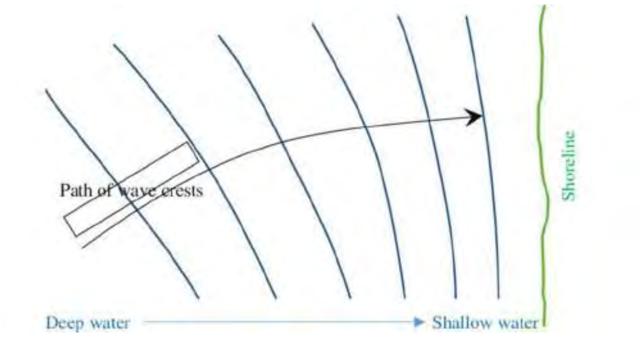

Figure 3: Refraction of waves [14].

Refraction has the following effects:

- The effect of refraction has significant impact as refraction and shoaling determine the wave height and hence the wave energy distribution. That is, for a specific depth and given incident wave characteristics in deep water (wave height in deep water H_0, period and direction of the wave), the wave height can be calculated.
- The change in direction that occurs in different parts of the wave field has the effect of concentrating or removing wave energy and practically affects the forces exerted on different parts of the structures.
- In addition to contributing to the concentration of sediments on the bottom, refraction affects erosion by depositing sediments on the bottom and altering by this way the bottom topography. A general description of bottom topography can be derived from aerial photographs containing refracted waves.

To estimate the wave height, the refractive index must be first calculated, as the relation that must be satisfied is expressed as follows:

$$H = K_r * K_S * H_O \quad \textit{Equation 5}$$

Where K_S the shoaling coefficient, K_r the refractive index and H_O wave height in deep water depths. Therefore, the refractive index should first be calculated, which presupposes the application of Snell's law. The following formulas relate to these calculations. Finally, using the diagrams listed below, wave height calculation is achieved.

$$c_0 = \frac{l_0}{\delta t} = \frac{s \sin a_0}{\delta t} \quad , \quad c = \frac{l}{\delta t} = \frac{s \sin \alpha}{\delta t} \quad \rightarrow \quad \frac{c}{c_O} = \frac{\sin \alpha}{\sin a_O} \quad \textit{Equation 6}$$

- a_O: the angle that wave crest forms with the contour line it crosses.
- α: the angle that wave crest forms with the next contour line
- c_O: the velocity at the depth of area 1
- c: the velocity at the depth of area 2

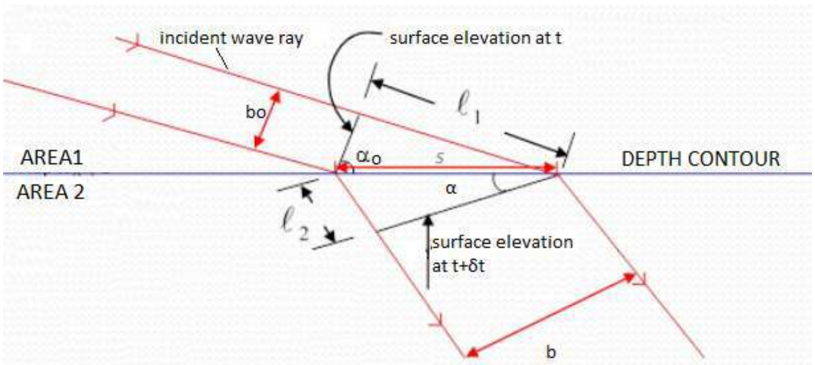

Figure 4: Snell's law [14]

Equation 6 is the basis for various geometric models that describe the traces of the rectangles from deep to shallow given the bottom topography. If b, bo are the distances between the rectangles in shallow water and in deep water depths respectively then:

$$\frac{H}{H_O} = \sqrt{\frac{b_O}{b}} * \sqrt{\frac{c_{g0}}{c_g}} = K_S * \sqrt{\frac{b_O}{b}} \qquad \text{Equation 7}$$

So, the refractive index can be expressed as follows:

$$K_r = \sqrt{\frac{b_O}{b}} = \sqrt{\frac{s\cos a_o}{s\cos a}} = K_s * \sqrt{\frac{b_O}{b}} \quad \text{Equation 8}$$

Then Equation 2 can be included:

$$H = K_r * K_S * H_O \quad or \quad \frac{H}{H_O} = K_r * K_S \quad \text{Equation 9}$$

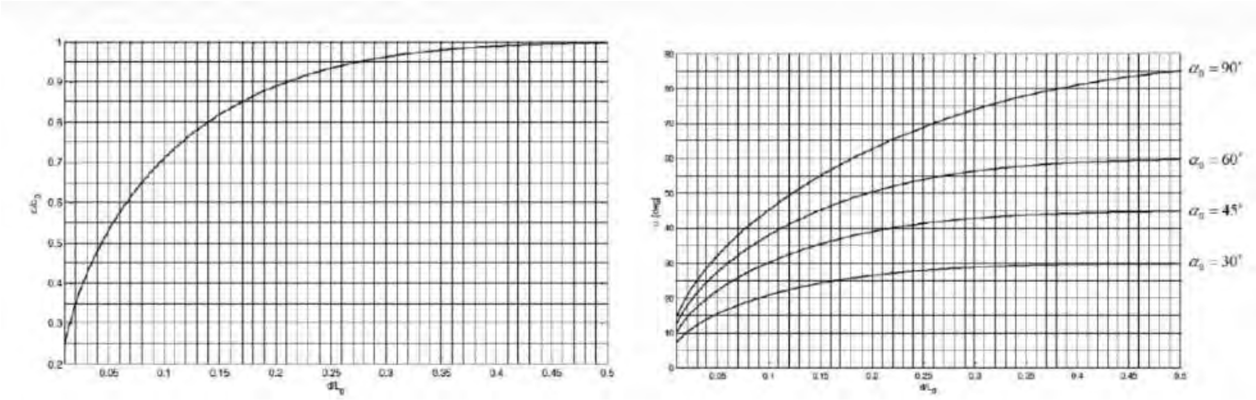

Figure 5: Ratio c/co – phase velocity shallow/deep water depth as function to d/Lo-local water wavelength shallow/deep water depth (left), wave propagation angle a as function of d/Lo given the deep-water propagation angle ao (right)

Diffraction: As diffraction is defined the transformation of waves when they encounter during their propagation a natural or artificial obstacle (e.g. breakwater, mull) which is impenetrable. Then a reduction in wave height and a curvature of the waves is observed around the edge of the obstacle. The waves change direction, and they propagate behind the obstacle, taking the form of concentric circular arcs of continuously reduced wave height.

The energy resulting from the wave propagation is transmitted to the back of the barrier which essentially acts as a source of energy, which in this way is transmitted not only longwise to the propagation direction of the waves but also transversely [15].

Diffraction theories are developed considering that: i) water is an ideal fluid (with zero viscosity and incompressible), ii) waves have a small amplitude and therefore a linear theory can be applied, iii) the flow is irrotational, and the Laplace equation defines the continuity of mass and lastly, iv) the depth upstream of the breakwater is constant.

Figure 6: Diffraction of waves around the tip of a breakwater [16]

The phenomenon of diffraction is of great practical importance in coastal engineering such as the quality and efficient construction design of breakwaters but also in general for the marine structures design. In the case of designing structures, mainly large-scale constructions, the flow is clearly affected, and this transformation must be considered. The complete mathematical description is difficult and complicated and the diagrams of the ratio of the refracted wave height to the incident wave height help to calculate the respective wave heights.

The images below correspond to wave diffraction and Weigel Table with multiple angles of incidence, while more cases are given by Wiegel in Shore Protection Manual. The diffraction coefficient K_D is the ratio of the height of the diffracted wave to the incident one and is calculated from the Weigel tables:

$$K_D(\theta, \beta, \frac{r}{L}) = \frac{H_{diffracted}}{H_{incintent}} \quad \text{Equation 10}$$

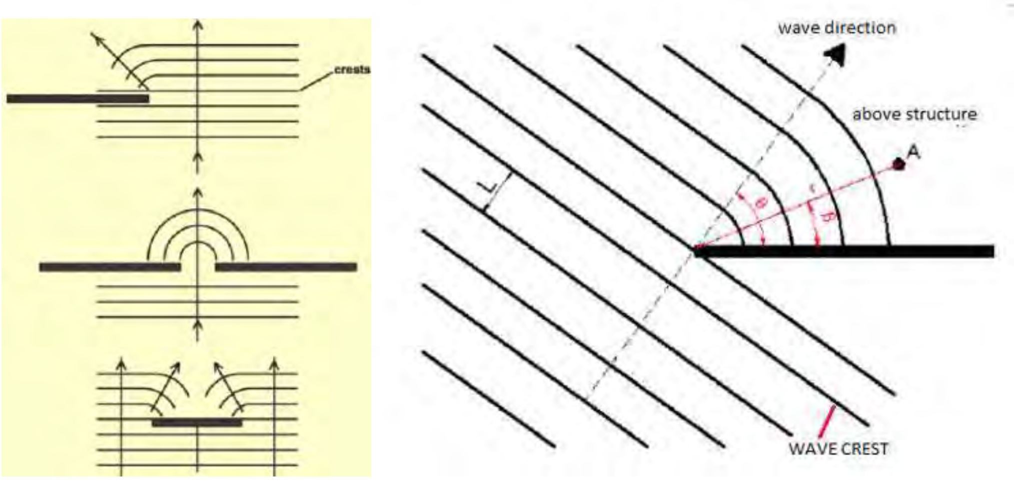

Figure 7: Examples of wave diffraction (left)[15], Wave diffraction analysis (right)

θ	r/L	β = 0	15	30	45	60	75	90	105	120	135	150	165	180
15	1/2	0.49	0.79	0.83	0.90	0.97	1.01	1.03	1.02	1.01	0.99	0.99	1.00	1.00
	1	0.38	0.73	0.83	0.93	1.04	1.04	0.99	0.98	1.01	1.01	1.00	1.00	1.00
	2	0.21	0.68	0.86	1.05	1.03	0.97	1.02	0.99	1.00	1.00	1.00	1.00	1.00
	5	0.13	0.63	0.99	1.04	1.03	1.02	0.99	0.99	1.00	1.01	1.00	1.00	1.00
	10	0.35	0.58	1.10	1.05	0.98	0.99	1.01	1.00	1.00	1.00	1.00	1.00	1.00
30	1/2	0.61	0.63	0.68	0.78	0.87	0.97	1.03	1.03	1.03	1.01	0.99	0.95	1.00
	1	0.50	0.53	0.63	0.78	0.95	1.06	1.03	0.98	0.99	1.01	1.01	0.97	1.00
	2	0.40	0.44	0.59	0.84	1.07	1.03	0.96	1.02	0.98	1.01	0.99	0.95	1.00
	5	0.27	0.32	0.55	1.00	1.04	1.04	1.02	0.99	0.99	1.00	1.01	0.97	1.00
	10	0.20	0.24	0.54	1.12	1.06	0.97	0.99	1.01	1.00	1.00	1.00	0.98	1.00
45	1/2	0.49	0.50	0.55	0.63	0.73	0.85	0.96	1.04	1.06	1.04	1.00	0.99	1.00
	1	0.38	0.40	[illegible]	0.59	0.76	0.95	1.07	1.06	0.98	0.97	1.01	1.01	1.00
	2	0.29	0.31	0.39	0.56	0.83	1.08	1.04	0.96	1.03	0.98	1.01	1.00	1.00
	5	0.18	0.20	[illegible]	0.54	1.01	1.04	1.03	1.02	1.00	0.99	1.01	1.00	1.00
	10	0.13	0.15	0.22	0.53	1.13	1.07	0.96	0.98	1.02	0.99	1.00	1.00	1.00
60	1/2	0.40	0.41	0.45	0.52	0.60	0.72	0.85	1.13	1.04	1.06	1.03	1.01	1.00
	1	0.31	0.32	0.36	0.44	0.57	0.75	0.96	1.08	1.06	0.98	0.98	1.01	1.00
	2	0.22	0.23	0.28	0.37	0.55	0.83	1.08	1.04	0.96	1.03	0.98	1.01	1.00
	5	0.14	0.15	0.18	0.28	0.53	1.01	1.04	1.05	1.03	0.99	0.99	1.00	1.00
	10	0.10	0.11	0.13	0.21	0.52	1.14	1.07	0.96	0.98	1.01	1.00	1.00	1.00
75	1/2	0.34	0.35	0.38	0.42	0.50	0.59	0.71	0.85	0.97	1.04	1.05	1.02	1.00
	1	0.25	0.26	0.29	0.34	0.43	0.56	0.75	0.95	1.02	1.06	0.98	0.98	1.00
	2	0.18	0.19	0.22	0.26	0.36	0.54	0.83	1.09	1.04	0.96	1.03	0.99	1.00
	5	0.12	0.12	0.13	0.17	0.27	0.52	1.01	1.04	1.02	1.03	0.99	0.99	1.00
	10	0.08	0.08	0.10	0.13	0.20	0.52	1.14	1.07	0.96	0.98	1.01	1.00	1.00
90	1/2	0.31	0.31	0.33	0.36	0.41	0.49	0.59	0.71	0.85	0.96	1.03	1.02	1.00
	1	0.22	0.23	0.24	0.28	0.33	0.42	0.56	0.75	0.96	1.07	1.03	0.97	1.00
	2	0.16	0.16	0.18	0.20	0.26	0.35	0.54	0.69	1.08	1.04	0.96	1.02	1.00
	5	0.10	0.10	0.11	0.13	0.16	0.27	0.53	1.01	1.04	1.03	1.02	0.99	1.00
	10	0.07	0.07	0.08	0.09	0.13	0.20	0.52	1.14	1.07	0.96	0.99	1.01	1.00
105	1/2	0.28	0.28	0.29	0.32	0.35	0.41	0.49	0.59	0.72	0.85	0.97	1.01	1.00
	1	0.20	0.20	0.24	0.23	0.27	0.33	0.42	0.56	0.75	0.95	1.06	1.04	1.00
	2	0.14	0.14	0.13	0.17	0.20	0.25	0.35	0.54	0.83	1.08	1.03	0.97	1.00
	5	0.09	0.09	0.10	0.11	0.13	0.17	0.27	0.52	1.02	1.04	1.04	1.02	1.00
	10	0.07	0.06	0.08	0.08	0.09	0.12	0.20	0.52	1.14	1.07	0.97	0.99	1.00
120	1/2	0.25	0.26	0.27	0.28	0.31	0.35	0.41	0.50	0.60	0.73	0.87	0.97	1.00
	1	0.18	0.19	0.19	0.21	0.23	0.27	0.33	0.43	0.57	0.76	0.95	1.04	1.00
	2	0.13	0.13	0.14	0.14	0.17	0.20	0.26	0.36	0.53	0.83	1.07	1.03	1.00
	5	0.08	0.08	0.08	0.09	0.11	0.13	0.16	0.27	0.52	1.01	1.04	1.03	1.00
	10	0.06	0.06	0.06	0.07	0.07	0.09	0.13	0.20	0.52	1.13	1.06	0.98	1.00
135	1/2	0.24	0.24	0.25	0.26	0.28	0.32	0.36	0.42	0.52	0.63	0.76	0.90	1.00
	1	0.18	0.17	0.18	0.19	0.21	0.23	0.28	0.34	0.44	0.59	0.78	0.95	1.00
	2	0.12	0.12	0.13	0.14	0.14	0.17	0.20	0.26	0.37	0.56	0.84	1.03	1.00
	5	0.08	0.07	0.08	0.08	0.09	0.11	0.13	0.17	0.28	0.54	1.00	1.04	1.00
	10	0.06	0.06	0.06	0.06	0.07	0.08	0.09	0.13	0.21	0.53	1.12	1.05	1.00
150	1/2	0.23	0.23	0.24	0.25	0.27	0.29	0.33	0.38	0.45	0.55	0.68	0.83	1.00
	1	0.16	0.17	0.17	0.18	0.19	0.22	0.24	0.29	0.36	0.47	0.63	0.83	1.00
	2	0.12	0.12	0.12	0.13	0.14	0.15	0.18	0.22	0.28	0.39	0.59	0.86	1.00
	5	0.07	0.07	0.08	0.08	0.08	0.10	0.11	0.13	0.18	0.29	0.55	0.99	1.00
	10	0.05	0.05	0.05	0.06	0.06	0.07	0.08	0.10	0.13	0.22	0.54	1.10	1.00
165	1/2	0.23	0.23	0.23	0.24	0.25	0.28	0.31	0.35	0.41	0.50	0.63	0.79	1.00
	1	0.16	0.16	0.17	0.17	0.19	0.20	0.23	0.26	0.31	0.40	0.53	0.73	1.00
	2	0.11	0.11	0.12	0.12	0.13	0.14	0.16	0.19	0.23	0.31	0.44	0.68	1.00
	5	0.07	0.07	0.07	0.07	0.08	0.09	0.10	0.12	0.15	0.20	0.32	0.63	1.00
	10	0.05	0.05	0.05	0.06	0.06	0.06	0.07	0.08	0.11	0.11	0.21	0.58	1.00
180	1/2	0.20	0.25	0.23	0.24	0.25	0.28	0.31	0.34	0.40	0.49	0.61	0.78	1.00
	1	0.10	0.17	0.16	0.18	0.18	0.23	0.22	0.25	0.31	0.38	0.50	0.70	1.00
	2	0.02	0.09	0.12	0.12	0.13	0.18	0.16	0.18	0.22	0.29	0.40	0.60	1.00
	5	0.02	0.06	0.07	0.07	0.07	0.08	0.10	0.12	0.14	0.18	0.27	0.46	1.00
	10	0.01	0.05	0.05	0.04	0.06	0.07	0.07	0.08	0.10	0.13	0.20	0.36	1.00

Figure 8: Wave Diffraction Calculation and Weigel Tables[14]

Reflection: Reflection is the transformation occurring when a wave meets an obstacle, and part or all its energy is reflected backwards. The presence of engineering structures in the coastal zone affects wave propagation. So, when waves hit the offshore structures, such as vertical fronts and breakwaters, they are reflected. The reflected wave is transmitted in the opposite direction to that of the incident wave, with which it interacts. The superposition of the incident wave with the reflected wave creates a standing wave. In the case of total reflection, the instantaneous surface elevation of a standing wave can be calculated simply by the sum of two waves of the same height with opposite directions. The reflection coefficient R is calculated as follows:

$$K_R = \frac{H_{max} - H_{min}}{H_{max} + H_{min}} \quad \text{Equation 11}$$

$$H = K_r * K_S * K_R * H_O \quad \text{Equation 12}$$

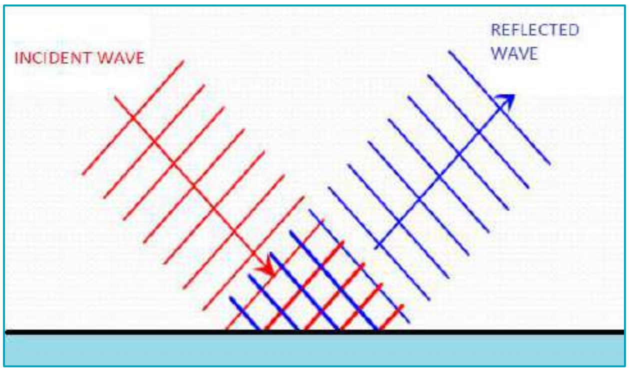

Figure 9: Reflection transformation: incident and reflected wave

When $K_R = 1$ then the reflection of the wave energy is total. In case of total reflection, the reflected wave has the same characteristics as the incident but moving in the opposite direction. The two waves are added and the so-called clapotis standing wave results.

$$\eta_s = H\cos(kx)\cos(\omega t)$$

$$\eta_s = \frac{H}{2}\cos(kx - \omega t) + K_R\cos(kx + \omega t)$$

$$H_{max} = (1 + K_R) * H \quad and \quad H_{min} = (1 - K_R) * H$$

$$H = \frac{1}{2}(H_{max} + H_{min}) \quad \text{Equation 13}$$

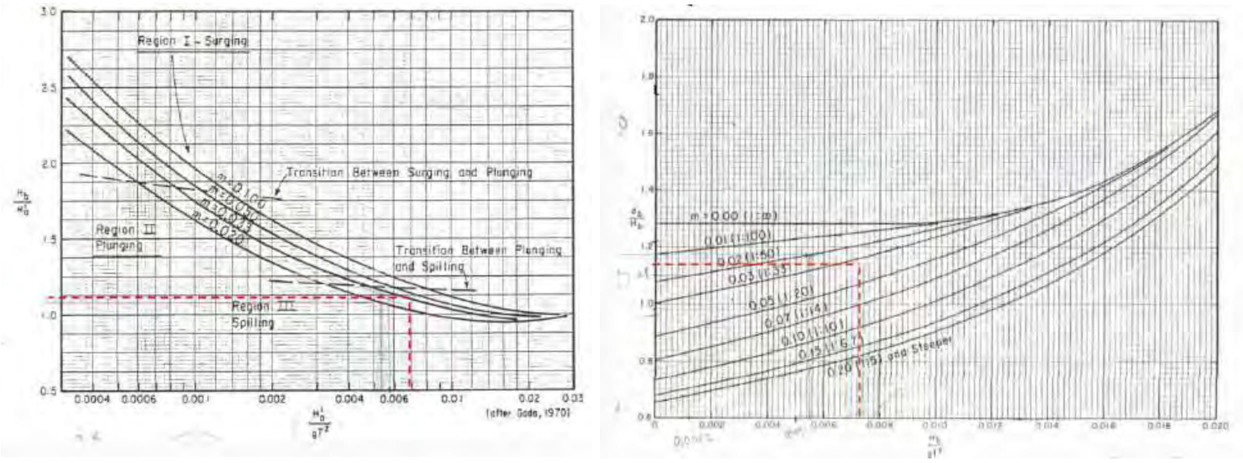

Figure 10: Breaking Depth Nomogram [14]

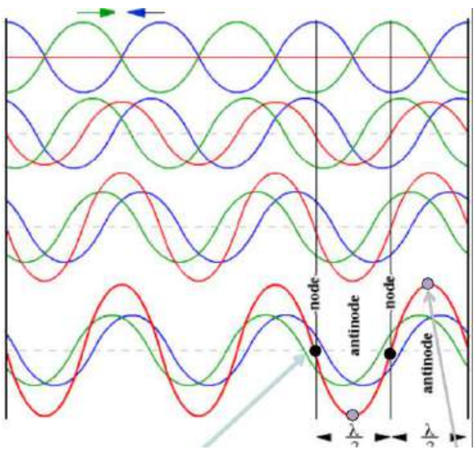

Figure 11: Reflection and resulting standing wave (blue: reflected wave, red: resulting wave-standing, green incident wave) [15]

Wave Breaking: As the waves are driven towards the shore, the effect of shoaling increases the wave height and the particle velocities, until the maximum horizontal velocity at the top of the wave tends to become greater than the propagation velocity itself. Then the water particles at the top of the wave detach, and wave breaking occurs. In detail, as the wave propagates to shallower water depths, its speed, c, decreases due to the decrease in depth, hence its kinetic energy. To maintain energy balance, there is an increase in dynamic energy by increasing the height H. This increase cannot continue indefinitely. At some point the wave becomes unstable and wave breaking occurs. This happens when:

1. The maximum horizontal velocity of wave particles exceeds the propagation velocity of the wave u>c.
2. The maximum vertical acceleration exceeds the acceleration of gravity $(\frac{dw}{dt})_{max} > g$.

Much research is devoted to the calculation of H_{max}.

1. In deep depths the limit is given by $\frac{H_{max}}{L_O} = 0.142$ (wave breaking criterion).
2. In shallow depths (for solitary waves): $\frac{H}{d} = 0.78$

   Miche criterion (1944): $\frac{H}{2} * k = 0.142\pi \tanh(kd)$

   Where for $d \rightarrow 0$ the Miche equation $\frac{H}{d} \rightarrow 0.89$

The above relations also constitute an upper limit of the height H of the wave, i.e. height wave greater than 0.142 L tanh(kd), does not exist [13].

Wave breaking is characterized by turbulent flow and energy loss with a reduction in wave height, and it continues until the wave rup-up is observed.

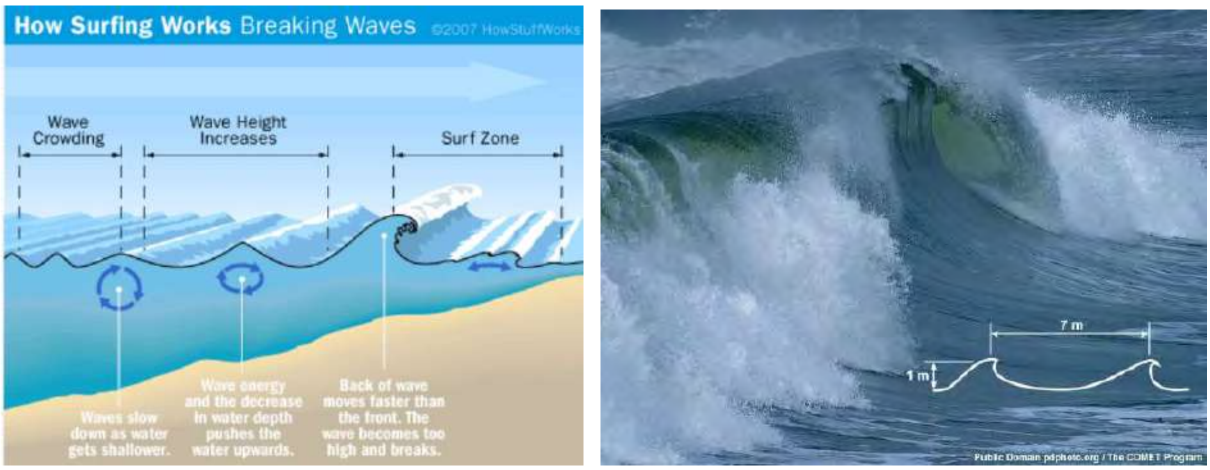

Figure 12: Wave Breaking [17],[18].

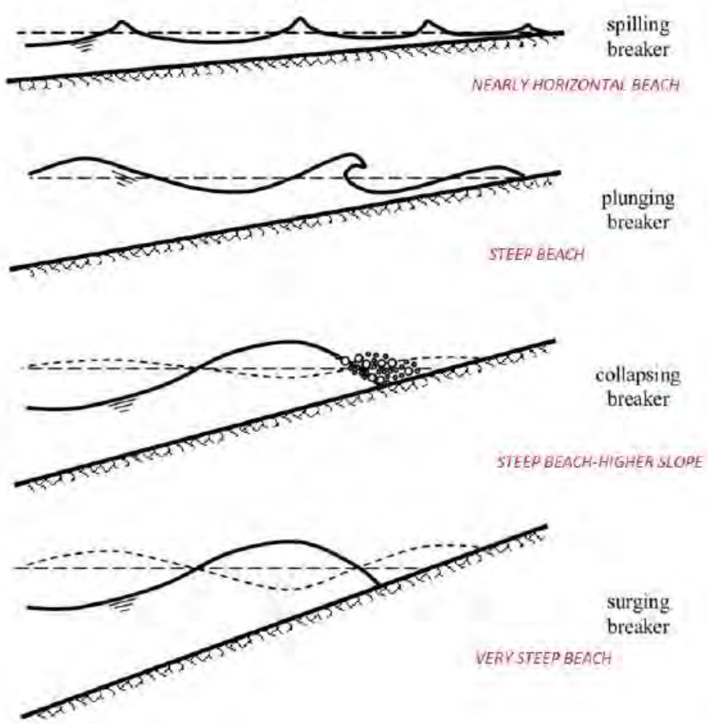

Figure 13: Types of Breaking Waves [19].

Wave Run Up: As wave run up (R) is defined the maximum height of the wave above the mean water level. After wave breaking, waves are transformed into moving hydraulic surges which propagate on the wave breaking zone and they "run-up". The maximum height R above still sea level where a wave runs-up can be estimated using the below classical Hunt relation [13]:

$$\mathrm{R} = H_o * \xi, \text{for } \xi < 2$$

The estimation of R is done through the following empirical relationship for the maximum wave run-up in real conditions [20]:

$$R = 1.1\left(0.35 \tan\beta_f \sqrt{H_o L_o} + \frac{H_o L_o \sqrt{0.563 \tan\beta_f^2 + 0.004}}{2}\right) \qquad \textit{Equation 14}$$

where $\tan\beta_f$ is the slope of the coast in the run up zone.

Wave over-topping: When waves meet on a sea front, a structure, or another barrier, they rise. When the crest level of the front is lower than the crest of the wave-run-up, wave overtopping takes place and part of the sea mass overflows to the inner face of the front [21]. In general, the wave overtopping occurs when:

$$R > h_c = \mathrm{h} - \mathrm{ds} \qquad \textit{Equation 15}$$

where:

- H: total height of the sea front
- ds: depth at the barrier front, which is calculated from mean water level,
- hc: front crest level above mean water level.

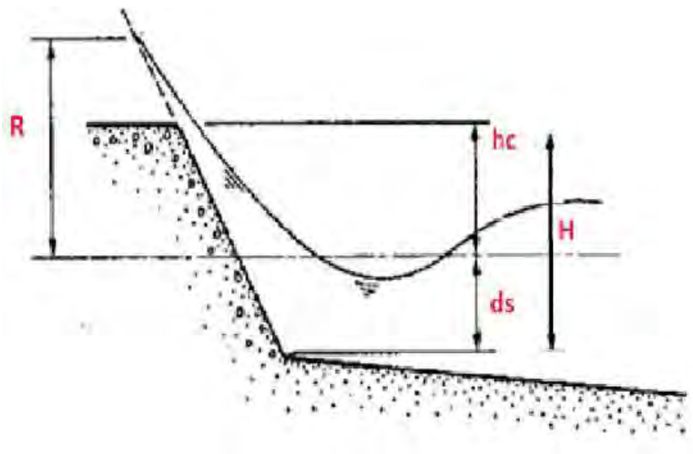

Figure 14: Wave-overtopping measurements [21].

Wave -Currents: Wave currents can be long shore currents or rip currents. Longshore currents are shore currents within the break zone resulting from obliquely breaking waves. The vertical component develops turbulence, and the shore-parallel component (rest) creates a parallel strong coastal current, a "marine river", that transports masses of water, pollution and granular material arising from the bottom or in suspension.

$$V = 20.7m\sqrt{g\,H_b\,sin(2\theta_b)} \qquad \textit{Equation 16}$$

Figure 15: Long shore and rip wave currents [22],[23].

Wave -Current Interaction: In the open sea, waves do not propagate under calm environmental conditions but in conditions of turbulent water flow over wave currents, tidal currents, estuaries, and river outflows. For wave currents, the speed of the current, U, is considered uniform, constant with water depth, and that the waves were created either upstream or in calm waters where the waves interact with the current. $U\sin(a)$ corresponds to the wave propagation direction of the current and the current U, could have the same or opposite direction with it.

Thus, when waves are studied for fixed axes in space, the characteristic measurements of angular frequency ω_α and wave propagation velocity c_α describe the kinematics, but while assuming a moving axis system which moves with velocity $U\sin(a)$, the characteristic measurements are now the relative angular frequency ω_r and the relative propagation velocity c_r. The following equation applies:

$$\omega_a = \omega_r + \vec{U} * \vec{k} \quad \textit{Equation 17}$$

$$\omega_r = \sqrt{g\, tanh(kd)} \quad \textit{Equation 18}$$

For known velocity U and wave direction a calculations can be held to estimate the wave number k, velocity components, u, w, and wave height η from linear theory for the moving axis system. By simple transformation the system can return to the fixed axis system.

Depending on the magnitude and direction of the wave current velocity, $U\sin(a)$, relative to the waves, the following cases show the fluctuations of the waves as they interact with the current. The index "c" indicates the effect of the current.

- $U\sin(a) > 0 \quad \rightarrow \quad c_{gc} > c_g \;\; and \;\; c_c > c$
- $U\sin(a) = 0 \quad \rightarrow \quad c_{gc} = c_g \;\; and \;\; c_c = c$
- $-c_{gc} < U\sin(a) < 0 \quad \rightarrow \quad c_{gc} < c_g \;\; and \;\; c_c < c$
- $-c_{gc} = U\sin(a) < 0$: *a) If the waves were initially propagated in still water, wave breaking occurs, b) If waves were created on the current:* $c_{gc} = 0,\; c_g > 0$.

For the following cases the waves must have been generated on the current:

- $-c < U\sin(a) < -c_{gc} \quad \rightarrow \quad c_{gc} < 0 \;\; and \;\; c_c < 0$
- $U\sin(a) = -c \quad \rightarrow \quad c_{gc} < 0 \;\; and \;\; c_c = 0$
- $U\sin(a) < -c \quad \rightarrow \quad c_{gc} < 0 \;\; and \;\; c_c < 0$

When the angle α≠0, the wave-current interaction is much stronger because the waves are simultaneously refracted by the current and both changes in wavelength and orthogonal direction and changes in ray direction occur. As waves propagate from one region to another the apparent period Ta remains constant. So:

$$\sqrt{\frac{d}{L_1} tanh(k_1 d)} = \sqrt{\frac{d}{L_O * a}} * \left(1 - \frac{T_a * U_1 * sin\, a_1}{L_1}\right) \quad \text{Equation 19}$$

$$\sqrt{\frac{d}{L_2} tanh(k_2 d)} = \sqrt{\frac{d}{L_O * a}} * \left(1 - \frac{T_a * U_2 * sin\quad_2}{L_2}\right) \quad \text{Equation 20}$$

From Snell's law: $\frac{L_1}{L_2} = \frac{\sin a_1}{\sin a_2}$, so *Equations 10 & 11* lead to the following:

$$\sqrt{\frac{d}{L_2} tanh(k_2 d)} = \sqrt{\frac{d}{L_O * a}} * \left(1 - \frac{T_a * U_1 * sin\, a_1}{L_1}\right) \quad \text{Equation 21}$$

The principle of conservation of wave propagation energy is applied to calculate the change in wave height between the two areas. Between successive rays there must be a constant flux of wave propagation $\frac{E}{\omega_r}$.

$$\left(\frac{E}{\omega_r} * c_{gr}\right)_1 * e_1 = \left(\frac{E}{\omega_r} * c_{gr}\right)_2 * e_2 \qquad \textit{Equation 22}$$

$$\frac{H_2}{H_1} = \sqrt{\frac{n_1}{n_2} * \frac{sin(2a_1)}{sin(2\,a_2)}} \qquad \textit{Equation 23}$$

If $U_1 = 0$ and $U_2 = U$, then:

$$\frac{c_2}{c_1} = 0.5 * \left[1 + \sqrt{\left(1 \pm \frac{4*U}{c_1}\right)}\right] \qquad \textit{Equation 24}$$

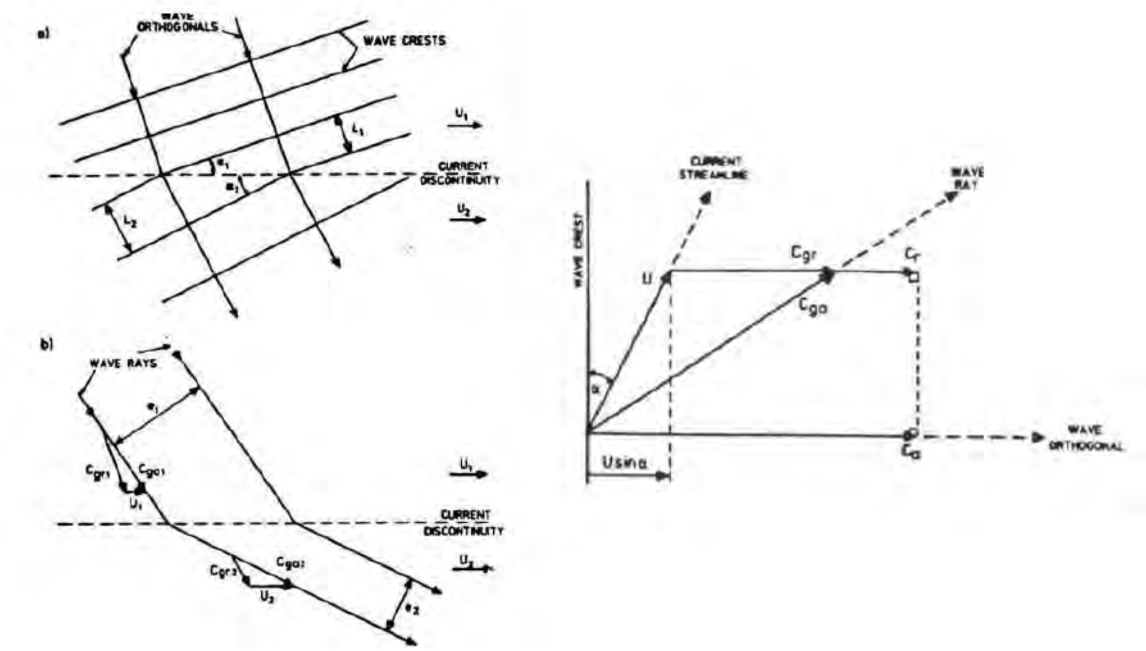

Figure 16: Wave – current interaction direction [14]

Bottom friction: The impact of bottom friction is of great importance for waves traveling in shallow water, as the friction of molecules on the bottom distorts the circular trajectories which become ellipses. This particle kinematics results in a reduction in both wave height and energy, and losses are observed.

White capping: an additional phenomenon occurs in deep water when wave breaking is caused by large wave steepness. Then white capping occurs with a very large wave height in relation to the wavelength.

2.3 Wave classification

A wave is defined as a set of disturbances interacting nonlinearly with each other in the open sea under turbulent conditions, travelling in random directions in waters of uneven density with various bottom slopes and permeability. Waves, depending on the return period and wavelength as well as the way they were created, can be classified into different categories. Wave disturbances can be created by wind, gravity, or even atmospheric pressure. The categories of waves are presented below.

Specific categories of waves arise from their generative cause. Waves that are created by the local wind with energy transfer from atmospheric layers that move on the sea surface are called *wind waves*. The tension leads this energy from wind to sea water and then pressure acts on wave crests and troughs. After the waves are created and travel away from the cause of their creation, they become *swells*. These travel long distances and correspond to a smooth sea surface**.** Surface tension also creates *capillary waves*, which are high frequency waves and so of small period. Another wind generated waves category is *storm surge.* The latter are long waves that occur as an unusual rise of water created by a storm, over and above the predicted tides. It is noted that strong onshore winds and decreased atmospheric pressure create this wave type.

Another cause of waves is gravity force. The latter creates the phenomenon of tides (about 2 times a day), during which the sea level periodically rises and falls. The rise of the water level is called flood *tide*, while the descent is called ebb or low tide. Gravity refers to the gravitational attraction of the Moon and the Sun on the Earth, as well as the rotation of these celestial bodies. In general, *gravity waves* are created within fluid medium or at their interface in order to restore equilibrium either by gravity itself or by the force of buoyancy, so the wave velocity in this case is a function of gravity. When the wave frequency is lower in the spectrum than this of the wind generated waves, then waves are called *infragravity waves*.

When waves propagate in the fluid medium by displacing a large volume of water, tsunami waves are created, and their generative cause is a large extreme event such as an earthquake, volcanic or underwater explosions.

Three categories are identified regarding the separation of waves in terms of the depth to which they propagate. There are *shallow, intermediate, and deep-water waves*. Intermediate water waves are the waves travelling between shallow and deep-water depths (could be considered around 500–1000 m). When the wave depth, d, is greater than ½ of the wavelength, λ, ($d > 0.5\lambda$) waves are referred as deep-water waves. In that case, the impact of the bottom is considered insignificant. The effect of bottom processes, on the contrary, is extremely important in the case of shallow water waves. A shallow water wave is one that occurs at depths less than the wavelength divided by 20 ($d < 0.05\lambda$).

Travelling or progressive wave is a wave propagating continuously in a medium in the same direction with constant amplitude and three subcategories of travelling waves are: longitudinal, transverse, and orbital waves. When two same in frequency and amplitude travelling waves propagating in opposite directions meet, their superposition creates a *stationary or standing wave*. The points of minimum amplitude of a stationary wave are called nodes, and the maximum amplitude points are called antinodes. *Seiches* are the standing waves that propagate in an enclosed or partially enclosed field such as lakes, reservoirs, harbors, and seas. The long wave created by strong onshore winds and decreased atmospheric pressure is called *storm surge*.

Other ocean classification

Extreme waves – freak/rogue wave: Extreme waves are characterized by their unexpected, particularly high height and they can cause failure to offshore structures. A typical example of a high-risk wave is the so-called *freak or rogue wave*. These waves are characterized by the concentration of the sea mass at a certain peak and by the strong directionality that leads to a rise in the wave height, which exceeds our statistical models. Accordingly, freak waves are waves that deviate from our predictions in terms of statistical data. One such well-known event is the famous New Year's wave that took place on January 1, 1995 at the Draupner jacket platform, in the North Sea at a depth of d = 70m. The freak wave reached a significant wave height Hs = 11.92 m (Hmax of 25.63 m)[24]. The characteristic form of *large waves* is close to that of the freak wave and therefore in any relevant research it is necessary to calculate the probability of exceedance (Hcrest / Hs).

Long and short crested waves: Further classification is done according to the peak of the wave: short crested or long crested waves. Waves on the surface of the sea which tend to become two-dimensional due to the characteristic shape of a large crest compared to the wavelength, are called long crested waves. In this case, a concentration of energy appears in a region-zone in the direction of wave propagation. Conversely, waves with a short crest in relation to the wavelength perpendicular to the direction of propagation are called short-crested waves and are the most numerous waves in the open sea.

Walls of water: walls of water are almost unidirectional waves, which cause enormous damage to offshore structures.

3. OFFSHORE STRUCTURES

Offshore structures are installed in the sea for oil and gas extraction and transportation, but also for the exploitation of the wind potential with the combined installation of offshore wind turbines (OWTs). Offshore gas or oil extraction platforms are installed with the aim of extracting and exploiting hydrocarbons from the marine environment, and they are complex large-scale structures. Their applications concern the exploration, drilling and extraction of oil or natural gas as well as the production and transmission of electricity (wind farms), while their design is a complex problem and a challenge for engineers. In addition, offshore platforms applications include navigation, ship loading and unloading, and bridges support. Accordingly, these structures host the oil and gas extraction and processing facilities and equipment or the wind power exploitation equipment. The structure also provides living quarters for the workforce.

The complexity is discussed clearly due to safety that must be ensured in a demanding environment, with strong wave and wind forces, with different environmental conditions each time of the open sea and for a lifetime of approximately 25 years. The dynamic response of the structure, which is studied in this document, is essential for the realistic design of a platform and requires both the depth and the geomorphology of the bottom to be considered for the selection of the type of the suitable platform for each area, as well as the protection of the workers in project and of the environment. These strict requirements have led to the establishment of national and international standards and guidelines (American Petroleum Institute-API, Det Norske Veritas-DNV), which are followed in the design.

Wind Farms Worldwide

- Hywind in Scotland, consisting of five 6MW Spar type wind turbines - October 2017.

- WindFloat Atlantic in Portugal, where three semi-submerged floating wind turbines with a power of 8.4 MW were installed.
- Kincardine in the United Kingdom which has a total of five floating wind turbines with a capacity of 9,525 MW as well as one with a capacity of 2 MW [25].
- In 2020, 16.83 MW floating wind power was installed, (16.8 MW is from Portugal and 0.03 MW from Spain) [26].
- As of 2020 power, a total of 73.33 MW net floating wind was installed globally, (32 MW is located in the UK, 25 MW in Portugal,12 MW in Japan, 2.3MW in Norway and 2 MW in France) [26].

For shallow and intermediate depths, wind turbines fixed to the bottom are used (bottom depth 20-40 m). For even smaller depths close to 10 m, gravity wind platforms are chosen, while for intermediate depths of 50-70 m, jacket-type wind turbines consisting of a complex truss structure are chosen. However, new technologies capable of being deployed in deeper waters with a bottom depth greater than 50 m are required to consider the construction and maintenance costs in these areas. This would be particularly useful as such a deep build presents the benefits mentioned in the Chapter 1: INTRODUCTION . Such constructions mainly refer to Spar wind turbines and semi-submersible floating platforms, such as the construction being studied.

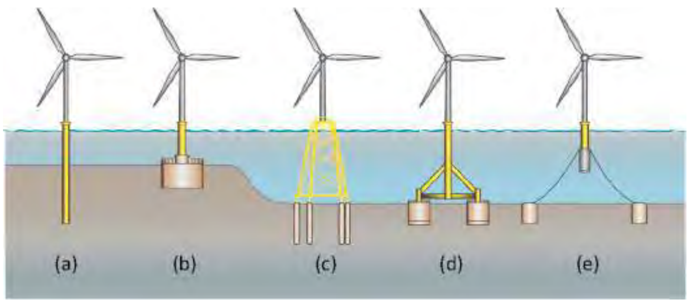

Figure 17: Foundation types for offshore wind plarforms: mono-pile (a), mono-pod (skirted caisson) (b), jacket structure (c), tripod (d) and floating wind turbine with anchors (e) [27]

The development of offshore technology, which is an important economic factor for several countries, began in the 1970s. It is noted that the first offshore wind farm in the world was built in 1991, Vindeby in Denmark, and had a capacity of 5 MV. Offshore wind power projects, as used for the exploitation of the potential of wind in open seas, are a very powerful solution to the energy crisis today. The need for renewable energy has brought the construction of offshore wind farms worldwide, which is a construction set consisting of a large number of OWTs. It is therefore a new technology that has rapidly gained traction in recent years, as the statistical data, which be cited below, prove.

According to 2022 renewable capacity statistics [28], renewables need to achieve around 40 per cent in total energy generation for all sectors by 2030. Total wind energy in Greece is clearly increased the last decade, but as presented in the following tables, all wind energy sources are related to onshore wind energy, while there are no offshore wind energy structures in Greece. In terms of technical criteria, according to experts, Greece can support up to 70 GW of floating wind farms.

Wind energy
Énergie éolienne
Energía eólica

CAP (MW)	2012	2013	2014	2015	2016	2017	2018	2019	2020	2021
Armenia	3	3	3	3	3	3	3	3	3	3
Azerbaijan	2	3	3	8	16	16	66	66	66	67
Georgia					20	20	20	21	21	21
Russian Fed	10	10	10	11	11	11	52	102	945	1 955
Turkey	2 261	2 760	3 630	4 503	5 751	6 516	7 005	7 591	8 832	10 607
Europe	107 196	118 181	130 209	143 010	155 763	170 624	181 904	196 339	207 878	222 052
Austria	1 337	1 675	2 110	2 489	2 730	2 887	3 133	3 224	3 226	3 524
Belarus	5	7	9	22	62	84	92	112	112	112
Belgium	1 370	1 780	1 944	2 176	2 370	2 788	3 268	3 863	4 681	4 780
Bosnia Herzg	0	0	0	0	0	0	51	87	135	135
Bulgaria	677	683	699	699	699	698	699	703	703	705
Croatia	180	254	339	418	483	576	586	646	801	988
Cyprus	147	147	147	158	158	158	158	158	158	158
Czechia	258	262	278	281	282	308	316	339	339	339
Denmark	4 162	4 819	4 886	5 077	5 245	5 489	6 115	6 103	6 259	7 014
Estonia	266	248	275	300	310	312	310	316	317	317
Faroe Islands	9	9	20	20	20	20	16	13	19	19
Finland	257	447	627	1 005	1 565	2 044	2 041	2 284	2 586	3 257
France	7 607	8 156	9 201	10 298	11 567	13 499	14 900	16 457	17 484	18 676
Germany	30 979	33 477	38 614	44 580	49 435	55 580	58 721	60 742	62 188	63 760
Greece	1 753	1 809	1 978	2 091	2 370	2 624	2 877	3 589	4 119	4 457
Hungary	325	329	329	329	329	329	329	323	321	321
Iceland		2	3	3	3	2	2	2	2	2

Onshore wind energy
Énergie éolienne terrestre
Energía eólica terrestre

CAP (MW)	2012	2013	2014	2015	2016	2017	2018	2019	2020	2021
Armenia	3	3	3	3	3 o	3 e	3 o	3 e	3 e	3 e
Azerbaijan	2 e	3	3	8	16 u	16 u	66 o	66 e	66	67
Georgia					20	20	20	21	21 o	21 o
Russian Fed	10	10	10 e	11 e	11 e	11 e	52 e	102 e	945	1 955 o
Turkey	2 261	2 760	3 630	4 503	5 751	6 516	7 005	7 591	8 832 o	10 607 o
Europe	102 183	111 497	122 234	132 014	143 130	154 822	163 141	174 282	182 964	194 237
Austria	1 337	1 675	2 110	2 489	2 730	2 887	3 133	3 224	3 226	3 524 u
Belarus	5	7	9	22	62	84	92	112	112	112 e
Belgium	989	1 072	1 236	1 464	1 658	1 910	2 082	2 308	2 419	2 518 o
Bosnia Herzg	0 o	0 o	0 o	0 o	0 o	0 o	51	87	135 u	135 u
Bulgaria	677	683	699	699	699	698	699	703	703	705 o
Croatia	180	254	339	418	483	576	586	646	801	988 u
Cyprus	147	147	147	158	158	158	158	158 o	158 o	158 e
Czechia	258	262	278	281	282	308	316	339	339	339 o
Denmark	3 240	3 548	3 615	3 806	3 974	4 225	4 414	4 402	4 559	4 708 o
Estonia	266	248	275	300	310	312	310	316	317	317 u
Faroe Islands	9 o	9 o	20 o	20 o	20 o	20 e	16 o	13 o	19 o	19 e
Finland	231 e	421 e	601 e	973 e	1 533 e	1 971	1 968 o	2 211	2 513	3 184 u
France	7 607	8 156	9 201	10 298	11 567	13 497	14 898	16 455	17 482	18 674 o
Germany	30 711 o	32 969 o	37 620 o	41 297 o	45 303	50 174	52 328	53 187	54 414	56 013 o
Greece	1 753	1 809	1 978	2 091	2 370	2 624	2 877	3 589	4 119	4 457 u
Hungary	325	329	329	329	329	329 u	329 o	323	321	321 e
Iceland		2	3	3	3	2	2	2	2	2 e

Offshore wind energy
Énergie éolienne maritime
Energía eólica marina

CAP (MW)	2012	2013	2014	2015	2016	2017	2018	2019	2020	2021
World	5 334	7 171	8 492	11 717	14 342	18 837	23 626	28 382	34 362	55 678
Asia	321	488	516	722	1 680	3 006	4 833	6 295	9 418	27 822
China	291	417	440	559	1 480	2 788 u	4 588 u	5 930	8 990 o	26 390 o
Chinese Taipei						8 u	8 u	128 o	128 o	237 o
Japan	25	50	50	53	60	65 u	65 u	65 o	65 o	65 o
Korea Rep	5	5	11	11	41	46 e	73 u	73 u	136 u	136 e
Viet Nam		16 e	16 u	99 u	99 o	99 o	99 e	99 u	99 e	994 e
Europe	5 013	6 684	7 976	10 996	12 633	15 802	18 763	22 058	24 915	27 814
Belgium	381	708	708	712	712	877	1 186	1 556	2 262	2 262 o
Denmark	922	1 271	1 271	1 271	1 271	1 264	1 701	1 701	1 701 o	2 306 o
Finland	26 u	26 u	26 u	32 u	32 u	73	73 o	73	73 u	73 u
France						2 u	2 o	2 u	2 u	2 u
Germany	268 o	508 o	994 o	3 283 o	4 132 o	5 406	6 393	7 555	7 774	7 747 o
Ireland	25	25	25	25	25	25 u	25 o	25	25 o	25 e
Netherlands	228 o	228 o	228 o	357 o	957 o	957 u	957 u	957 u	2 460	2 460 o
Norway	2 u	2 u	2 u	2 u	2 u	2 o	2 u	2 u	2 e	6 u
Portugal	2	2	2	2				8	25	25 u
Spain		5 u	5 u	5 u	5 u	5 u	5	5 o	5 e	5 o
Sweden	163	212	213	213	203	203 e	203	203 u	203 u	203 u
UK	2 995 o	3 696 o	4 501 o	5 093 o	5 293 o	6 988	8 217	9 971	10 383 o	12 700 u
European Union (27)	2 015	2 985	3 472	5 900	7 337	8 812	10 545	12 085	14 529	15 108
N America			0	0	29	29	29	29	29	42
USA			0 u	0 u	29	29	29 o	29 o	29 o	42 o

Figure 18: Total Wind Energy, Onshore Wind Energy and Offshore Wind Energy in Greece by IRENA 2022 source [28].

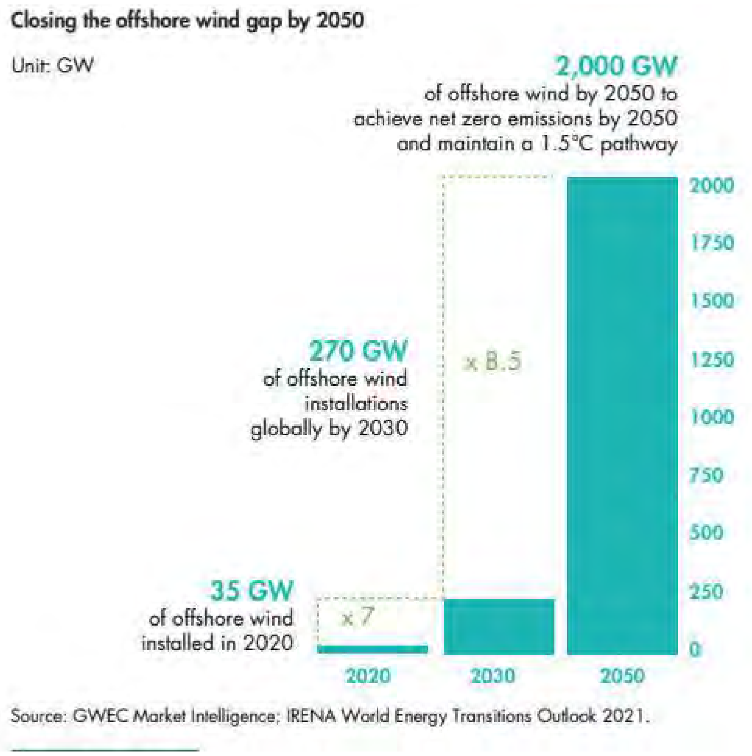

Figure 19: Offshore wind gap to be closed by 2050 and new offshore installations by GWEC 2021 source [26].

3.1 Offshore structure types

The first category of offshore wind structures concerns *stationary platforms* founded at the sea bottom, which do not move and include fixed jacket platforms, compliant towers, jack-up platforms and gravity-based structures, also called GBS. The second category refers to *Mobile Offshore Drilling Units – MODU Mobile Platforms*, which are facilities designed for drilling and exploration activities and can be moved without significant effort. This is achieved by tugboats or motor vehicles. The latter includes tension leg platforms-TLP's, semi-submersible platforms and spar platforms. As stationary platforms are fixed to the bottom, they are more stable and so, more resistant in time, comparing to MODU Mobile Platforms. The subcategories are described below.

STATIONARY PLATFORMS

Fixed Jacket Platforms

The jacket offshore platforms rest on the bottom with a truss base which supports the deck carrying various pieces of equipment for the purposes of the platform. These are significantly stable structures due to their strong foundation on the bottom which resists strong wind and wave loads. The legs of the structure are concrete or steel or a mix of both tubular structures, usually steel, joined together with cross braces forming the structure. The vertical members of the base are fixed on the bottom with piles and are usually four, six or eight. As can be understood, this is a proper type for shallow and intermediate water depths, as a similar construction in deep water would have enormous economic and construction costs. They are therefore recommended for depths located in water depths up to 500 meters (Figure 20).

Compliant towers (CTs)

Compliant Towers are fixed offshore platforms that, like jacket platforms, support a deck for oil or gas exploitation and other purposes. Because of their base structure, they can receive significant lateral forces, as it is a jacket steel base anchored with piles into the seabed, with the characteristic difference of a narrower and longer structure compared to jacket, but also of more flexible tubular elements that connect the platform legs. These flex elements for the base construction prevent resonance and high wave impact so that compliant towers can sustain huge latteral forces even in hurricane conditions. The lower part of the flexible tower base is a narrow steel jacket structure in tension and their upper part includes buoyant tanks (up to 12) that control the amount of buoyancy by maintaining the appropriate tension in the members of the structure during the act of wind and wave loads.

For this type of platform, it is customary to install a mooring system of high-strength cables or wire ropes, which anchor the tower to the seabed. The jacket offshore platforms rest on the bottom with a truss base which supports the deck but a compliant tower, due to its design, can operate in deeper waters than a jacket platform. Typical water depth for the construction of compliant towers ranges between 450 and 900 meters. The cost of construction and operation of a compliant tower is increased compared to that of a fixed jacket platform (Figure 20).

Figure 20: Stationary platform categories: (from left to right) fixed jacket platform, compliant tower, jack-up platform (up) and gravity-based structure (down) [29],[30], 128],[33]

TLP platforms (Tension Leg Platform-TLP)

Tension leg platforms are floating structures permanently anchored to the seabed by a mooring system of tendons. These platforms have been used mainly for oil and gas extraction since the early 1980s with the first applications appearing in the North Sea. The tendons of the structure are grouped at each of its corners creating a group called a "tension leg" and are essentially long cables in constant tension. The name of the structure is since it does not support directly its weight on the seabed, but it is stabilized through buoyancy in the upper part of the structure, with the tensioned legs transferring the forces to the bottom. This operation of the tendons results in the elimination of any vertical movements of the structure. However, the tendons allow small horizontal movements so that the platform can withstand lateral loads without the risk of the tendons breaking. Tension leg platforms have a high construction and operational cost and at the same time their consolidation is a complex process, however they are extremely stable structures with great strength that can operate in water depths of up to 2000 meters (Figure 22).

GBS structures (gravity-based platform)

Gravity based platforms (GBS) are steel or concrete structures, based on the seabed which stand by their self-weight. Their material is reinforced concrete, and their structural system consists of a cellular base, which surrounds three to six columns, extending above the surface of the water, to support the deck of the platform. GBS structures are mainly installed in water depths between 20-350 meters and are the safest offshore construction type. They have significantly low maintenance costs and a long lifecycle, and it is possible to use their base as a storage space oil.

A prerequisite for the construction of such a platform is the geotechnical study of the bottom of the area of interest in order to determine the geotechnical parameters and the loads between the structural base and seabed, and to ensure the appropriate strength and stability of the construction. An average shell thickness of the columns must be chosen, suitable, so that they do not break due to the weight of the deck they support, but also not so thick that it increases the platform weight and makes it impossible to float for transporting the platform. These studies must therefore include checking the stability of the structure against overturning and sliding, but also against the increased hydrostatic pressure it receives during the sinking and an accurate assessment of the loads that will be applied. Therefore, gravity-based platforms are found in areas where the bottom geological conditions are strong and piling foundations are not feasible (Figure 20).

Installation: The steps of construction and installation are the construction of the base, the construction of columns and the support of the deck onsite. The process starts away from the final site, in a special port facility (tank) where the base cells are cast, not including their tops, then the tank is filled with water to sail, and the cell system is transported and moored in a sheltered deep-water-depth seaport. There, the concrete columns are placed on the base and the overall system is sunk to support the deck and related equipment. It is then raised to be transported by tugboat to the intended location, where it sinks very slowly. At this point, any gaps in the base are filled with soil material, ensuring the stability of the structure, and all the necessary materials and machinery are placed on the deck.

MOBILE OFFSHORE DRILLING UNITS (MODU)

Jack-up platforms

Jack-up rigs are mobile platforms suitable for shallow water depths up to 190 meters. They consist of three to four piles or legs as they are otherwise called, which support the floating deck. They are self-elevating mobile platforms whose mobile legs raise the floating deck above the surface of the sea. The legs that support the structure are a truss consisting of high strength tubular steel members which offer mobility to the platform and to this fact the platform owes its name, jack -up, from the word “jack”. This mobility is achieved by a system of gears which gives the ability to raise or lower the deck depending on whether the rig is in operation or not. The foundation of the legs is done by penetrating piles into the seabed, if the soil is soft, or in the case of stiff soils, it is supported on the bottom with cylindrical steel bases.

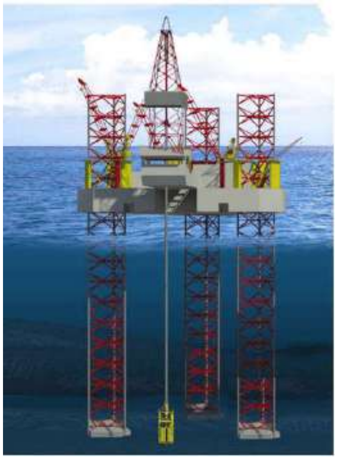

Figure 21: MODU Platforms- Jack up platform[32]

The transportation and movement of the platform is done by uncoupling the legs when the purpose of the construction (e.g. drilling) has been completed. Uncoupling leads to the lifting of the deck and thus the platform becomes free to move to a new location. As it is not self-propelled, the platform is moved from one location to another by special ship tugs. The operation of structure of this type is not applicable in deeper water depths, as the actions of raising and lowering the deck are not a practical task. A significant disadvantage is the fact that they have limited storage capacity (Figure 21).

SPAR platforms

Spar platforms are large offshore structures of extremely large diameter that extend to great depths. It is a type of floating platform, used for deep water up to 3000 meters. They consist of a large diameter cylinder on which the deck rests. The cylinder is mostly submerged, and its base includes a chamber made of heavy material, denser than water. This heavy material carries the center of gravity of the structure is lower than the center of buoyancy, and so the construction is characterized by great stability. The platform is anchored to the seabed permanently by a cable system. Due to its design, the structure shows great resistance to wind loads as well as to wave loads and sea currents. There are three types of spars classic, truss, and cell, which are described below (Figure 23). From classic to truss and after to cell spar, there have been significant structural and operational improvements, while achieving a lower cost and higher efficiency.

Classic SPAR: The first type is classical spar and is the earliest type to appear. It consists of a long buoyant cylinder, which has heavy tanks at its base, acting as heavy ballast of the structure. It is common for the shell to contain spiral fins, which direct the flow downwards, reducing the pressure difference in front and behind the cylinder and thereby providing stability to the structure.

Truss SPAR: The spar type consists of three parts: a short length cylindrical shell, a truss integrated in its base and heavy tanks for heavy ballast at the bottom of the structure. The truss of the shell consists of four tubular vertical members, which are connected by X-braces and horizontal plates, which reduce vertical movement. This type of spar platform is better option financially than the classic type, as less steel is required for its construction.

Cell SPAR: Cell SPAR is the latest, most modern type of spars and smaller than the others. A cell spar consists of a set of small diameter cylinders (usually 6), which surround a seventh cylinder. The cylinders can be buoyancy and ballast cylinders or buoyancy only. To ensure stability of the structure, the cylinders are connected through structural steel members. At the base of the system is placed the tank with the heavy material, as is the case with the other two types of spars. Compared to the other types it has a lower construction cost.

Semi-submersible platforms

The semi-submersible platforms are floating structures that have a large deck connected to horizontal buoyant members, the pontoons. Semi-submersible platforms are mobile platforms, and because of the legs they have, they have a high resistance to lateral loads whose height is high so that the deck is protected from extreme waves of high wave height but also so that there is enough gap to neutralize the strong wind loads. So, they are suitable for very deep depths up to 3000 meters.

Four or six vertical columns, supported on horizontal cylindrical members, support the deck, the weight of which is distributed evenly among these columns. With this design, the horizontal cylinders can be submerged while the weight of the platform is evenly distributed to keep it in place while it is anchored to the bottom with a chain and cable combination mooring system and thus a floating structure is achieved. There are submersible platforms, which allow the structure to be raised and lowered by changing the amount of water they contain. So, while during its operation the platform is partially submerged in water, when it is transported, it floats completely on the surface. This fact facilitates its transportation, which is carried out by tugboats, while some platforms are self-propelled. However, a disadvantage is the high cost of its construction (Figure 22).

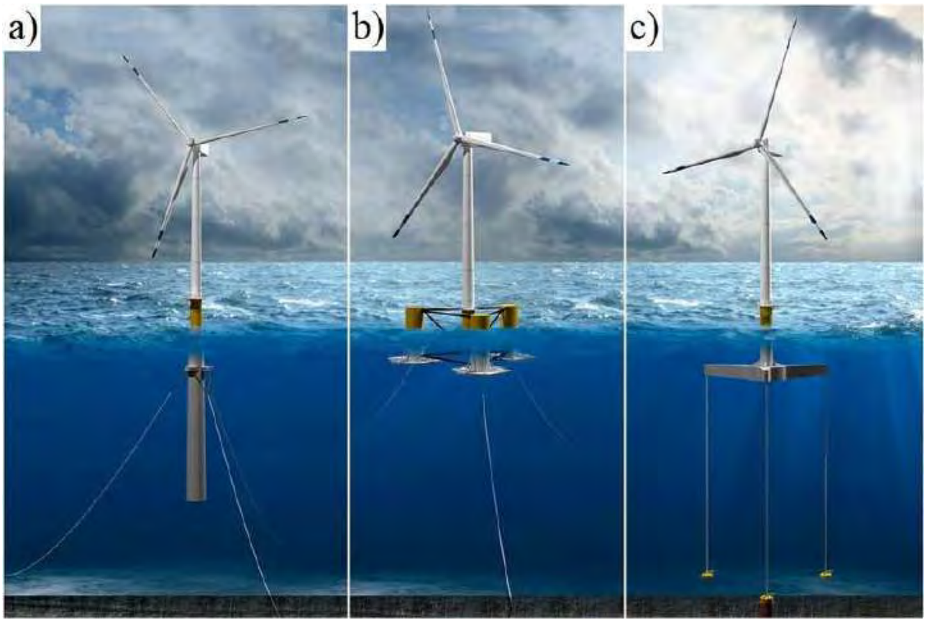

Figure 22: Three main floater categories: a) spar, b) semi-submersible, c) TLP [34].

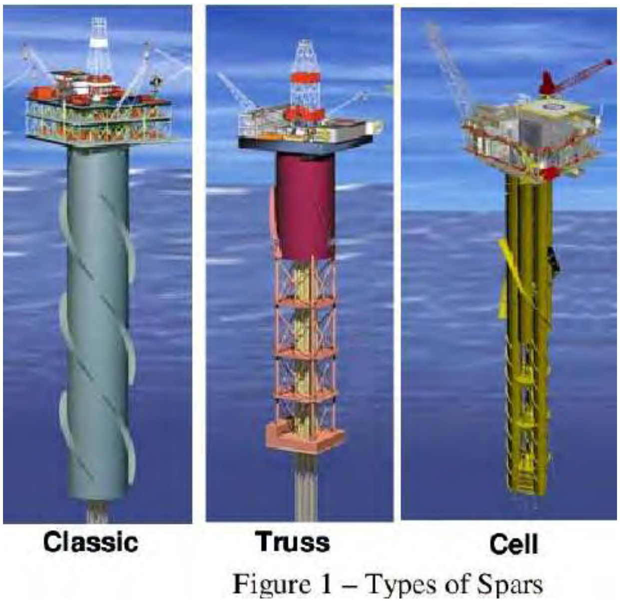

Figure 23: Types of Spar Platforms [35].

3.2 Loads of waves exerted on offshore structures.

The loads that an offshore construction can receive from the waves are the following:

- Initially, horizontal load on the piles, which is permissible loading.
- Deck loading, leading to failure.
- Vertical charge due to vertical velocities and accelerations resulting from the elliptical shape of the motion of the particles. Such loads lead the structure to rise and fall through the buoyancy and are considered only in the design of the anchors.
- Loading from the bottom up, the so-called air gap.

Offshore wind platforms, monopiles are not chosen in Greece due to deeper seabed. Specifically, for the Greek depths of 60, 70 and even 500m, floating or jacket constructions are considered more suitable.

4. WAVE THEORIES AND WAVE MODELLING

A wave is defined as a set of disturbances, periodic or not, interacting nonlinearly with each other in the open sea under turbulent conditions, travelling in random directions in waters of uneven density with various bottom slopes and permeability. To understand the behavior of the wave field and the effects that its action has on ships and structures it encounters, it is necessary to study the wave particles, their kinematics, and their properties. The calculation of the wave particle kinematics, namely particle velocity, acceleration, and pressure, as well as the elevation of the free surface, are key quantities for the accurate estimation of wave loads. Various wave models are used to calculate the above-mentioned parameters, which are required to capture as accurately as possible the three foundation properties that govern the real sea: irregularity, non-linearity, and directionality [9].

The term *irregularity* describes wave dispersion to frequency spectrum, *non-linearity* refers to the interaction between the wave field frequencies generating new waves, and *directionality* indicates that waves of the open sea have multidirectional components, while wave energy propagates in numerous different directions. Short-crested waves are generated, and the wave shape is affected by these procedures by changing in the transverse direction at a faster rate the more directional the field becomes. As waves travel to shallower depths, as discussed in the chapter 2.2Wave transformation: mechanism description, there is an increase in wave height up to wave breaking. However, two additional processes in this process make *skewness* and *asymmetry* important characteristics of waves. Initially, asymmetry is observed with respect to the horizontal axis, while a sharpening and rise of the wave crest is observed, with simultaneous flattening of the trough, a phenomenon called *skewness*. Also, asymmetry with respect to the vertical axis is observed as an increase of wave steepness of the wave front before wave breaking occurs with consistency a forward tilt.

There two categories of wave models to describe water waves: steady wave and random wave models, depending on the consideration of a monochromatic or spectral field.

4.1 Steady waves

This category refers to regular waves, which are monochromatic/non- random waves studied in two-dimensional conditions. Particularly, steady wave models assume that every and each wave component preserves its shape and its characteristics in each period, leading to analytical periodic wave solutions. Therefore, this assumption concludes to simple mathematical calculations, neglecting the real sea wave spectrum and, accordingly, wave directionality. However, the effect of directionality on the wave field can be considered by using the reduction factor ϕ, which is uniformly applied in depth to the final values of the velocity and acceleration components.

In the general case, wave spectrum in case of regular waves is considered as a point in the frequency domain, corresponding to a single frequency around which total wave energy is concentrated. So, this frequency value will also correspond to maximum amplitude of the wave. The most appropriate theory can be chosen based on wave steepness, which is the key parameter to approach more realistic non-linear solutions, using the Dean & Le Méhaute diagram. Steady wave models are described as follows.

1. Airy or Stokes 1st order theory (linear solution)
2. 2nd order Stokes theory (2nd order nonlinear solution)
3. 5th order Stokes theory (5th order nonlinear solution)
4. 18th order Fourier or Stream function solutions theory (18th order nonlinear solution)

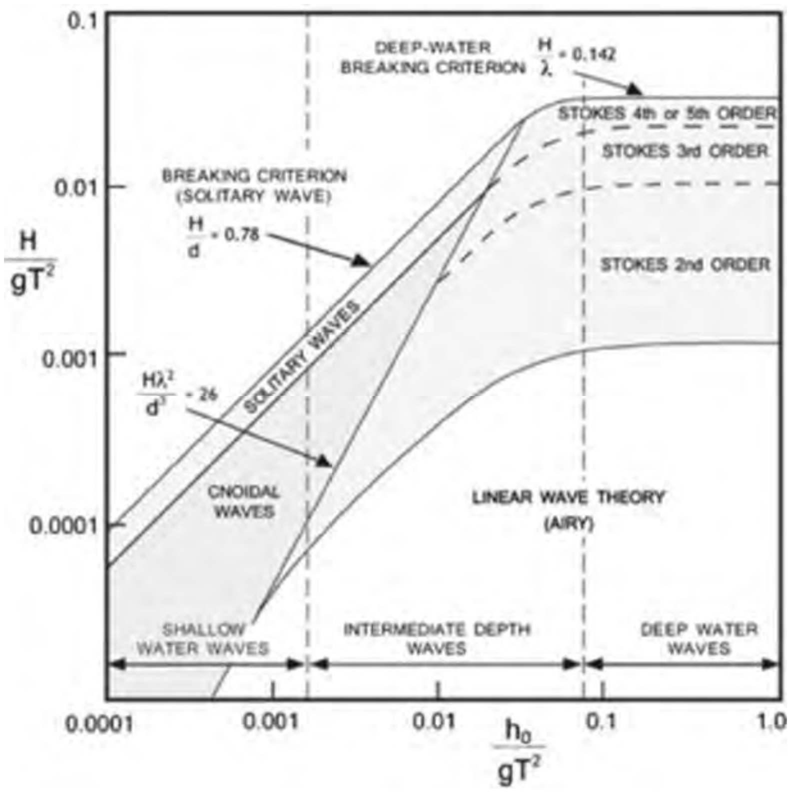

Figure 24: Dean & Le Méhaute diagram [36].

4.1.1. Airy or Stokes 1st order theory (linear solution)

The Airy wave theory (1845), known as linear wave theory or Stokes 1st order (1847) is a sinusoidal linearized description of the surface gravity waves propagation on a homogeneous fluid layer. This theory, published by George Biddell Airy in the 19th century, adopts the following assumptions: that the fluid is ideal, the bottom is constant (in terms of depth), impermeable and horizontal, the flow is irrotational, the pressure on the free surface is zero and the wave height, H, is much less than the depth d and the length L. It is the simplest wave model to estimate wave kinematics, as the fluid layer is of infinite width, leading to a simplified two-dimensional study.

Considering the assumptions adopted, the mathematical problem arises as follows.

- The fluid is homogeneous and incompressible, so the shear stress on the surface is considered negligible. Thus, the *continuity equation* is valid.

$$div\vec{U}(x,y,z) = 0 \Rightarrow \frac{\partial u}{\partial x} + \frac{\partial w}{\partial z} = 0 \quad \text{Equation 25}$$

were $\vec{\mathrm{U}}(\mathrm{x},\mathrm{y},\mathrm{z}) = \vec{\mathrm{U}}(\mathrm{u},\mathrm{w})$ is the 2D velocity vector.

- The bottom is constant, impermeable, and horizontal (constant depth).
- The flow is irrotational. This means that no shear stress occurs at the air-fluid interface and at the seabed. Therefore, the relation for a *irrotational flow* is valid.

$$\nabla x\vec{U}(x,y,z) = 0 \Rightarrow \frac{\partial w}{\partial x} - \frac{\partial u}{\partial z} = 0 \quad \text{Equation 26}$$

- The fluid is ideal and the pressure on the free surface is zero. The fluid is ideal (μ = 0), as the boundary layer at the seabed is considered very small. Thus, from the general Navier-Stokes motion equations and through the irrotational flow hypothesis, the *Bernoulli equation* is derived:

$$\rho\frac{\partial\varphi}{\partial t} + \rho gz + \rho\frac{u^2+w^2}{2}\, p_o = ct \quad \text{Equation 27}$$

- The amplitude of the waves is much smaller in relation to the depth of the water as well as the wavelength (a << d and a << L). Through this hypothesis, the validity of linear theory is limited to cases of small wave height, which occurs in deep and intermediate water depths. For shallow water depth the Airy theory cannot be applied.

Airy theory is based on the potential function φ (x, z, t) to calculate the characteristics of the wave field, which are free surface profile, particle kinematics and wave propagation velocity. Due to the assumption of the irrotational flow, the directional velocity components at each point of the flow are expressed through the flow potential function applied in *Equation 26*, as follows:

$$\vec{U}(x,y,z) = grad\varphi \Rightarrow u = \frac{\partial\varphi}{\partial x} \; and \; w = \frac{\partial\varphi}{\partial z} \quad \text{Equation 28}$$

Then by assuming the mass continuity equation, *Equation 25*, which considers the fluid incompressible, the Laplace equation results in terms of flow potential and in terms of velocity:

$$\nabla^2\varphi = 0 \Rightarrow \frac{\partial^2\varphi}{\partial x^2} + \frac{\partial^2\varphi}{\partial z^2} = 0 \quad \textit{Equation 29}$$

$$\nabla^2 u = 0 \Rightarrow \frac{\partial^2 u}{\partial x^2} + \frac{\partial^2 u}{\partial z^2} = 0 \quad \textit{Equation 30}$$

For the description of the free surface and the wave particle kinematics, it is necessary to establish and apply boundary conditions, which concern both the bottom and the surface of the wave. Through the hypothesis of "small" waves, it is possible to linearize the boundary conditions of the surface, with the upper order terms being neglected [9]. The application of the boundary conditions is done at the still water level, instead of the free surface.

Kinematic bottom boundary condition – KBBC: The bottom layer is considered horizontal and impenetrable. This means that the bottom does not contribute to energy transfer and does not reflect wave energy. This condition implies that there is no vertical flow at the bottom and therefore the vertical velocity is zero.

$$\frac{\partial\varphi}{\partial z} = 0 \; for \; z = -d \quad \textit{Equation 31}$$

Kinematic free surface boundary condition – KFSBC: This boundary condition expresses the fact that wave particles remain on the surface, and they do not detach from the rest of the water mass. Therefore, the flow velocity on the free surface must coincide to the velocity on the surface in the vertical direction.

$$\frac{\partial\varphi}{\partial z} = \frac{\partial\eta}{\partial t} + \frac{\partial\varphi}{\partial x}\frac{\partial\eta}{\partial x} \Rightarrow \frac{\partial\varphi}{\partial z} = \frac{\partial\eta}{\partial t} \quad for \; z = 0 \quad \textit{Equation 32}$$

Dynamic free surface boundary condition -DFSBC: The pressure on the free surface is constant. Through this condition the effects of wind flow are ignored. Therefore, the pressure difference, due to wind, between a wave crest and a trough is negligible. Applying the Bernoulli equation, *Equation 27,* results in the following equations:

$$\frac{\partial \varphi}{\partial t} + gz + \frac{1}{2}\left[\left(\frac{\partial \varphi}{\partial x}\right)^2 + \left(\frac{\partial \varphi}{\partial z}\right)^2\right] = 0 \; for \; z = \eta$$

$$\frac{\partial \varphi}{\partial t} + g\eta = 0, \quad for \; z = 0 \qquad \textit{Equation 33}$$

The above assumptions and equations derived lead to analytical solutions of periodic waves which maintain their shape in each period.

While combining Laplace equation, the bottom kinematic condition, and the surface dynamic condition (*Equations 29, 30, 31 and 33 respectively*), the analytical solution for the potential function is obtained and for a wave with a given frequency ω, the potential function is calculated:

$$\varphi(x, y, z) = \frac{\omega}{\kappa} \alpha \frac{cosh(k(z+d))}{sin \;\; (kd)} sin(kx - \omega t) \quad \textit{Equation 34}$$

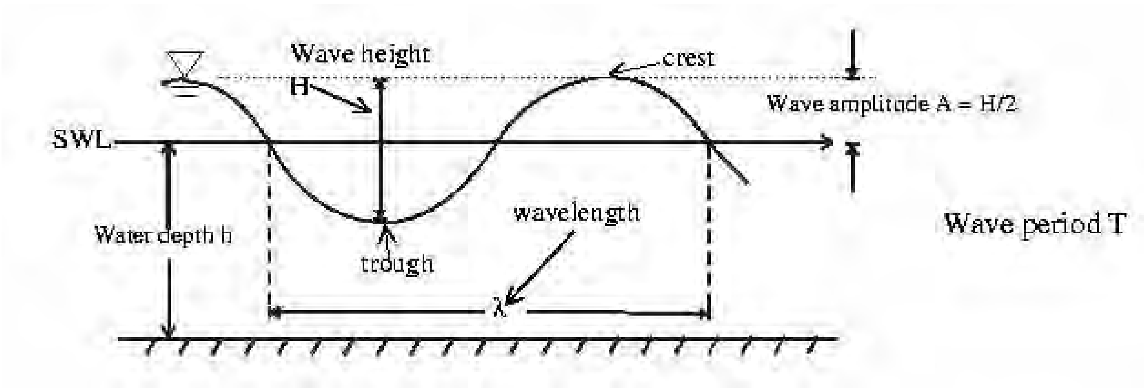

Figure 25: Free surface profile, Airy Wave Theory[37]

To describe the propagation of a wave in two dimensions, the coordinate system is first defined:

• X-axis represents the Still Water Level (SWL), the surface of the fluid in the absence of waves. The direction of x-axis indicates the direction of propagation of the waves, which is considered positive from left to right.

• Z-axis is perpendicular to the x-axis and takes positive values upwards the still water level (where z = 0). The direction of gravity corresponds to that of the negative z axis. As a result, z-axis takes values from a to $-d$, where a is the amplitude of the wave and d the water depth (distance of the still water level to the bottom).

Combining the potential function and the dynamic surface condition (*Equation 33, Equation 34*), the free surface elevation is obtained. The free surface is described by a harmonic function of the horizontal distance x and time t and is defined as follows:

$$\eta(x,t) = 0 \Rightarrow \alpha\, cos(kx - \omega t) \quad \textit{Equation 35}$$

where:

- a: wave amplitude, in meters [m], It is the vertical distance of each crest or trough from the still water level of the sea and so $-a < \eta < a$. Also, wave height H is defined as the vertical distance between a crest and a trough in a period. Thus, for the wave height of regular linear waves the following holds: $H = 2a$.
- ω: the angular frequency of the wave (angular frequency), in rad per second [rad / s]. The angular frequency, ω, and the wave number, k, are the spatial parameters of the wave. Parameters ω and k are related to the time parameters of the wave, which are the wave period, T, and the wavelength, λ, respectively.
- k: the wave number, in rad per meter [rad / m].
- λ: the wavelength represents the horizontal distance between two subsequent crests or troughs.
- T: the wave period is defined as the minimum time required for a fixed point of the wave to return to the same phase, i.e., between two successive crests or

troughs (one wavelength). The equations that associate these parameters as well as their units of measurement are presented below.

$$T = \frac{2\pi}{\omega}\ [s] \quad and \quad \lambda = \frac{2\pi}{k}\ [m] \quad \text{Equation 36}$$

From Figure 25, it is concluded that the profile of the free surface is symmetrical with respect to the still water level, which for linear waves is identical to the mean water level (MWL).

Wave number and frequency are not independent parameters. They are related to each other, as surface gravity waves display frequency dispersion, and thus, each wave number has its own frequency and propagation velocity. This is expressed through the linear dispersion relation, which results from the dynamic surface boundary condition (DFSBC), *Equation 33*:

$$\omega^2 = gk\,tanh(kd) \quad \text{Equation 37}$$

As period is the time the wave needs to traverse a distance equal to the wavelength, the propagation velocity of a wave is defined as follows:

$$c = \frac{\lambda}{T} \quad \text{Equation 38}$$

The velocity components of each wave particle, in the horizontal (u) and vertical (w) directions, are obtained according to *Equations 28 and 34* as follows:

$$u(x,y,z) = \frac{\alpha\omega cosh(k(z+d))}{sinh(kd)}\ cos(kx-\omega t) \quad \text{Equation 39}$$

$$w(x,y,z) = \frac{\alpha\omega sinh(k(z+d))}{sinh(kd)}\ sin(kx-\omega t) \quad \text{Equation 40}$$

Moreover, the acceleration components of each wave particle, in the horizontal (a_x) and vertical (a_z) directions, are obtained:

$$a_x(x,y,z) = u\frac{\partial u}{\partial x} + w\frac{\partial u}{\partial z} + \frac{\partial u}{\partial t} \quad \text{Equation 41}$$

$$a_z(x,y,z) = u\frac{\partial w}{\partial x} + w\frac{\partial w}{\partial z} + \frac{\partial w}{\partial t} \quad \text{Equation 42}$$

where:

- the first two terms, on the left, express the rate of change of the velocity in the corresponding directions relative to wave particle position – *convective acceleration*, and
- the last term expresses the rate of change of velocity to the respective directions with respect to time - *local acceleration*.

Convective acceleration includes 2nd order velocity terms, which are considered too small due to the initial hypothesis of "small" waves and can be ignored. Therefore, the components of the particle acceleration in the horizontal and vertical directions are respectively:

$$a_x(x,y,z) = \frac{\alpha\omega^2 cosh(k(z+d))}{sinh(kd)} \, sin(kx - \omega t) \quad \text{Equation 43}$$

$$a_z(x,y,z) = -\frac{\alpha\omega^2 sinh(k(z+d))}{sinh(kd)} \, cos(kx - \omega t) \quad \text{Equation 44}$$

Figure 26 shows that free surface elevation is symmetrical with the horizontal component of velocity. The same applies to the vertical velocity and horizontal acceleration components, which show a phase difference of π / 2 with the above mentioned.

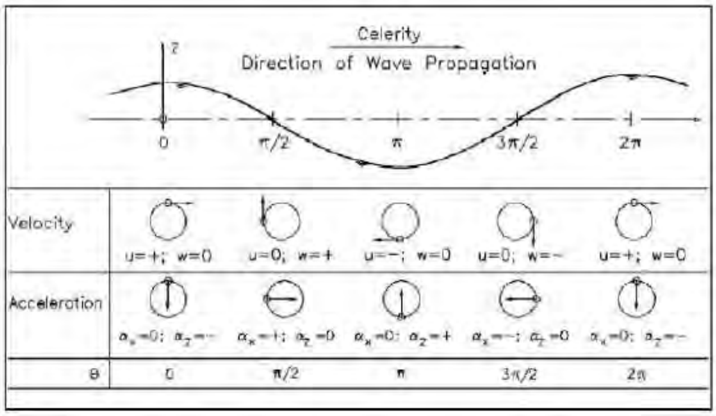

Figure 26: Wave particle velocities and accelerations [38]

Equations 39-43, do not consider the required properties of the wave field, as directionality governs the real sea, is neglected. To include directionality, a reduction in velocity and acceleration measurements should be applied, and this is achieved by applying the coefficient Φ. So, the final values of the components of velocity and acceleration, are leading to linear reduction:

$$u_\varphi = u\Phi \quad and \quad w_\varphi = w\Phi \quad \textit{Equation 45}$$

$$a_{x,\varphi} = a_x\Phi \quad and \quad a_{z,\varphi} = a_z\Phi \quad \textit{Equation 46}$$

As a wave propagates, from left to right, as defined by the free surface profile, this movement of the surface causes the movement of the wave particles below the surface, which follow a clockwise orbital motion. Specifically, the orbits of the particles are closed curves, circles in deep water and elliptical in intermediate and shallow water depths (Figure 27).

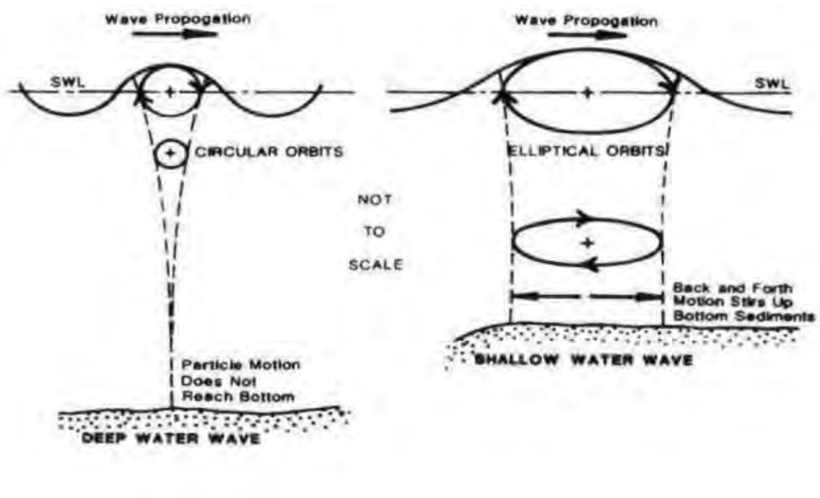

Figure 27: Wave particles motion in deep and shallow water [39]

In any water depth, the wave particle velocity as well as the diameter of the orbits decreases with the depth. In the case of finite depth, the elliptical orbits of the wave particles become more and more elongated near the bottom. Due to the linear description of the waves, energy transfer takes place in each period, while no mass is transferred. The energy is transferred to the wave propagation direction, with the fluid particles below the surface moving around a specific-average position at a velocity different from the velocity of wave propagation.

Regarding the pressure distribution, the Bernoulli equation is used, *Equation 27*. Assuming a "small" wave (α <<), it holds that $u << u^2$ and therefore the term ρ $(u^2 + w^2)$ / 2 can be omitted. By introducing the potential function, the pressure P (x, z, t) at each point of the wave field is given by *Equation 47.* Examining the above relation, the first term corresponds to the constant atmospheric pressure, the second the hydrostatic pressure that changes with depth and the third the dynamic pressure that depends on both depth and time Figure 28.

$$P(x,z,t) = p_o - \rho g z + \rho \alpha g \frac{cosh(k(z+d))}{cosh(kd)} cos(kx - \omega t) \quad \textit{Equation 47}$$

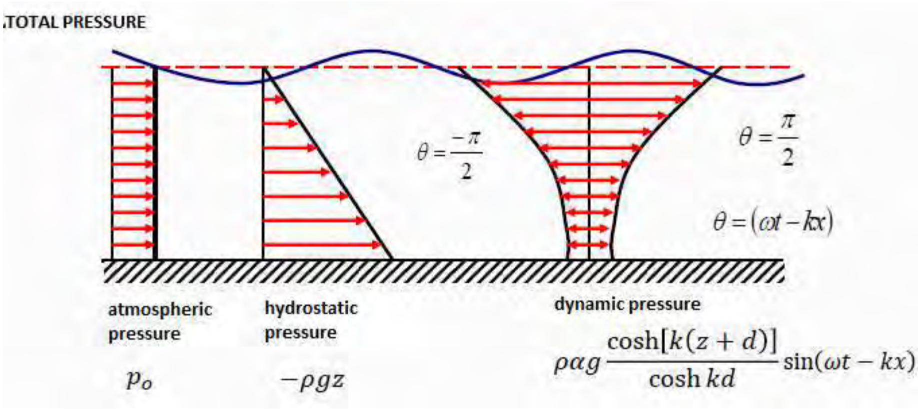

Figure 28: Total pressure of wave particles [14]

4.1.2. 2nd order Stokes theory (2nd order nonlinear solution)

As the three main characteristics of waves, irregularity, directionality, and nonlinearity, govern the real sea, wave theories attend to integrate them into a mathematical problem. Nonlinearity has been approached by Sir George Stokes (1847), who extended Airy's linear theory to 2nd order solutions. The description of the waves is done through the perturbation method. According to this method, each dependent variable is expressed using Fourier series, which have as their main growth parameter the wave steepness. Wave steepness is defined as $\varepsilon = ak$, where a is the wave amplitude as described in linear wave theory and k is the wave number. Stokes 2nd order wave theory also applies to regular waves and gives more accurate results in deep water too.

Based on the same assumptions with Airy theory, Stokes 2nd order theory considers two-dimensional flow, which satisfies the mass continuity equations for incompressible fluid (*Equation 25*), the Laplace equation for irrotational flow (*Equation 29, Equation 30).* and the Bernoulli equation (*Equation 27*). The wave field is described by the potential function φ (x, z, t) and therefore for the velocity components u $(x, z, t) = grad\varphi$. In addition, the bottom and surface boundary conditions mentioned in the previous paragraph apply. However, in the case of 2nd order Stokes theory, the boundary conditions apply to the free surface. This means that the 2nd order terms, which are ignored in linear theory, are now important and considered.

Kinematic bottom boundary condition – KBBC: The bottom layer is horizontal and impenetrable.

$$\frac{\partial\varphi}{\partial z} = 0 \; for \; z = -d \quad \text{Equation 48}$$

Kinematic free surface boundary condition – KFSBC: Wave particles remain on the surface.

$$\frac{\partial\varphi}{\partial z} = \frac{\partial\eta}{\partial t} + \frac{\partial\varphi}{\partial x}\frac{\partial\eta}{\partial x} \Rightarrow \frac{\partial\varphi}{\partial z} = \frac{\partial\eta}{\partial t} \quad for \; z = 0 \quad \text{Equation 49}$$

Dynamic free surface boundary condition -DFSBC: The pressure on the free surface is constant. Applying the Bernoulli equation – *Equation 27* results in:

$$\frac{\partial\varphi}{\partial t} + gz + \frac{1}{2}\left[\left(\frac{\partial\varphi}{\partial x}\right)^2 + \left(\frac{\partial\varphi}{\partial z}\right)^2\right] = 0 \; for \; z = \eta \quad \text{Equation 50}$$

Based on the above assumptions, it is possible to extract analytical solutions, which relate to periodic waves that propagate while maintaining their form in each period. The wave field is described by the potential function, which by introducing the Laplace equation into the kinematic bottom boundary condition and the dynamic surface boundary condition, results:

$$\varphi(x, y, z) = \frac{\omega}{\kappa}\alpha\frac{cosh(k(z+d))}{sinh(kd)}sin(kx - \omega t) + \alpha^2\omega\frac{3cosh(2k(z+d))}{8\,sinh^4(kd)}sin(2\theta) \quad \text{Equation 51}$$

where:

- $\theta = kx - \omega t$: wave phase [rad]

Stokes 2nd order wave theory mathematically describes the elevation of the free surface as a periodic function of the parameters x, t, which consists of two terms:

$$h_{stokes\ 2n}\ (x,t) = h_1 + h_2 = \frac{H \cos\theta}{2} + \frac{(H^2 k cosh(kd))(2+cos\ \ (2kd))\, cosh(2\theta)}{16\, si\ \ \ {}^3(kd)}\quad \textit{Equation 52}$$

the first term is the equation of the free surface according to Airy theory.

The elevation profile of the free surface, as shown in Figure 29, is not symmetric with respect to the still water level ($\eta_{max} > H\ /\ 2$ and $|\ \eta_{min}\ | < H\ /\ 2$). The crests appear taller, and the troughs are shallower than in the Airy linear theory, while the wave height remains constant over time ($\eta_{max} + |\ \eta_{min}\ | = H$). Due to the high crests, the waves show bigger slopes. Therefore, a large slope of the free surface, $\frac{\partial\eta}{\partial t}$, implies large accelerations. This, in turn, leads to greater forces exerted on the construction.

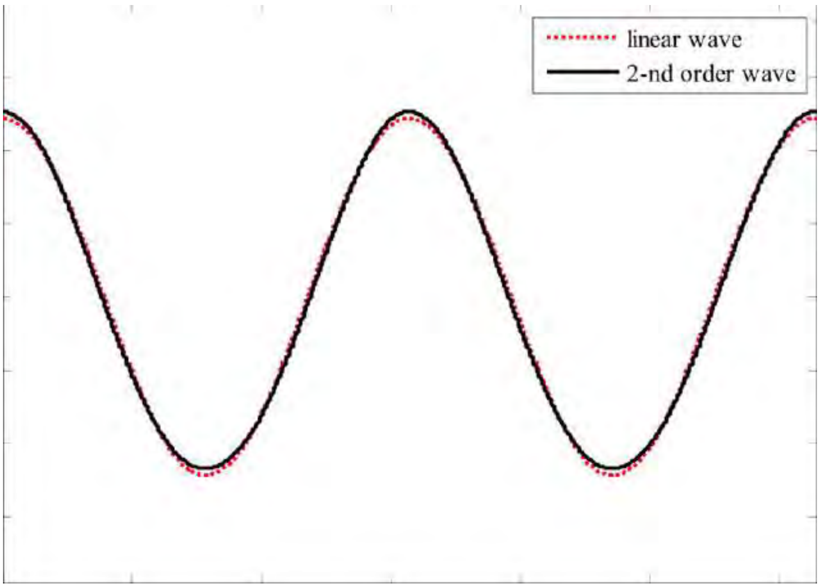

Figure 29: Free surface profiles for 2nd order Airy and Stokes wave theories [40].

The linear dispersion equation remains same in the case of the 2nd order nonlinear waves and is the same as that mentioned in Airy theory:

$$\omega^2 = gk\, tanh(kd)\quad \textit{Equation 53}$$

Similarly, the equations expressing the velocities and local accelerations of the particles in the two directions consist of two terms, a 1st order, and a 2nd order term.

$$u(x,z,t) = \frac{\partial \varphi}{\partial x} = \frac{H\omega c \quad (k(z+d))}{2sinh(kd)} \cos\theta + \frac{3H^2\omega kcosh(2k(z+d))}{16\, sinh^4(kd)} cos(2\theta) \quad \text{Equation 54}$$

$$w(x,z,t) = \frac{\partial \varphi}{\partial z} = \frac{H\omega cosh(k(z+d))}{2sinh(kd)} \sin\theta + \frac{3H^2\omega kcos \quad (2k(z+d))}{16\, sinh^4(kd)} sin(2\theta) \quad \text{Equation 55}$$

$$a_x(x,z,t) = \frac{\partial u}{\partial t} = \frac{H\omega^2 cosh\big(k(z+d)\big)}{2sinh(kd)} \sin\theta + \frac{16 \quad {}^2\omega^2 kcosh(2k(z+d))}{16\, sin \quad {}^4(kd)} sin(2\theta) \quad \text{Equation 56}$$

$$a_z(x,z,t) = \frac{\partial w}{\partial t} = -\frac{H\omega^2 sinh\big(k(z+d)\big)}{2sinh(kd)} \cos\theta - \frac{16H^2\omega^2 ksin \quad (2k(z+d))}{16\, sinh^4(kd)} cos(2\theta) \quad \text{Equation 57}$$

The final values of the velocities and accelerations, with the introduction of the directionality,

$$u_\varphi = u\Phi \quad and \quad w_\varphi = w\Phi \quad \text{Equation 58}$$

$$a_{x,\varphi} = a_x\Phi \quad and \quad a_{z,\varphi} = a_z\Phi \quad \text{Equation 59}$$

4.1.3. 5th order Stokes theory (5th order nonlinear solution)

Stokes 5th order wave theory corresponds to a model of regular waves, according to which individual waves propagate without changing their shape. These are detailed two-dimensional flow solutions where directionality is difficult to introduce. Based on Stokes 2nd order theory, Sir George Stokes (1880) extended his previous theory to 5th order solutions, approaching the problem as a series of disturbances. The waves are described using Fourier series. The basic formulation parameter of the series is the quantity ak, where a is the amplitude of the wave according to the linear wave theory and k the wave number. The coefficients used in the Fourier series are calculated based on the free surface boundary conditions and are increased for higher wave heights. Each wave, then, results in a sum of five harmonics, describing both free and bound waves. Due to the different steepness of each wave, the higher order harmonics are not necessarily of same phase with the previous ones.

Correspondingly, the model is only accurate for waves not too long and too high in relation to the wave depth and applies more accurately in deep water depths. It is noted that in the case of waves characterized by sharper crests and flatter troughs than in a sine wave, in relation to the depth, the Cnoidal wave theory must be applied, in contrast to Stokes theory. According to Hedges (1995), the limits of application of the 5^{th} order Stokes theory are determined based on the dimensionless parameter known as the Ursell number:

$$U_r = \frac{\frac{H}{d}}{(\frac{d}{\lambda})^2} \rightarrow U_r < 40 \,, \quad \textit{Equation 60}$$

Along with Stokes theory, other theories for regular 5^{th} order nonlinear waves were developed, such as those of De and Skjelbreia and Hendrickson. All the above theories assume that waves propagate according to Stokes' first definition of wave velocity. This leads to erroneous results, as demonstrated by Fenton (1985) [41], as it does not consider the change of the shape of the waves over the surface of the water as they propagate.

Fenton presented a mathematically more precise version of Stokes theory to describe regular, non-linear waves travelling in deep water. According to Fenton, in addition to the commonly used design values (wave height H, wave period T and water depth), it is important to determine the flow velocity or the mass flux. This is necessary, as in most cases the waves travel on a finite stream or current, which is determined by the oceanography and topography of the area. The velocity of the waves as perceived by a stationary observer is directly related to the finite flow, as the waves travel faster in the direction of the flow than in the opposite direction of the flow. This implies that the period measured by a stationary observer depends on the velocity of the waves and therefore on the current, in the sense that it is calculated according to the Doppler displacement. In addition, the current velocity must be added when calculating the horizontal component. Therefore, if the current is known, the problem is fixed. Like the Stokes theory, Fenton describes the waves using Fourier series. However, as formulation parameter of the Fourier series is used the wave steepness, $\varepsilon = Hk / 2$. In addition, the coefficients of the series are expressed as active depth kd functions, as presented by Fenton. Therefore, for the solution of the equations, the calculation of the wave number is sufficient, which in this case does not follow the linear dispersion equation presented earlier (*Equation 37 and Equation 53*).

The solution concerns a reference system (x, y) moving at speed $c = \lambda / T$, the speed of the wave. The fluid is considered ideal, incompressible, while the flow is irrotational and the bottom is horizontal and impermeable. For incompressible fluid the equation of mass continuity (*Equation 25*) applies and for irrotational flow the Laplace equation in terms of potential and velocity (*Equation 29* and *Equation 30*, respectively) as well as the Bernoulli equation (*Equation 27*). In addition, the bottom (*Equation 48*) and surface (*Equation 49* and *Equation 50*) limit conditions apply. Note that, in all the equations mentioned above, the parameter z has been replaced by the parameter y as well as the vertical component of velocity w has been replaced by v. This is because the vertical axis is now measured from the horizontal bottom in a positive upward direction and not from the still water level (Figure 29). Therefore, it holds that $y = z + d$ and $\partial y = \partial z$.

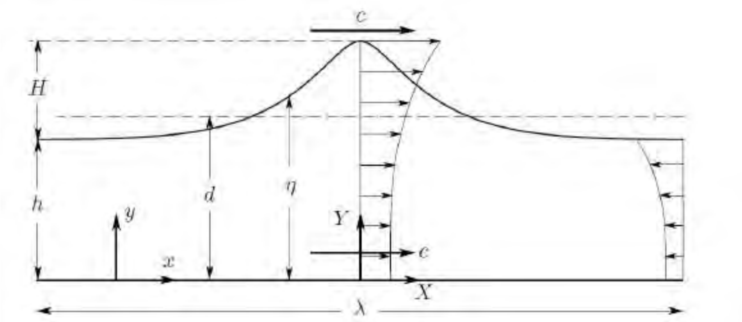

Figure 30: Stokes 5th theory: A wave of a steady train, showing principal directions, coordinates, and velocities [41].

The dynamic surface boundary condition in combination with the Bernoulli equation led to the following equation:

$$R = \frac{1}{2}\left[\left(\frac{\partial\varphi}{\partial x}\right)^2 + \left(\frac{\partial\varphi}{\partial z}\right)^2\right] + gh \qquad \textit{Equation 61}$$

where:

- R: the positive Bernoulli constant to which:

$$\frac{R}{g} = \frac{1}{2}{C_0}^2 + kd + \varepsilon^2 E_2 + \varepsilon^4 E_4 + 0(\varepsilon^6) \qquad \textit{Equation 62}$$

where:

- C C_0, E_2, E_4: coefficients according to Fenton
- O: the Landau order parameter symbol, which determines the order of a series. In this case, the terms greater than or equal to the 6th order are neglected.

The waves evolve, in the positive direction of the x axis, with speed $c = \lambda\ /\ T$. The following applies to the flow rate (c):

$$\vec{c} = \vec{u} + \overrightarrow{c_E} \qquad \textit{Equation 63}$$

where:

- $\vec{u}$ the average horizontal velocity of water, for which the following is valid: $\vec{u}(\frac{k}{g})^{1/2} = C_0 + \varepsilon^2 C_2 + \varepsilon^4 C_4 + 0(\varepsilon^6)$
- $\overrightarrow{c_E}$: average over time velocity of the fluid according to Euler
- in a reference system, with respect to which the current velocity is zero, the following holds $\overrightarrow{c_E} = 0$ and $|\overrightarrow{c_E}| = |\vec{u}|$

To calculate the wave number k, the transcendentally nonlinear equation is applied, which results from the dynamic surface boundary condition (DFSBC) (*Equation 50*) as:

$$\sqrt{\frac{k}{g}}c_E - \frac{2\pi}{T\sqrt{gk}} + C_0(kd) + \varepsilon^2 C_2(kd) + \varepsilon^4 C_4(kd) = 0 \ \textit{Equation 64}$$

As the wave number is known, the potential function results, which describes the properties of the wave field. The potential function for each frequency ω arises from a combination of the Laplace equation, the bottom kinematic condition, and the surface dynamic condition (*Equation 29, Equation 49*, and *Equation 50*, respectively).

$$\varphi(x,y,t) = -\bar{u}x + C_0\left(\frac{g}{k^3}\right)^{\frac{1}{2}} \sum_{i=1}^{5} \varepsilon_i \sum_{j=1}^{i} A_{ij}\, cosh(jky)\, sin(jkx) \quad \textit{Equation 65}$$

where:

- g: the acceleration of gravity, [m / s^2]
- Aij: coefficients according to Fenton

The free surface profile is expressed as the sum of five terms as follows:

$$kh_{stokes\ 5th}(x,y,t) = kd + \sum_{i=1}^{5} \sum_{j=1}^{i} \varepsilon_i B_{ij}\, cos(jkx) \ \textit{Equation 66}$$

where:

- Bij: coefficients according to Fenton

The velocities and local accelerations of the wave particles are defined based on the potential function:

$$u(x,y,t) = \frac{\partial\varphi}{\partial x} = -\bar{u} + C_0\left(\frac{g}{k^3}\right)^{\frac{1}{2}} \sum_{i=1}^{5} \varepsilon_i \sum_{j=1}^{i} A_{ij}\, cosh(jky)\, cos(jkx) \cdot jk \quad \textit{Equation 67}$$

$$v(x,y,t) = \frac{\partial\varphi}{\partial y} = C_0\left(\frac{g}{k^3}\right)^{\frac{1}{2}} \sum_{i=1}^{5} \varepsilon_i \sum_{j=1}^{i} A_{ij}\, sinh(jky)\, sin(jkx) \cdot jk \quad \textit{Equation 68}$$

$$a_x(x,y,t) = \frac{\partial u}{\partial t} = C_0\left(\frac{g}{k^3}\right)^{\frac{1}{2}} \sum_{i=1}^{5} \varepsilon_i \sum_{j=1}^{i} A_{ij}\, cosh(jky)\, sin(jkx) \cdot j^2 k\omega \quad \textit{Equation 69}$$

$$a_z(x,y,t) = \frac{\partial y}{\partial t} = -C_0\left(\frac{g}{k^3}\right)^{\frac{1}{2}} \sum_{i=1}^{5} \varepsilon_i \sum_{j=1}^{i} A_{ij}\, sinh(jky)\, cos(jkx) \cdot j^2 k\omega \quad \textit{Equation 70}$$

To compare the results of the theory with the directional solutions to eliminate again the reduced coefficient Φ in the final values of velocities and accelerations.

$$u_\varphi = u\Phi \quad and \quad v_\varphi = v\Phi \quad \textit{Equation 71}$$

$$a_{x,\varphi} = a_x\Phi \quad and \quad a_{y,\varphi} = a_y\Phi \quad \textit{Equation 72}$$

The pressure P (x, y, t), at each point, satisfies the Bernoulli equation and is presented according to Fenton as follows:

$$P(x,z,t) = R - gY - \frac{[(u-c)^2+v^2]}{2} \quad \textit{Equation 73}$$

where:

- ρ: the density of water, [kg / m^3]

Note that *Equation 65*, *Equation 46*, and *Equation 70* can be expressed in a new time-constant coordinate system (X, Y). As shown in Figure 30, the following applies to the new system: $X = x + ct$ and $Y = y$. In the new coordinate system, the potential function, the velocities, and the local accelerations of the wave particles are defined as follows:

$$\Phi(X,Y,t) = (\vec{c} - \vec{u})X + C_0\left(\frac{g}{k^3}\right)^{\frac{1}{2}} \sum_{i=1}^{5} \varepsilon_i \sum_{j=1}^{i} A_{ij}\, cosh(jkY)\, sin(jk(X-ct)) \quad \textit{Equation 74}$$

$$U = \frac{\partial\varphi}{\partial x}, V = \frac{\partial\varphi}{\partial y},\ A_x = \frac{\partial U}{\partial t},\ A_y = \frac{\partial V}{\partial t} \quad \textit{Equation 75}$$

4.1.4. 18th order Fourier or Stream function solutions theory (18th order nonlinear solution)

Fourier theory refers to the development of the flow function in Fourier series and it is based on the theory developed by Dean (1965). It is a model for regular waves, which applies either to data of wave height H, wave period T and depth of wave field d, either to a given time series, $\eta(t)$. The flow is described using the flow function in two dimensions ψ (x, z), (*Equation 76*), which satisfies the Laplace equation (*Equation 77*). The model is valid to a wide range of depths, in respect of the Dean & Le Méhauté Chart Figure 24, while giving more accurate results in intermediate and shallow waters.

More specifically, in cases where the wave height is greater than 50% of the breaking height, the method of flow function gives more accurate results than linear theory.

$$u + U = \frac{\partial \psi}{\partial z}, w = \frac{\partial \psi}{\partial x} \quad \textit{Equation 76}$$

Where:

- U is the velocity of the current (if existing)

$$\nabla^2 \psi\,(x, z) = 0 \quad \textit{Equation 77}$$

The assumptions on which Fourier theory is based are the same as those on regular waves: the flow is two-dimensional, the depth is uniform, and the wave motion is periodic. The bottom and surface boundary conditions are then defined:

Kinematic bottom boundary condition – KBBC: The bottom layer is horizontal and impenetrable.

$$\frac{\partial \varphi}{\partial z} = -\frac{\partial \psi}{\partial x} = w = 0, \quad for\ z = -d \quad \textit{Equation 78}$$

Kinematic free surface boundary condition – KFSBC: Wave particles remain on the surface.

$$\frac{\partial \eta}{\partial t} + (u + U)\frac{\partial \eta}{\partial x} = w, \quad for\ z = \eta \quad \textit{Equation 79}$$

Dynamic free surface boundary condition -DFSBC: The pressure on the free surface is constant.

$$\frac{p(x)}{\rho g} + \frac{1}{2g}[(u + U)^2 + w^2] - \frac{1}{g}\frac{\partial \varphi}{\partial t} = 0, \quad for\ z = \eta \quad \textit{Equation 80}$$

$p\ (x)\ \rho g$ + 12g [(u + U) 2 + w2] + η – 1$g\partial\varphi\partial t$ = 0, $\sigma\tau o\ z = \eta$ *Equation 81*

where:

- $p\ (x)$, is the atmospheric pressure (constant)

If the wave propagates with velocity c, without changing its shape and its characteristics, the horizontal component of velocity is defined as $u + U - c$, while the vertical component remains unaffected. Therefore, the surface boundary conditions (*Equation 79* and *Equation 80*) are simplified in *Equation 81* and *Equation 82*, respectively.

$$\frac{\partial \eta}{\partial x} = \frac{w}{u+U-c} \quad \textit{Equation 82}$$

$$\frac{p(x)}{\rho g} + \frac{1}{2g}[(u+U)^2 + w^2] + \eta = constant = Q \quad \textit{Equation 83}$$

In reference system, moving with velocity, c, the flow function can be approximated as follows:

$$\psi(x,z) = \left(\frac{L}{T} - U\right) z + \sum_{n=4,6,8}^{N-1} sinh(n-2)\frac{n}{L}(d+z)\left(X(n)\,cos(n-2)\frac{\pi}{L}x + X(n+1)\,sin(n-2)\frac{\pi}{L}x\right) \quad \textit{Equation 84}$$

where:

- N: the class of theory, in this case $N = 18$
- X_n: coefficients, the values of which are determined by the method of least squares adapted to the boundary conditions of the free surface
- L: the wavelength
- T: the wave period

By introducing the flow function (*Equation 84*) in the dynamic surface condition (*Equation 83*), the elevation profile of the free surface is obtained:

$$\eta = \frac{\psi(x,z)}{(\frac{L}{T}-U)} - \frac{1}{(\frac{L}{T}-U)} \sum_{n=4,6,8}^{N-1} sinh(n-2)\frac{n}{L}(d+z)\left(X(n)\,cos(n-2)\frac{\pi}{L}x + X(n+1)\,sin(n-2)\frac{\pi}{L}x\right) \quad \textit{Equation 85}$$

where:

- $X_n\psi$ $(x, z = \eta)$: the value of the flow function on the free surface, which is constant, as the free surface is a flow line

In fact, the elevation components in Fourier theory do not apply to Airy and Stokes theories. More specifically, the first order term according to Fourier does not correspond to that of the Airy theory, the second does not correspond to that of the 2nd order Stokes theory and so on. This is because the Fourier model develops the sequence in terms of flow function and not potential function.

The velocities in the two directions, u in the horizontal direction and w in the vertical direction, are obtained according to *Equation 76*. The local accelerations are calculated $a_x = \frac{\partial u}{\partial \mathrm{t}}$ and $a_z = \frac{\partial w}{\partial \mathrm{t}}$. It is noted that the model allows the introduction of the reduction coefficient Φ for directional waves in the final values of the kinematic quantities.

4.2. RANDOM WAVES

Wave models that consider random waves of the real sea state are included in the category of random wave theories. Random waves, also known as irregular, unsteady or spectral waves, are described in three dimensions and therefore the directionality is considered. In this wave models the shape of each wave varies with time, while the characteristics of the wave remain unchanged. Random waves are approximated by estimating the energy scattering in the frequency domain using an appropriate frequency spectrum.

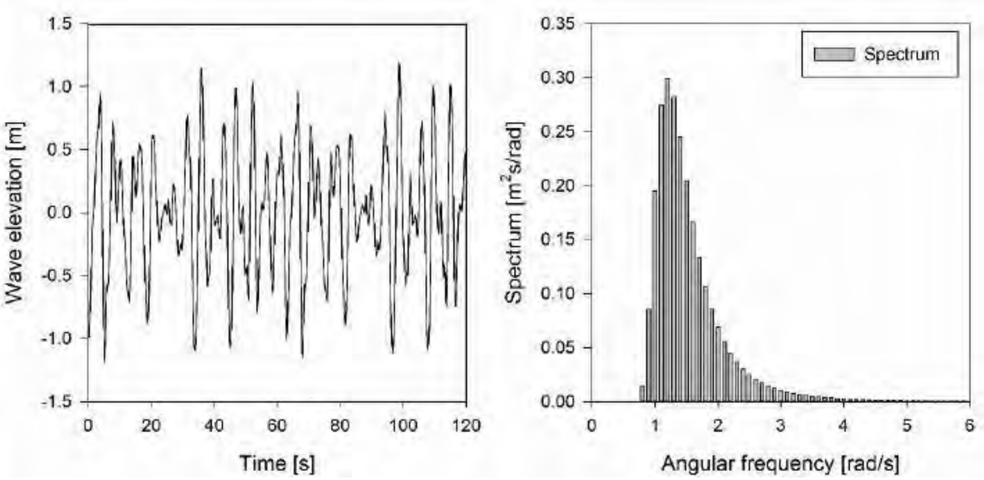

Figure 31: Random waves spectrum [38]

Specifically, the waves are described by a range of frequency values, each of which corresponds to a different wavelength Figure 31. The narrower the time history of the wave (small amplitude range), the narrower the frequency range (shorter range) [9]. If the amplitude value range is too small, then the wave tends to be described by a regular wave model. As a result of the irregularity of the waves, the shape of each wave varies with time, while the characteristics of the wave remain unchanged.

For fully developed seas, Pierson-Moskowitz spectrum is used, while JONSWAP spectrum describes fetch-limited seas. JONSWAP spectrum is the most used spectrum in the North Sea, where the Torsethaugen spectrum is also used. Torsethaugen is a double peaked spectrum which refers to sea environmental conditions including swells created in distance and local wind-generated waves. In the present study, JONSWAP spectrum was applied as most suitable for the present environmental conditions.

The spectral models applied in the present study are the following:

1. Linear Random Wave Theory (linear solution)
2. 2^{nd} order or Sharma & Dean random wave theory (2nd order non-linear solution)

4.2.1. Linear random wave theory - LRWT

In order to include the irregularity of the waves into the mathematical calculations, LRWT theory assumes a random state of the sea, which is described by a large number of linear, free waves or, otherwise, wave components. The free surface elevation and the wave particle kinematics are calculated as the linear sum of the contribution of every directional component (frequency component). The LRWT gives a satisfactory description of the irregularity that governs the real sea, as it considers the fluctuation of the free surface in the frequency domain. Describing the wave field by the assumption of the linearity, the theory gives simple equations that facilitate the mathematical calculation, in contrast to the nonlinear theories.

For the mathematical description of the free surface elevation, LRWT considers a random state of the sea, consisting of N >> 1 free wave components of different frequencies, phases, and amplitudes. The wave components propagate in the positive direction of the axis x, which is perpendicular to the axis y, measured from the still water level in a positive upward direction. Within LRWT, the potential function and the free surface profile are obtained from the linear sum of the individual waves giving:

$$\Phi(x, y, z, t) = \sum_{i=1}^{N} b_i \frac{cosh(k_i(z+d))}{cosh(k_i d)} sin\left(\overrightarrow{k_\iota}\vec{x} - \omega_i t + \varepsilon_i\right) \quad \text{Equation 86}$$

$$\eta = \frac{1}{g} \sum_{i=1}^{N} b_i\, \omega_i\, cos\left(\overrightarrow{k_\iota}\vec{x} - \omega_i t + \varepsilon_i\right) \quad \text{Equation 87}$$

where:

- bi: coefficient of the amplitude, $bi = \frac{\mathrm{ai\omega i}}{\mathrm{g}}$
- ki: wave number vector, determined based on the direction of the waves θ_{i} as $(\mathrm{k_{ix}, k_{iy}}) = (|\ \mathrm{k_i}\ |\ cos\theta_{\mathrm{i}}, |\ \mathrm{k_i}\ |\ sin\theta_{\mathrm{i}})$
- i: the phase of each wave component

The relation that connects the respective frequency ω_{i} with the corresponding wave number $\overrightarrow{\mathrm{k_\iota}}$, is given through the linear dispersion relation equation:

$$\omega_i^2 = g|\vec{k_i}|\tanh(\vec{k_i}d), \quad 1 < i \leq N \qquad \text{Equation 88}$$

Then, from the potential function (*Equation 86*) the components of wave particle velocities and accelerations in the horizontal and vertical direction are derived.

However, the fact that the model neglects all the non-linear terms, as well as the existence of bound waves, introduces a significant error in the case of random waves. Specifically, when calculating the wave particle kinematics at the surface of water, the linear sum of the components results in the phenomenon known as high-frequency contamination. The phenomenon is due to the addition of high frequency components to those of lower frequency and leads to an overestimation of the maximum horizontal velocities and accelerations, ie those developed near the water surface. While linearly summing two components, one of which is low frequency and the other high frequency, it is not considered that the second wave is not integrated into the first but propagates on it. However, the real sea is characterized by strong non-linearity and, so, the interaction of the two waves would be different. The long-crested wave (low frequency) would remain unaffected, while the short-crested wave (high frequency) would be shaped to occur:

- taller and at the same time shorter at the peaks of the long-crested wave and
- shallower and at the same time longer at the troughs of the long-crested wave

Various empirical methods have been proposed to deal with the phenomenon of overestimation of maximum velocities. The first method has been presented by Wheeler (1969), known as Wheeler stretching, and it is an empirical correction of the phenomenon. In fact, according to Wheeler's empirical relation [42], to correct the overestimated maximum velocities and accelerations, a stretching factor is introduced into the vertical wave coordinates. Specifically, the velocity equations use the variable depth z^* instead of the original z, which is calculated from the relation:

$$z^* = \frac{z-\eta(t)}{1+\frac{\eta(t)}{d}} \qquad \text{Equation 89}$$

As the Wheeler's method is empirical, it does not satisfy the mass continuity equation. However, the results of the method deal the phenomenon of high-frequency contamination, giving reduced kinematic quantities close to the surface, compared to the overestimated values resulting from a simple application of LRWT. Therefore, although fundamentally wrong, the method satisfactorily approaches values correction.

4.2.2. Second order random wave theory – Sharma & Dean

In 1960, Longuet-Higgins and Stewart [43], assuming a linear representation of the wave field, they proposed the solution of interaction between two linear wave components by recognizing the terms of frequency-sum and frequency- difference. Based on these results, Sharma and Dean (1981) [44] summed the resulted interactions from each possible pair of free linear wave components in a random state of the sea, resulting in a nonlinear 2^{nd} order solution. Their model, known as the Second Order Wave Random Theory (SD) model, provides a first approach to the effect of nonlinearity and can be combined with the NewWave model to accurately describe the shape of the most probable "large" waves. The free surface elevation corresponds to a focused wave group, otherwise, a second order NewWave.

NewWave theory represents a state of the sea, consisting of many wave components with different frequency, phase, and amplitude. The most probable shape of a "large" wave occurs when the phase difference between the waves becomes zero and the wave amplitudes become proportional to the underlying spectrum. The solution is then normalized to achieve the desired wave height (H_{max}) or peak elevation (η_{max}), corresponding to a specific probability of exceedance. Regarding NewWave linear theory, the process mentioned above is simple. On the contrary, for non-linear NewWave theories it is necessary to apply an iterative procedure to achieve the desired wave height or peak elevation.

Sharma and Dean's 2nd order model gives a more realistic description of the shape of the most probable large wave than linear theory. However, achieving this accuracy with respect to the introduction of directionality requires a large number of components, making the method particularly time consuming. For this reason, the model is not applied often enough.

Regarding the accuracy of 2nd order random wave solutions, a study by Katsardi and Swan (2005) [5] showed that for waves with high wave steepness the application of the model close to the free surface is likely to produce erroneous velocity calculations. The problem lies in the difficulty of describing the distribution of the velocities, due to the last part of the spectrum (spectrum queue). In contrast to the linear theory, in which empirical velocity correction is used to deal with the phenomenon, regarding the 2nd order model a cut of the energy spectrum is applied to a multiple of the spectral peak. The cut-off point of the spectrum is usually defined between $3\omega_p$ and $3.5\omega_p$, where ω_p is the peak frequency of the spectrum. The cut-off rate should be considered with great care, as the results depend directly on it.

According to Sharma and Dean's model, it applies that the fluid is incompressible, and the flow irrotational. Therefore, the mass continuity equation for incompressible fluid $div\vec{U} = 0$ holds, where $\vec{U} = (u, v, w)$ the velocity in the three directions as well as the Laplace equation $\nabla^2\varphi = 0$ in terms of potential flow. The boundary conditions considered are based on the perturbation theory, with the potential, the free surface elevation and Bernoulli's coefficient, being developed into forces of wave steepness, e, as follows:

$$\varphi(x, y, z, t) = \varphi^{(1)}(x, y, z, t) + \varphi^{(2)}(x, y, z, t) \quad \text{Equation 90}$$

$$\eta(x, y, z, t) = \eta^{(1)}(x, y, z, t) + \eta^{(2)}(x, y, z, t) \quad \text{Equation 91}$$

$$Q(t) = Q^{(1)}(t) + Q^{(2)}(t) \quad \text{Equation 92}$$

where:

- the exponent 1 corresponds to the linear term and

- the exponent 2 corresponds to the term 2nd class

Kinematic bottom boundary condition – KBBC

$$\frac{\partial \varphi^{(1)}}{\partial z} = 0 \; for \; z = -d \quad \text{Equation 93}$$

$$\frac{\partial \varphi^{(2)}}{\partial z} = 0 \; for \; z = -d \quad \text{Equation 94}$$

Kinematic free surface boundaty condition – KFSBC

$$\frac{\partial^2 \varphi^{(1)}}{\partial t^2} + g\frac{\partial \varphi^{(1)}}{\partial z} - \frac{\partial Q^{(1)}}{\partial t} = 0, \;\; for \; z = 0 \quad \text{Equation 95}$$

$$\frac{\partial^2 \varphi^{(2)}}{\partial t^2} + g\frac{\partial \varphi^{(2)}}{\partial z} - \frac{\partial Q^{(2)}}{\partial t} = \eta^{(1)}\frac{\partial}{\partial z}\left(\frac{\partial^2 \varphi^{(1)}}{\partial t^2} + g\frac{\partial \varphi^{(1)}}{\partial z}\right) - \frac{\partial}{\partial t}\left(\left|\vec{\nabla}\varphi^{(1)}\right|^2\right), \;\; for \; z = 0 \quad \text{Equation 96}$$

Dynamic free surface boundary condition -DFSBC

$$\eta^{(1)} = -\frac{1}{g}\left[\frac{\partial \varphi^{(1)}}{\partial t} - Q(t)\right], \;\; for \; z = 0 \quad \text{Equation 97}$$

$$\eta^{(2)} = -\frac{1}{g}\left[\frac{\partial \varphi^{(2)}}{\partial t} + \frac{1}{2}\left|\vec{\nabla}\varphi^{(1)}\right|^2 + Q^{(2)} + \eta^{(1)}\frac{\partial^2 \varphi^{(1)}}{\partial t \partial z}\right], \;\; for \; z = 0 \quad \text{Equation 98}$$

It is noted that, for small formulation parameters, the surface boundary conditions are applied at the still water level, as the surface equation is unknown.

The linear term of potential and free surface is derived from LRWT (*Equation 86* and *Equation 87*, respectively). The 2nd order terms refer to the sum terms and the difference terms, which appear in $2\omega_p$ and at the beginning of the spectrum, respectively. It is noted that the difference terms are out of phase and their contribution to the final profile of the elevation is particularly important in the case of intermediate and shallow water depths. According to Sharma and Dean the expression of the potential and the elevation of the 2nd order are defined as follows:

$$\varphi^{(2)}\,(x,y,z,t)=\frac{1}{4}\sum_{i=1}^{N}\sum_{j=1}^{N}b_i b_j\frac{cosh\left(k_{ij}{}^{-}(z+d)\right)}{cosh\left(k_{ij}{}^{-}d\right)}\frac{D_{ij}{}^{-}}{\sigma_i-\sigma_j}sin\left(\psi_i-\psi_j\right)+\frac{1}{4}\sum_{i=1}^{N}\sum_{j=1}^{N}b_i b_j\frac{cosh(k_{ij}{}^{+}(z+d))}{cosh(k_{ij}{}^{+}d)}\frac{D_{ij}{}^{+}}{\sigma_i+\sigma_j}sin\left(\psi_i+\psi_j\right)$$ *Equation 99*

where:

- $k_{ij}{}^{-} = |k_i - k_j|$

- $k_{ij}{}^{+} = |\, k_i + k_j|$

- $\psi_i = \overrightarrow{k_i}\vec{x} - \omega_i t + \varepsilon_i$

- b_i: coefficients of the wave amplitude, $bi = \frac{ai\omega i}{g}$

- $D_{ij}{}^{-}$, $D_{ij}{}^{+}$: coefficients according to Sharma & Dean

$$\eta^{(2)}\,(x,y,z,t)=\frac{1}{4}\sum_{i=1}^{N}\sum_{j=1}^{N}a_i a_j\left[\frac{D_{ij}{}^{-}-[\overrightarrow{k_i k_j}+(R_i R_j)]}{\sqrt{(R_i R_j)}}+(R_i+R_j)\right]\frac{cosh\left(k_{ij}{}^{-}(z+d)\right)}{cosh\left(k_{ij}{}^{-}d\right)}cos\left(\psi_i-\psi_j\right)+\frac{1}{4}\sum_{i=1}^{N}\sum_{j=1}^{N}a_i a_j\left[\frac{D_{ij}{}^{+}-[\overrightarrow{k_i k_j}-(R_i R_j)]}{\sqrt{(R_i R_j)}}+(R_i+R_j)\right]\frac{cos\,\left(k_{ij}{}^{-}(z+d)\right)}{cosh\left(k_{ij}{}^{-}d\right)}cos\left(\psi_i+\psi_j\right)$$

Equation 100

where:

- Ri, Rj: coefficients according to Sharma & Dean

The equations that give velocity (Equation 101) and local acceleration (Equation 102) consist of two terms: a linear term, derived from LWRT, and a 2nd order term.

$$u=\frac{\partial\varphi}{\partial x}, v=u\frac{\partial\varphi}{\partial y}, w=\frac{\partial\varphi}{\partial z}$$ *Equation 103*

$$a_x=\frac{\partial u}{\partial t}, a_y=u\frac{\partial v}{\partial t}, a_z=\frac{\partial w}{\partial t}$$ *Equation 104*

4.2.3 HOS (High-Order Spectral) theory

To achieve fully non-linear modelling solutions, the high-order spectral method HOS wave theory is developed. This fully non-linear method takes into account the propagation of the wave both at different frequencies and in different directions (Guillaume Ducrozet et al, 2015)[45].

Considering a quadratic fluid potential theory defined in Cartesian coordinates and making use of the continuity equation, the Laplace equation in terms of flow potential is obtained.

$$\vec{\nabla}\varphi + \frac{\partial^2\varphi}{\partial z} = 0 \quad \textit{Equation } 105$$

Defining the boundary conditions of the free surface after their description by the elevation (n) as well as the velocity potential $(\tilde{\varphi})$ of the corresponding surface gives the following relations:

$$\frac{\partial\eta}{\partial t} = (1 + |\nabla n|^2)w - \nabla\tilde{\varphi}\nabla n \quad \textit{Equation 106}$$

$$\frac{\partial\tilde{\varphi}}{\partial t} = -gn - \frac{1}{2}|\nabla\tilde{\varphi}|^2 + \frac{1}{2}(1 + |\nabla n|^2)w^2 \quad \textit{Equation 107}$$

Using the Fourier transform (FFTs) in conjunction with the Laplace equation assuming zero vertical velocity at the bottom, infinite field in width and calculating the vertical velocity w (West et al, 1987) over the free surface then the surface elements can be expressed as following.

$$n(x,t) = \sum_m B_m^n \, exp(i \cdot k_m \cdot x) \quad \textit{Equation 108}$$

$$\tilde{\varphi}(x,t) = \sum_m B_m^{\tilde{\varphi}} \, exp(i \cdot k_m \cdot x) \quad \textit{Equation 109}$$

Finally, having knowledge of the above data, the surface vertical velocity of the wave can be derived. Based on a serial expansion in the wave slope, ε, up to order M with ϕ(m), ε(m) quantities it is obtained.

$$\varphi(x,z,t) = \sum_{m=1}^{M} \varphi^{m}(x,z,t) \quad \textit{Equation 110}$$

5. FLOATING OFFSHORE STRUCTURE DESCRIPTION & SIMULATION

5.1 STRUCTURE DESCRITION: OC4-DEEPCWIND PLATFORM

This chapter presents the elements of the geometry of the floating part of the OC4 wind turbine platform with the aim of understanding the structure. In detail, the names and structure of the individual sections will be described and there the wave loading will be applied to study the floating platform's response. It is noted that the general position and geometry of the mooring system should be governed by basic principles based on the regulations described below. In order to understand the whole structure, the analysis of the distribution of the masses is also presented.

The floating offshore structure was selected for this study due to the numerous advantages it presents for the Greek seas and the geomorphology of Greece, as presented in the introduction. These advantages include the use of high-power wind turbines due to higher wind speed as the Aegean offers suitable sea conditions in the presence of strong winds without obstacles, easy transport, smaller environmental footprint, reduced visual and acoustic disturbance away from the shore, reduced cost of installation and maintenance, cost-effective solution in comparison with rigid structures due to the great depth and uneven geomorphology of the bottom of the Greek seas.

OC4 PLATFORM GEOMETRY: The OC4 semi-submersible floating platform geometry consists of four columns, which are submerged below sea water level (SWL). There are three offset columns each of which is divided into two separate columns, one of small and one of larger diameter at the bottom (named UC: upper columns [1,2,3] and BC: base columns [1,2,3] respectively), and the main column, named MC. The three offset columns of the structure extend to a height of 12 m above the sea water level, while the main one ta a height of 10 m. On the latter, MC column, rests the part of the wind turbine. The larger diameter columns at the base of the offset columns of the bottom part helps to suppress motion [47]. These columns are connected to each other with individual cross members and pontoons, creating a joined-up structure. The diameter of the offset columns is 12m in the upper part, but this changes to 24 m, when the column depth exceeds 14m below sea water level. For this reason, they are described by a different name compared to the rest of their part ("UC" corresponds to D=12m and "BC" corresponds to D=24m). The main column, however, maintains a constant diameter along its entire length equal to 6.5 m. The diameter of the pontoons and cross brasses is constant and equal to 1.6 m. The origin of the axes is initially defined as the center of the inner main column, where the x-axis also indicates the wave filed direction. The offset columns centers' distance of the is equal to 50m. Also, the angle formed successively by the external columns on the plane is equal to 60° where the point of intersection of the bisectors of the angles is also the center of the main column. The three offset columns (UC [1,2,3]) start above the SWL and continue under water[47].

The following figures -Figure 32, Figure 33- show the geometry and names of the parts of the OC4 platform. The illustration concerns the cross section and plan view of the floating part.

Figure 32: DeepCwind semisubmersible OC4 platform (as-built)[47].

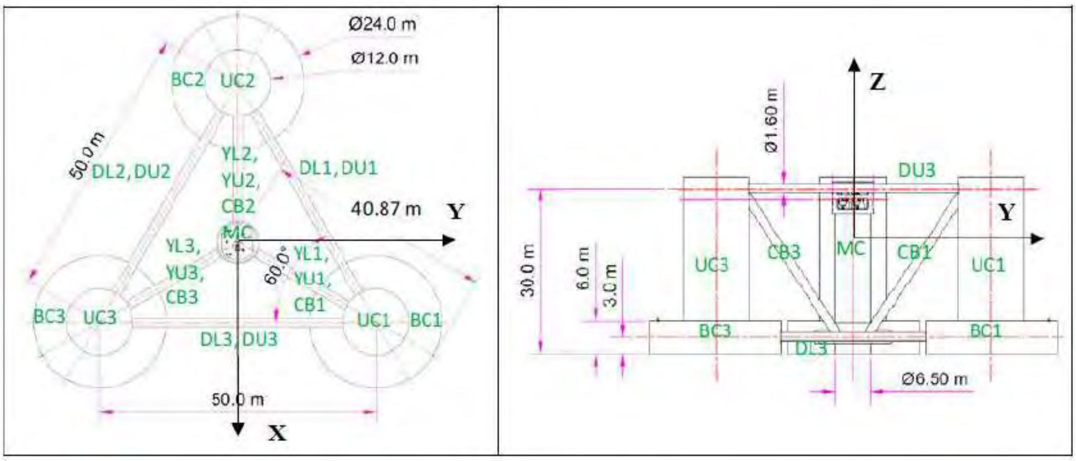

Figure 33: Plan and side view of the OC4 platform (left and right respectively) [47]

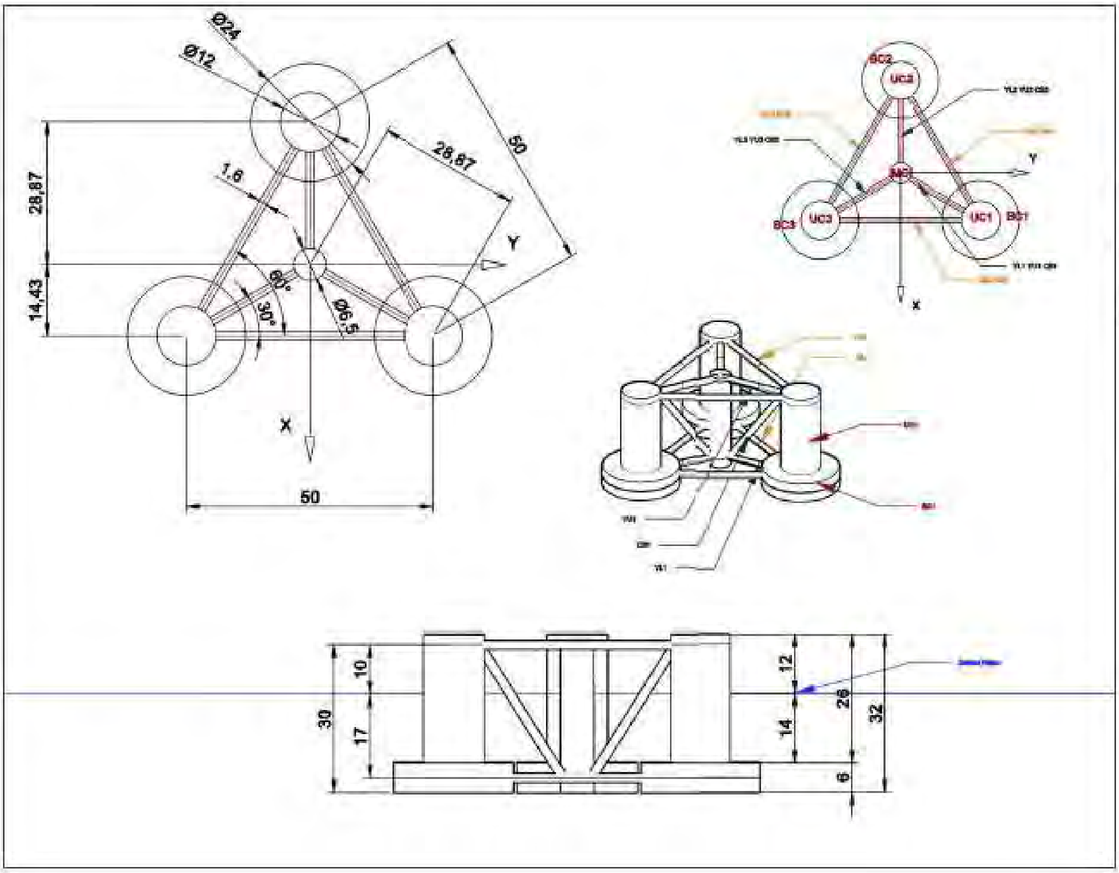

Figure 34: Geometric characteristics of the DeepCwind semisubmersible platform [25]

The connecting system of cross braces and pontoons includes the following parts:

- Six pontoons (grouped at two sets of three), which connect the offset columns shaping a triangle (or delta), at the top (DU) and bottom (DL) of the OC4 platform.
- Six pontoons (grouped at two sets of three), which the offset columns with the main column shaping a y-connection at the top (YU) and bottom (YL) of the OC4 platform.
- Three cross braces which fasten the bottom of the main column with the top of the offset columns [47].

The following tables show extensively the coordinates of the floating platform members [47], when the axis system is set at the center of the MC column and with the wave direction taken in the analyzed Figure 33 whereas zero point of the z-axis was assumed to be the sea water level.

Column Name	Abbr.	Start location (X,Y,Z)	End location (X,Y,Z)	Length (m)	Wall Thick. (m)
Main Column	MC	(0, 0,-20)	(0, 0,10)	30	0.03
Upper Column 1	UC1	(14.43, 25, -14)	(14.43, 25, 12)	26	0.06
Upper Column 2	UC2	(-28.87, 0, -14)	(-28.87, 0, 12)	26	0.06
Upper Column 3	UC3	(14.43, -25, -14)	(14.43, -25, 12)	26	0.06
Base Column 1	BC1	(14.43, 25, -20)	(14.43, 25, -14)	6	0.06
Base Column 2	BC2	(-28.87, 0, -20)	(-28.87, 0, -14)	6	0.06
Base Column 3	BC3	(14.43, -25, -20)	(14.43, -25, -14)	6	0.06
Delta Pontoon, Upper 1	DU1	(9.20, 22, 10)	(-23.67, 3, 10)	38	0.0175
Delta Pontoon, Upper 2	DU2	(-23.67, -3, 10)	(9.20, -22, 10)	38	0.0175
Delta Pontoon, Upper 3	DU3	(14.43, -19, 10)	(14.43, 19, 10)	38	0.0175
Delta Pontoon, Lower 1	DL1	(4, 19, -17)	(-18.47, 6, -17)	26	0.0175
Delta Pontoon, Lower 2	DL2	(-18.47, -6, -17)	(4, -19, -17)	26	0.0175
Delta Pontoon, Lower 3	DL3	(14.43, -13, -17)	(14.43, 13, -17)	26	0.0175

Y Pontoon, Upper 1	YU1	(1.625, 2.815, 10)	(11.43, 19.81, 10)	19.62	0.0175
Y Pontoon, Upper 2	YU2	(-3.25, 0, 10)	(-22.87, 0, 10)	19.62	0.0175
Y Pontoon, Upper 3	YU3	(1.625, -2.815, 10)	(11.43, -19.81, 10)	19.62	0.0175
Y Pontoon, Lower 1	YL1	(1.625, 2.815, -17)	(8.4, 14.6, -17)	13.62	0.0175
Y Pontoon, Lower 2	YL2	(-3.25, 0, -17)	(-16.87, 0, -17)	13.62	0.0175
Y Pontoon, Lower 3	YL3	(1.625, -2.815, -17)	(8.4, -14.6, -17)	13.62	0.0175
Cross Brace 1	CB1	(1.625, 2.815, -16.2)	(11.43, 19.81, 9.13)	32.04	0.0175
Cross Brace 2	CB2	(-3.25, 0, -16.2)	(-22.87, 0, 9.13)	32.04	0.0175
Cross Brace 3	CB3	(1.625, -2.815, -16.2)	(11.43, -19.81, 9.13)	32.04	0.0175
Upper Col. Top Cap	UCTC				0.06
Upper Col. Bottom Cap	UCBC				0.06
Base Col. Top Cap	BCTC				0.06
Base Col. Bottom Cap	BCBC				0.06
Main Col. bottom cap	MCBC				0.03

Figure 35: Member Geometry of the DeepCwind semisubmersible platform[47]

Depth of platform base below SWL (total draft)	20 m
Elevation of main column (tower base) above SWL	10 m
Elevation of offset columns above SWL	12 m
Spacing between offset columns	50 m
Length of upper columns	26 m
Length of base columns	6 m
Depth to top of base columns below SWL	14 m
Diameter of main column	6.5 m
Diameter of offset (upper) columns	12 m
Diameter of base columns	24 m
Diameter of pontoons and cross braces	1.6 m

Figure 36: Floating platform geometry[47]

FLEXIBILITY AND COORDINATE SYSTEM: Steel is the material used for al the parts of the structure and wall thickness is defined in Figure 33. Platform density is equal to 7850 kg/m^3. In their analysis of ANSYS model, Robertson et al., (2014) [47] increased the steel Young's modulus from the value 2.10E+2GPa to 2.10E+4GPa, which is a value two orders higher in order to approach realistic values of bending stiffness. Otherwise, this would be achieved by changing the size of the structure parts, but simultaneously with consistency to the DeepCwind geometric properties and weights. If the system is modeled as beams, the effective bending stiffness (EI) that should be achieved should approach the properties of members with wall thickness and Young's Modulus. The calculation of the properties of effective bending (EI), torsional (GJ) and extensional stiffness (EA) is based on the geometry of the cross section. This approach of a beam system modelling may not be suitable for the base columns of the platform, due to their low aspect ratio, according to Robertson et al., (2014) [47]. The Poisson's ration is considered equal to 0.33 and with this value shear modulus (G) was calculated. The value for the structural damping ratio of the platform is equal to 1%. It should be noted that the end caps are inside the cylinder [47].The coordinate system is the orthogonal x, y, and z of the inertial reference frame. The sea water level is considered as the plane XY while the z-axis points at the opposite of the gravity direction (upwards) along the centerline of the MC. The X axis is the nominal wind direction, and the Y axis is lateral to the left when looking downwind[47].

Member Name	Metal mass (*kg*)	Mass per unit length (*kg/m*)	*EI* (*N-m²*)	*GJ* (*N-m²*)	*EA* (*N*)
MC	1.436E+05	4.787E+03	6.701E+13	5.038E+13	1.281E+13
UC	4.594E+05	1.767E+04	8.423E+14	6.333E+14	4.726E+13
BC	2.125E+05	3.542E+04	6.789E+15	5.105E+15	9.476E+13
DU	2.599E+04	6.830E+02	5.720E+11	4.301E+11	1.827E+12
DL	1.778E+04	6.830E+02	5.720E+11	4.301E+11	1.827E+12
YU	1.329E+04	6.830E+02	5.720E+11	4.301E+11	1.827E+12
YL	9.164E+03	6.830E+02	5.720E+11	4.301E+11	1.827E+12
CB	2.142E+04	6.830E+02	5.720E+11	4.301E+11	1.827E+12
UCTC	5.221E+04	--	--	--	--
UCBC	5.327E+04	--	--	--	--
BCTC	1.577E+05	--	--	--	--
BCBC	2.109E+05	--	--	--	--
MCBC	7.671E+03	--	--	--	--

Figure 37: Flexible properties of the platform [16]

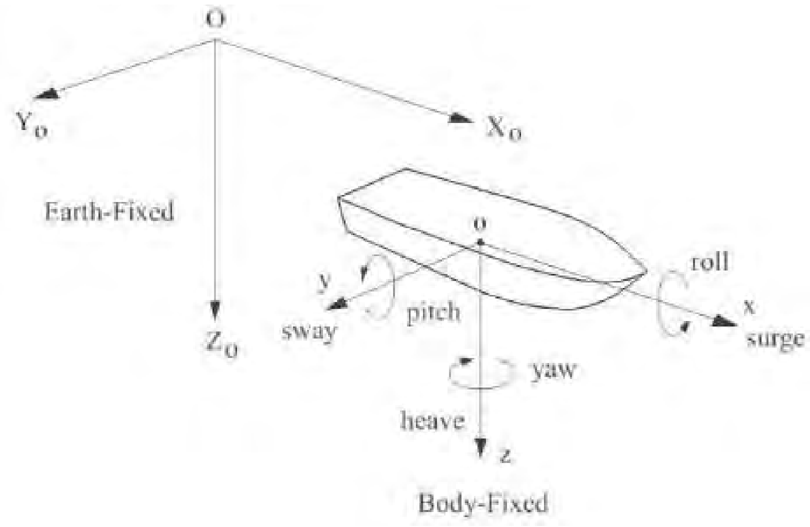

Figure 38: Ship motions and reference frames [47]

While examining a rigid-body platform, there are 6 degrees of freedom (DOFs). These are the following: translational surge, sway, and heave motions and rotational roll, pitch, and yaw motions [47]. X-axis defines the surge and positive surge corresponds to positive x-axis. The sway is the movement around the y-axis, and heave is along the z-axis. Respectively, positive roll refers to the positive x-axis, pitch is about the Y-axis, and yaw is approximately the Z axis [47].

OC4 MOORING SYSTEM AND ULS DESIGN: Open sea waves thrust on the floating structure causing the floating part to move according to the prevailing wave conditions. Therefore, it is necessary to include a system which will restore the state of equilibrium. This safety factor is provided by the platform mooring system, which is a cable system with a weight and geometry such that the construction is safe in the ultimate limit state of failure (Ultimate Limit State-ULS) [25]. Through the Ultimate Limit State of failure, the resistance of each individual cable under the influence of extreme sea conditions is ensured. Specifically, regarding the OC4 platform, the cable and floating part mooring point occurs 14 m below sea water level. The structure consists of three cables that reach the bottom at a depth of 50 m from the structure centerline. These cables develop an angle of 120° successively. In this paper a depth of

50m below sea water level was chosen for the mooring system, so that it corresponds to specific Aegean positions depths. Regarding the basic geometry of the location of the mooring system, the remote ends of the cables at the points anchored to the bottom inscribe a circle of radius 837.6m considering the center of the MC column as the center. Finally, the net length of the cable is given as 835.5 m.

In the present analysis, the mooring system is the main object of study with the platform concentrating the mass at one point and from there connecting the cables. As will be described in the next chapter, the effect of waves incident on the platform must first be studied on this large-scale mooring system, as its movement is the one that primarily affects the stability of the platform's floating system.

Number of Mooring Lines	3
Angle Between Adjacent Lines	120°
Depth to Anchors Below SWL	200 m
Depth to Fairleads Below SWL	14 m
Radius to Anchors from Platform Centerline	837.6 m
Radius to Fairleads from Platform Centerline	40.868 m
Unstretched Mooring Line Length	835.5 m
Mooring Line Diameter	0.0766 m
Equivalent Mooring Line Mass Density	113.35 kg/m
Equivalent Mooring Line Mass in Water	108.63 kg/m
Equivalent Mooring Line Extensional Stiffness	753.6 MN
Hydrodynamic Drag Coefficient for Mooring Lines	1.1
Hydrodynamic Added-Mass Coefficient for Mooring Lines	1.0
Seabed Drag Coefficient For Mooring Lines	1.0
Structural Damping of Mooring Lines	2.0%

Figure 39: Mooring System Properties [25]

ULS REGULATIONS: According to the ultimate limit state (ULS) design criteria, the structure should provide efficiency in terms of both generation and transmission of the generated energy. This means that the movement of the structure should be limited to a specific range. Also, the mooring cables must not exceed their breaking point and resist all possible loading conditions. It is noted that during the life of the project the length of the cable located on the bottom should not be violated in terms of its total elevation, as such a condition is likely to cause vertical forces at its anchor point with the bottom, capable of causing failure of the structure. Lastly, the length of the cable rising from the bottom to the floating part must have pre-tension and not be “loose” as otherwise its failure is possible [49].

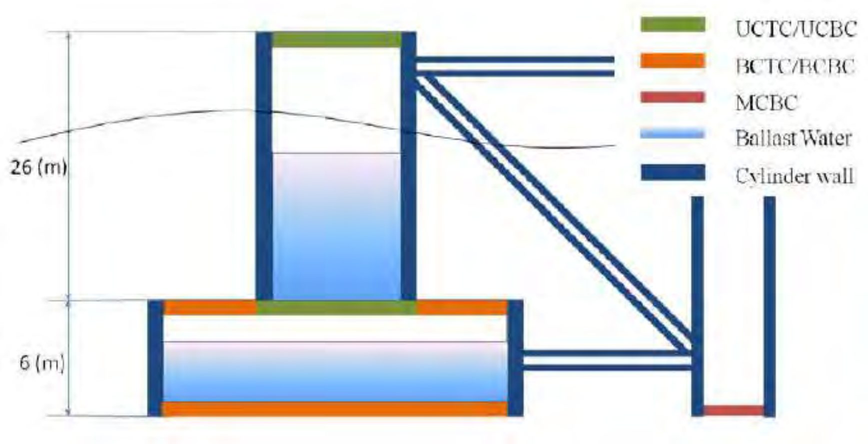

Figure 40: Side view of platform walls and caps[47].

MASS DISTRIBUTION OF THE STRUCTURE: The structure consists of three main parts: the mooring system, the floating part where the wave loads are applied, and finally the wind turbine placed on the platform for energy production. The largest part of the mass of the structure accounts for the floating part which refers to the mass of the metal part as well as the mass of water with a density of 1025 kg/m3 which is placed inside the columns UC and BC columns. The mass of water in each column UC and BC is not in motion but is presented as constant during the movement of the platform filling the columns UC to a height of 7.8m above its base and the BC respectively to a height of 5.1m. The total mass of the water on the platform is equal to 9.6208E+6 kg and the total mass of the metal corresponds to 3.8522E+6kg [25].

Platform mass, including ballast	1.3473E+7 kg
CM location below SWL	13.46 m
Platform roll inertia about CM	6.827E+9 kg-m^2
Platform pitch inertia about CM	6.827E+9 kg-m^2
Platform yaw inertia about CM	1.226E+10 kg-m^2

Figure 41: Floating platform structural properties [47]

PLATFORM OC4 WIND TURBINE: The wind turbine that will be placed on top of the MC column is the NREL 5 MW. The tower that is located on the main column of the platform has distributed properties which are founded on the base of diameter equal to that of the main column, d=6.5m. The Young's modulus is equal to 210 GPa, the shear modulus 80.8 GPa, while the effective density of the steel is considered 8,500 kg/m3. The common value of density would be equal to 7,850 kg/m3, but an increase was decided for the calculations as other properties as bolts, flanges, welds, and paint, where ignored in the considered thickness, so by this increase the right properties can be approached. bolts, welds, and flanges that are not included in the tower thickness data. This increase concerns the tower of the platform and its properties, and not the rest of the structure. The total calculated tower mass is 249,718 kg and is centered at 43.4 m along the tower centerline above the SWL, as the overall tower length is known and measured 77.6 m. Another property that needs to be considered for the tower is the structural-damping ratio, equal to1% for all modes of the isolated tower. In the present study, the force of the weight of the tower exerted on the floating platform was simulated as a gravity load.

Elevation to Tower Base (Platform Top) Above SWL	10 m
Elevation to Tower Top (Yaw Bearing) Above SWL	87.6 m
Overall (Integrated) Tower Mass	249,718 kg
CM Location of Tower Above SWL Along Tower Centerline	43.4 m
Tower Structural-Damping Ratio (All Modes)	1%

Elev (m)	HtFr (-)	TMassDen (kg/m)	TwFAStif (N-m^2)	TwSSStif (N-m^2)	TwGJStif (N-m^2)	TWEAStif (N)	TwFAIner (kg-m)	TwSSIner (kg-m)
10.0	0.0	4667.00	603.903E+9	603.903E+9	464.718E+9	115.302E+9	24443.7	24443.7
17.76	0.1	4345.48	517.644E+9	517.644E+9	398.339E+9	107.354E+9	20952.2	20952.2
25.52	0.2	4034.76	440.925E+9	440.925E+9	339.303E+9	99.682E+9	17847.0	17847.0
33.28	0.3	3735.44	373.022E+9	373.022E+9	287.049E+9	92.287E+9	15098.5	15098.5
41.04	0.4	3447.32	313.236E+9	313.236E+9	241.043E+9	85.169E+9	12678.6	12678.6
48.80	0.5	3170.40	260.897E+9	260.897E+9	200.767E+9	78.328E+9	10560.1	10560.1
56.56	0.6	2904.69	245.365E+9	245.365E+9	165.729E+9	71.763E+9	8717.2	8717.2
64.32	0.7	2650.18	176.028E+9	176.028E+9	135.458E+9	65.475E+9	7124.9	7124.9
72.08	0.8	2406.88	142.301E+9	142.301E+9	109.504E+9	59.464E+9	5759.8	5759.8
79.84	0.9	2174.77	113.630E+9	113.630E+9	87.441E+9	53.730E+9	4599.3	4599.3
87.60	1.0	1953.87	89.488E+9	89.488E+9	68.863E+9	48.272E+9	3622.1	3622.1

Elev = Elevation
HtFr = Height Fraction
TMassDen = Tower Mass Density
TwFAStif = Tower Fore/Aft Stiffness
TwSSStif = Tower Side/Side Stiffness
TwGJStif = Tower GJ Stiffness
TWEAStif = Tower EA Stiffness
TwFAIner = Tower Fore/Aft Inertia
TwSSIner = Tower Side/Side Inertia

Figure 42: Tower Properties [47]

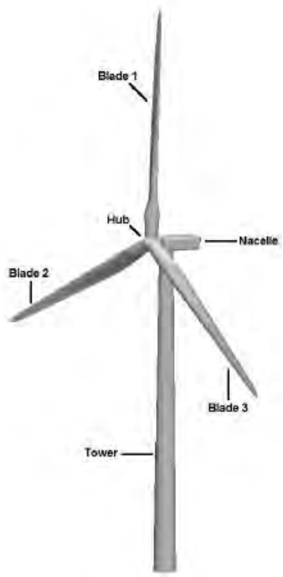

Figure 43: Indicative position of the members of the wind turbine carrier [50]

5.2 FEM analysis, MSC Marc & simulation parameters

5.2.1 Finite Element Analysis

The Finite Element Method is a numerical method using calculations to approximate solutions resulting from the solution of partial differential equations. Finding approximate solutions becomes necessary as deriving an analytical solution from the equations that describe the physical and technical phenomena is rarely possible. This can only be achieved in very simple geometries and small loads, which is not representative of the more complex reality.

The approximate solutions resulting from this method are reliable results and can be applied to all kinds of problems, making the method particularly effective and versatile. It requires enormous computing power to solve complex computational problems, and consequently this droves the development of the computing tools observed nowadays. The finite element method is an evolution of the matrix methods of numerical solution of differential equations and had been approached by various great scientists such as Ioannis Argyris, Ray Clough, Walter Ridge, Boris Galerkin and others.

Finite Element Analysis Steps:

- First, the geometry of the construction or material is entered into a CAD design program and the 3D model is created.
- The structure is then divided into small individual elements, the finite elements, forming a mesh.
- Then, the various parameters of the problem are introduced (material properties, cross-sections, boundary conditions, loads, etc.). This process is done with programs called pre-processors.
- When the above data has been selected, they are entered into a program which will carry out the solution of the problem. Such programs are called solvers and use numerical methods to approach the solutions.

- When solving is done, a program, called a post processor, must be used to enable the researcher to view the results.

5.2.2 MSC Marc Mentat

The history of the software begins in 1963, when Richard MacNeal and Bob Schwendler founded the MacNeal-Schwendler Corporation (MSC) [51]. Marc was the first commercial general purpose nonlinear finite element software being developed by the scientists Pedro V. Marcal and David Hibbitt [51]. Today Marc Mentat is distributed by the MSC Software Corporation. Mentat is the exclusive pre- and post-processor used to support Marc. Marc can solve problems across many industries from oil, gas industry and construction, to electromechanical and biomedical industry.

The program used to simulate the floating construction system in this paper *is MSC Marc*. It is a non-linear finite element analysis software that can be used for a multitude of applications with extreme complexity in terms of material properties and the magnitude of deformations and strains. Simulations can be about natural phenomena with their thermal, piezoelectric, electrostatic, magnetostatic, and electromagnetic behaviors combined with structural elements. For this purpose, it uses automatic two-dimensional and three-dimensional remeshing.

The interaction of the members of the structures with each other and with other materials of different properties is complex and characterized by non-linearity, just as in the specific subject the interaction of fluid (sea waves) and offshore construction. The nonlinearities affect the geometry, materials, and boundary conditions. Marc performs finite element analysis calculations for structures taking into account all these nonlinearities, in one, two and three dimensions, so it was the appropriate choice for this task.

5.3. Floating offshore structure simulation using MSC Marc software.

The subject of this study is the wave impact on the balance of the floating platform mooring system, where the wind turbine tower will be located. The wave load action mainly concerns the mooring system of the structure, consisting of three steel mooring lines, which connect the floating part to the seabed. The effect of the external forces on the structure, displacing the floating part and the mooring system, is what restores the whole system to its original state. For this reason, the simulation concerns this basic part of the mooring lines.

Below is presented the schematic illustration of the floor plan and the 3d model of the system in Marc software as well as the illustration with the geometrical sizes as given by the Robertson et al. (2014) [47].

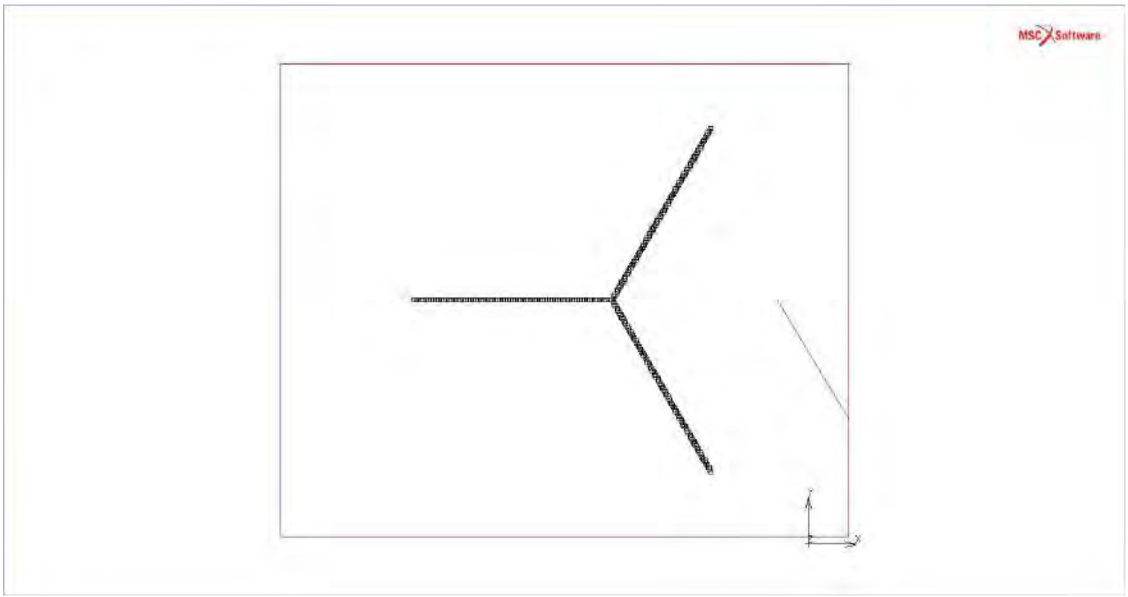

Figure 44: Initial MARC schematic illustration of platform mooring system.

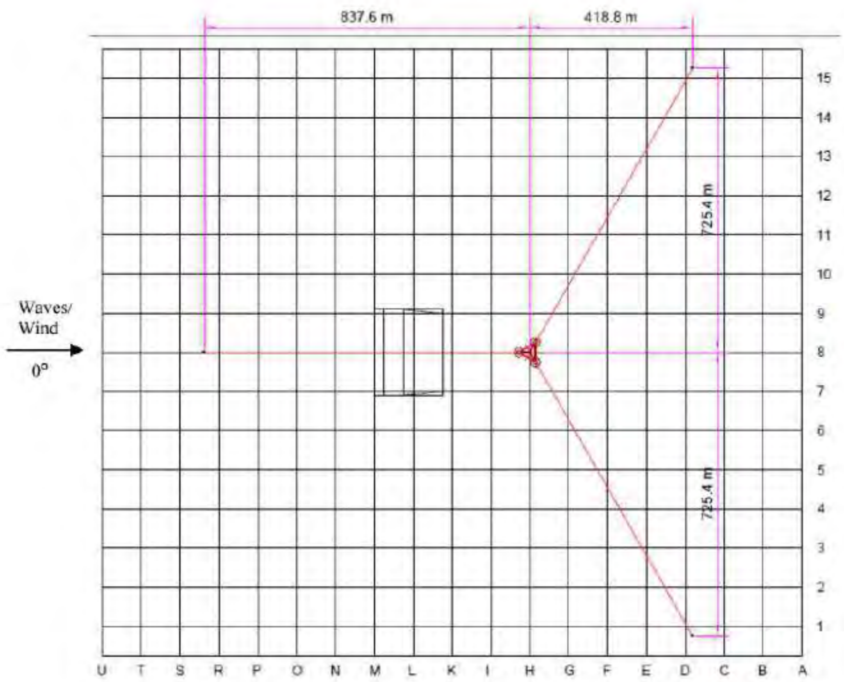

Figure 5-1: Mooring line arrangement

Figure 45: Mooring line arrangement [47]

In detail, from a construction point of view, the floating platform and the cables are connected at a depth of 50m below the SWL (still water level) developing an angle of 120° between them successively. Center is considered the center of column MC. The net length of the unstretched cables is 835.5m and their diameter is 0.0766m.

For the simulation of the system using Marc Mentat, a simplified modeling of a point was carried out which represents the floating part of total mass 1.3473E+07 kg and at which point the three cables are connected with their properties (Figure 44: Initial MARC schematic illustration of platform mooring). The central point therefore receives the following forces:

- the weight of the floating structure plus the weight of the tower plus the water inside the columns of the platform

- *z displacement z=50, which applies to the central node and transfers the platform from the seabed(z=-50m) to free surface(z=0m).*
- the self-weight of the cables anchored to the bottom,
- the timeseries of the force due to wave loading
- a large force at the last node of each mooring line representing the anchoring.

The structure is modeled in Marc Mentat with the following procedure.

CAD and MESH generation discretization: First, the platform node (node A) is created, to MSC MARC software, to which point the 3 steel cables mooring system are connected as *truss elements* (9, 64). Node A constitutes the modeling of the platform. Mooring lines are then divided into regular finite elements with the help of the mesh created through the "*subdivide*" command. In continuation of these steps, the surface of the seabed was created, as a square plane at the level of XY axis where the structure is located, but of much larger dimensions than it *(command Geometry and Mesh tab →Geometry →Surfaces*).

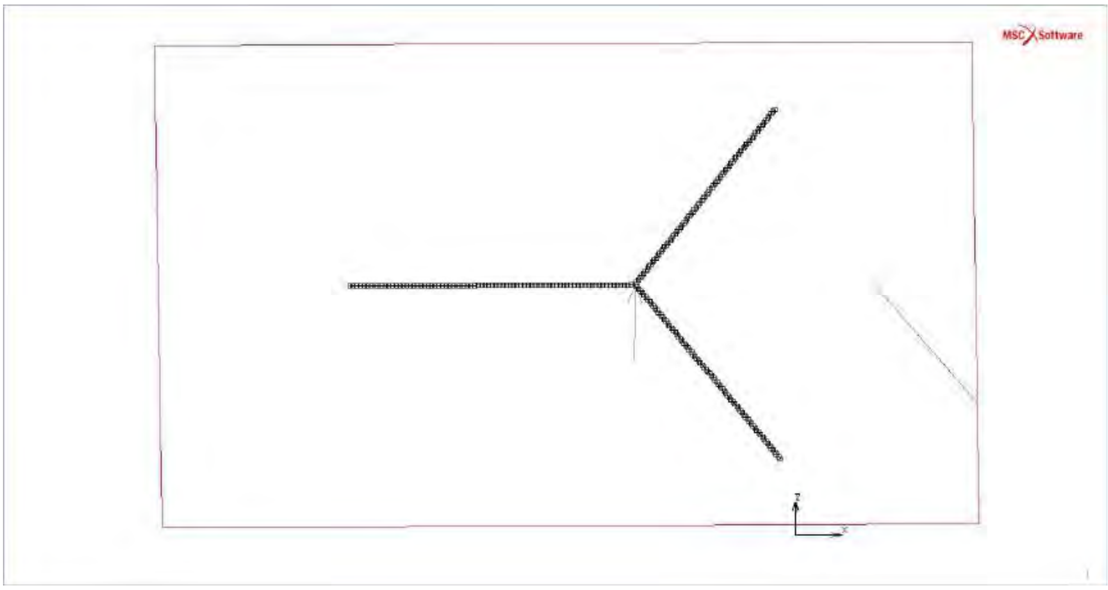

Figure 46: Cad and mesh generation of the model.

Material properties: The chains material is steel and it is introduced to the model as shown in the figure below *(Material Properties → New → Finite Stiffness Region → Standard*).

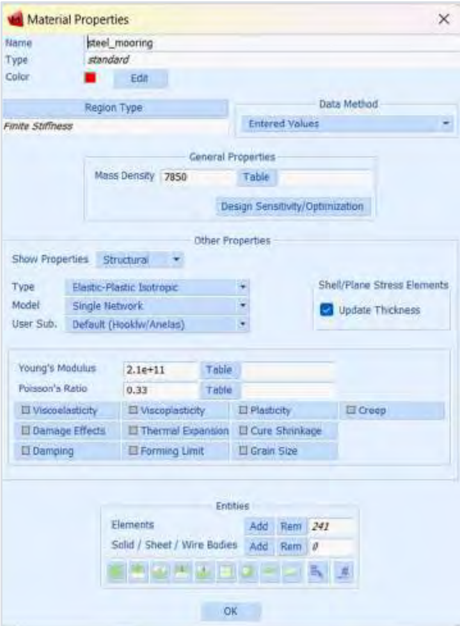

Figure 47: Material Properties

Contact bodies: Then, three contact bodies of the meshed deformable category were defined, one for each mooring line, and one contact body of the geometric category, representing the seabed, as presented in the following figure.

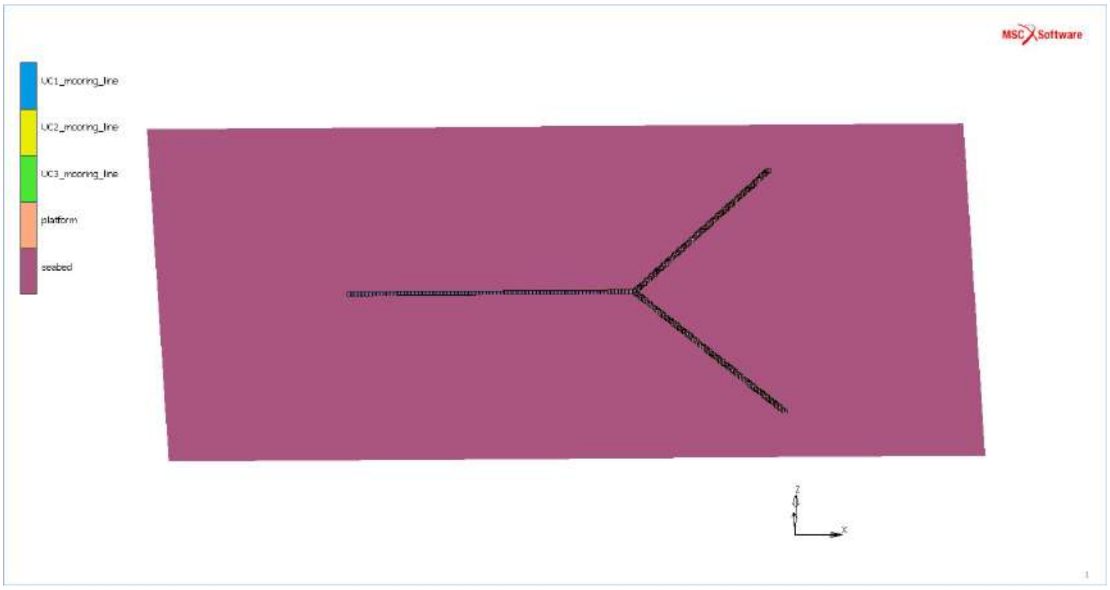

Figure 48: Material Properties

***Contact table*:** The interaction of the aforementioned contact bodies is described in the contact table, glued or touching. In this step, we define a friction coefficient between seabed and chains μ=0.9, in the interaction Meshed deformable vs. Geometric.

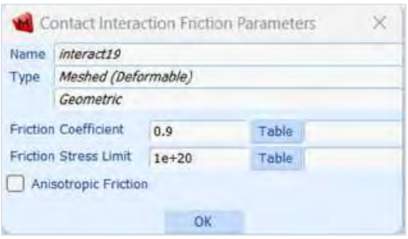

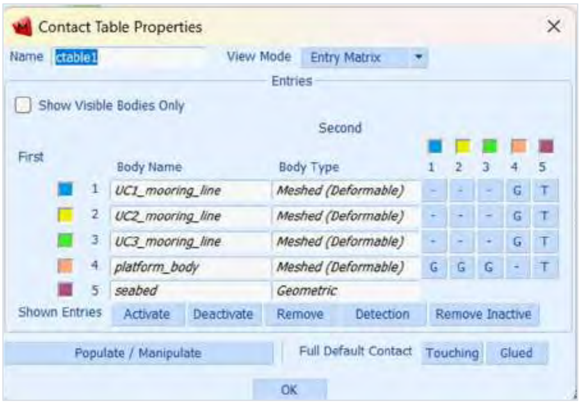

Figure 49: Contact Table

Timetables: As far as the timetables are concerned, to begin with, the whole system is in the xy plane.

- Initially a displacement z=50 is given to the central node to rise the system to the surface (seabed depth 50m) (*t=0 - 2, timetable time_disp2*).
- Once the node reaches the free surface, a large order of magnitude vertical force is applied to the ends of the chains, which represents the force of the anchor (*t=2.1 - end, timetable anchor*).
- Finally, at this point the wave loadings of various theories are applied (*t=4 - end, timetable wave_load).*

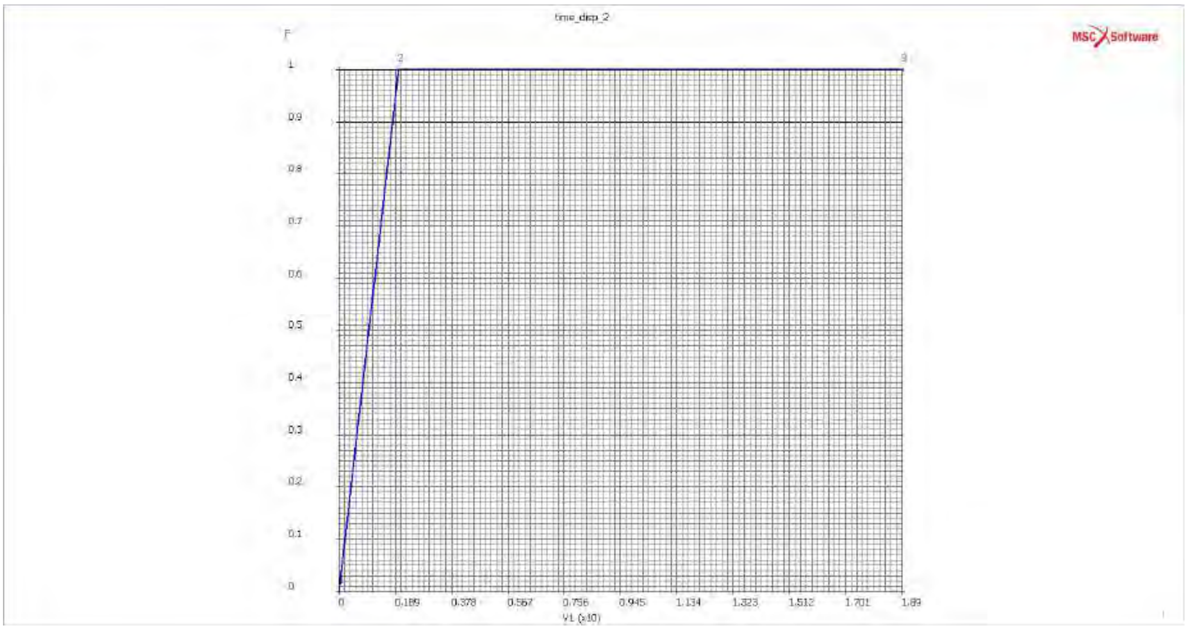
time_disp_2
F
MSC Software
V1 (x10)

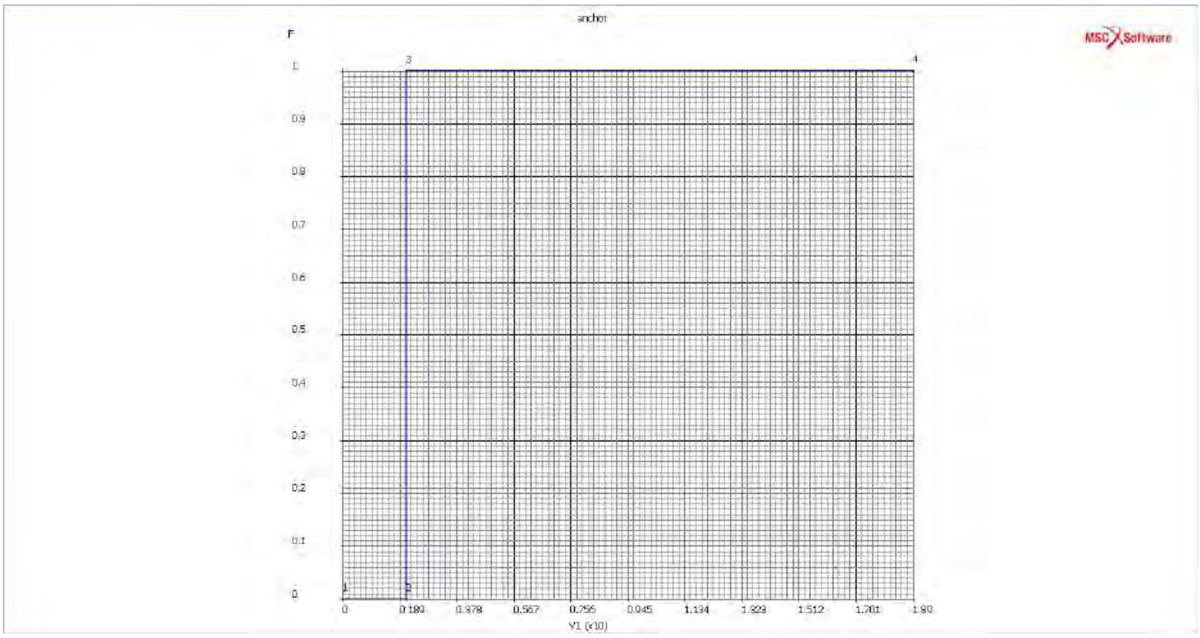
anchor
F
MSC Software
V1 (x10)

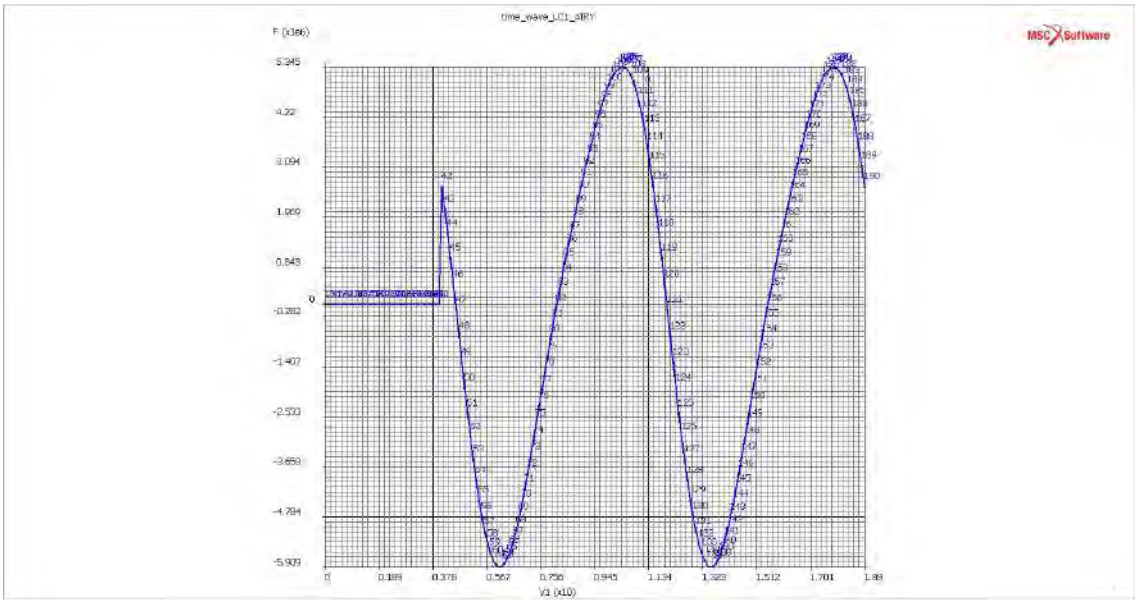

Figure 50: Timetables of the simulation

Boundary Conditions: The abovementioned timetables are matched to the boundary conditions of the problem: the fixed displacement to displacement z=50m, the anchoring as point load and the wave load also as a point load.

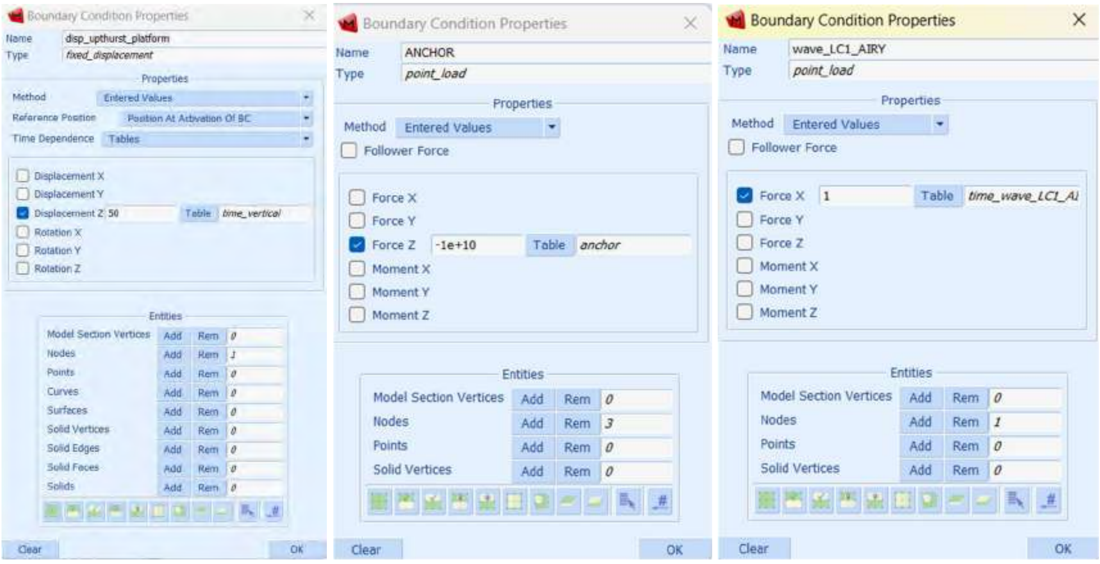

The weight of the chains is entered as a gravity load as follows.

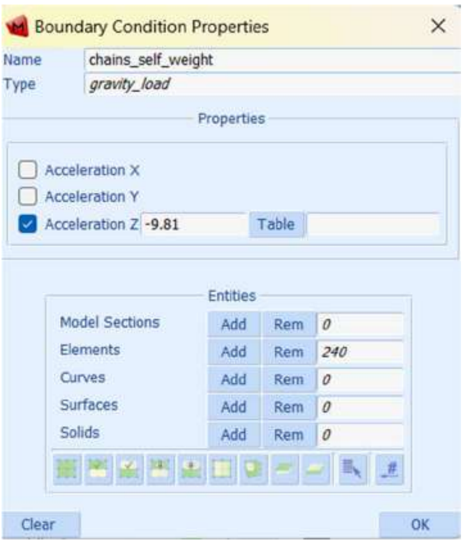

Figure 51: Boundaty conditions

Load case -Job: The simulation is carried out by including all the above boundary conditions, a process that is achieved using one *loadcase* with the appropriate use of timetables for applying the loads. The system from being submerged at the level 2d z=-50m, is raised to the surface of the sea z=0m. This part derives the geometry of the mooring system of the structure on which the wave load will be applied after the chains are anchored to the bottom. So, in the next period, after the system has been lifted, the ends are anchored, i.e. the large vertical force, and simultaneously the wave loading is imposed, through the appropriate time series given in the corresponding boundary condition. Then, a *job* is created and after selecting the *loadcase*, the analysis is conducted.

6. WAVE LOADING

The wave load that will be applied on the floating offshore semi-submergible platform OC4-DeepCWind, which was simulated with the characteristics described in the above chapters, have been taken from the literature, and specifically from 2 previous diploma thesis (Papadomichelakis, 2022)[25] and (Kanaki, 2017)[11]. These loads are applied to the floating part of the structure. Their calculation is based on Morison's equation, and they extracted load time series considering the geometry of the structure and the wave field parameters, using MATLAB.

Through the Morison equation, the forces exerted on the structure by the wave field are calculated as the sum of two individual terms with different impact in terms of total loading. These terms depend on the physical features of the wave field and the floating structure members and are detailed as follows:

- wave particle velocity
- wave particle acceleration,
- diameter of the elements to which the wave is applied.
- coefficients C_d, C_m

$$F = \underbrace{\frac{1}{2} C_d \, p \, u \, |u|}_{drag\ force} + \underbrace{\frac{1}{4} C_m \, p \, \pi \, \frac{\partial u}{\partial t} \, D^2}_{inertia\ force} \qquad \text{Equation 111}$$

The two terms are shown in the above equation and the first part of the equation concerns *drag force* and is significantly determined by the velocity obtained, while the second term is referred to as *inertia force* and indicative of the acceleration of the wave particles. The most important measure that determines if the phenomenon is drag or inertia dominated, is the diameter of the structure element. As resulted by the Equation 111, the large diameter parts will exhibit increased inertial forces compared to the drag forces.

The force exerted on the structure is obtained as a sum of the inertia and drag forces of the Equation 111, and is given per unit length (N/m)[25]. The coefficients Cm and Cd are practically the components of the inertial and drag forces, respectively, and were obtained for each wave theory and each loading condition separately.

The wave height calculation, but also the wave particle velocity and acceleration, were obtained for each wave theory, (steady and random wave theories) given the significant wave height, the peak period of the spectrum for each load case (LC1, LC6, LC8 shown in the following table) and the bottom depth. In the research [25], the wave loads on the floating part of the structure were calculated using a matlab code which detects the height of the wave, the velocity and the acceleration according to its position in space but also the time. These calculations were achieved taken under consideration Morison's equation, which estimates the total force in each element by integrating for each member of the structure. A time range of two periods was obtained. For members of the structure that are not exerted perpendicular to the wave propagation direction, the vertical component corresponding to this part of the structure had been taken, taking the appropriate angle in each case depending on the structure's geometry.

Load cases.

	U_{ref} [m/s]	T_I –	H_s [m]	T_p [s]	U_c [m/s]	Seeds –	Simulation length [s]	Turbine status
LC1	4	0.258	1.96	9.72	–	10	12 000	Operational
LC2	8	0.174	2.53	9.85	–	10	12 000	Operational
LC3	12	0.146	3.20	10.11	–	10	12 000	Operational
LC4	16	0.132	3.97	10.44	–	10	12 000	Operational
LC5	20	0.124	4.80	10.82	–	10	12 000	Operational
LC6	24	0.118	5.69	11.23	–	10	12 000	Operational
LC7	32	0.111	7.64	12.08	–	10	12 000	Parked
LC8	40	0.110	9.77	12.95	–	10	12 000	Parked
LC9	40	0.110	9.77	12.95	1.0	10	12 000	Parked

Figure 52: Load Cases – Wave Loading[52]

The resulted measurements used for this present study as wave loads and will be applied to the structure through MARC simulation, are described below. The diagrams of the time series are presented in Figure 53, Figure 54, Figure 55.

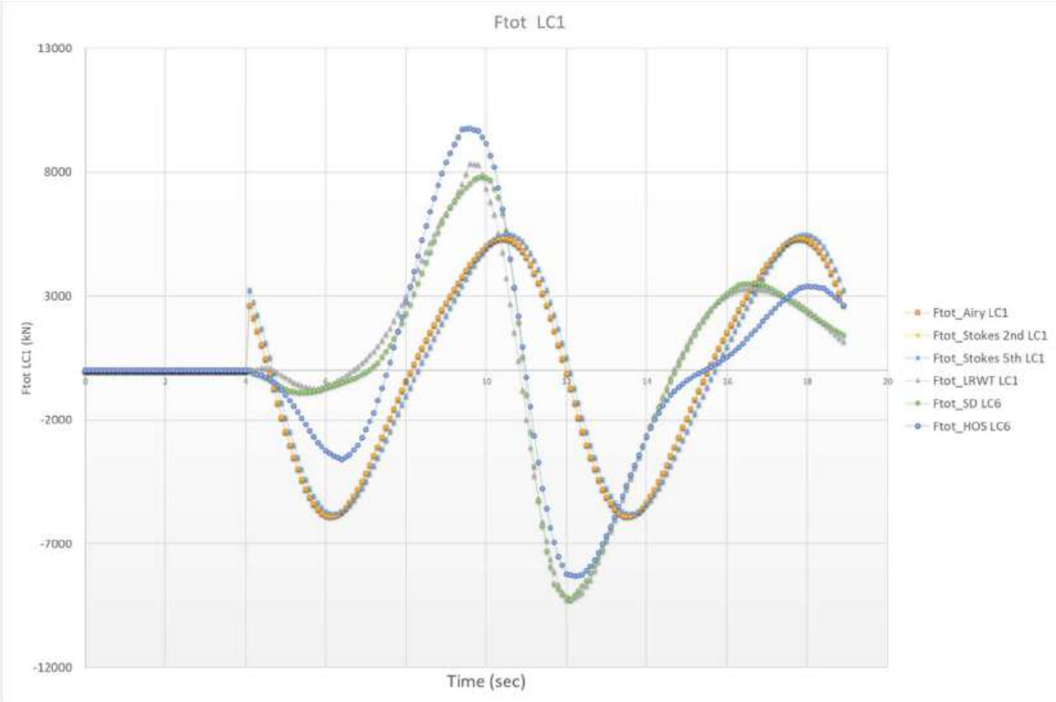

Figure 53: Total forces of wave modelling with the theories a) Airy, b) Stokes 2nd, c) Stokes 5th, d) LRWT, e) SD, f) HOS, for the load case LC1.

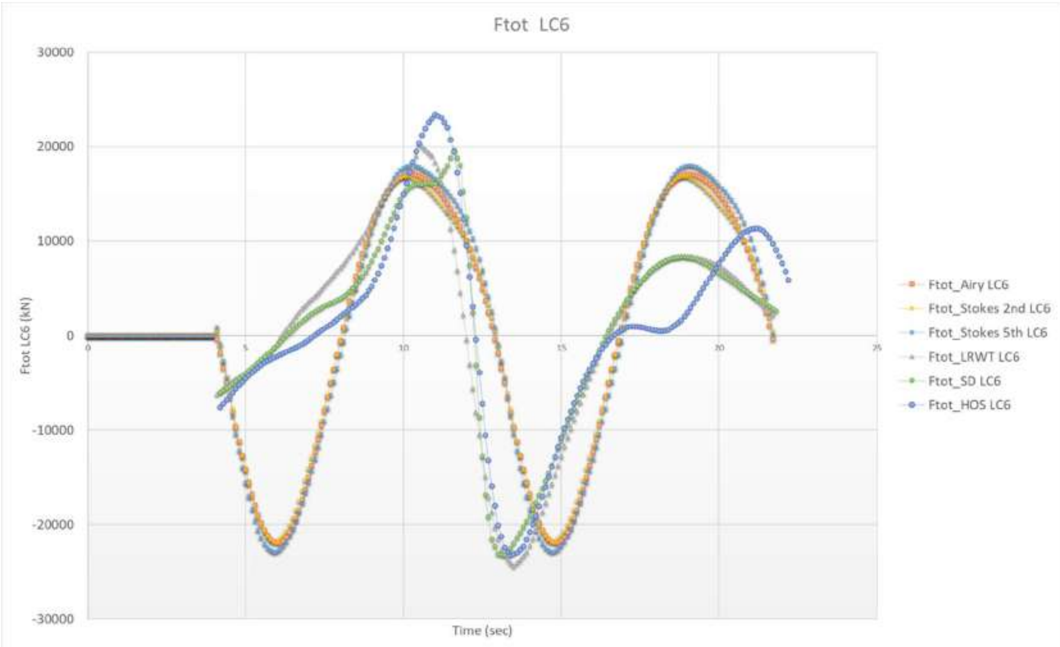

Figure 54 : Total forces of wave modelling with the theories a) Airy, b) Stokes 2nd, c) Stokes 5th, d) LRWT, e) SD, f) HOS, for the load case LC6.

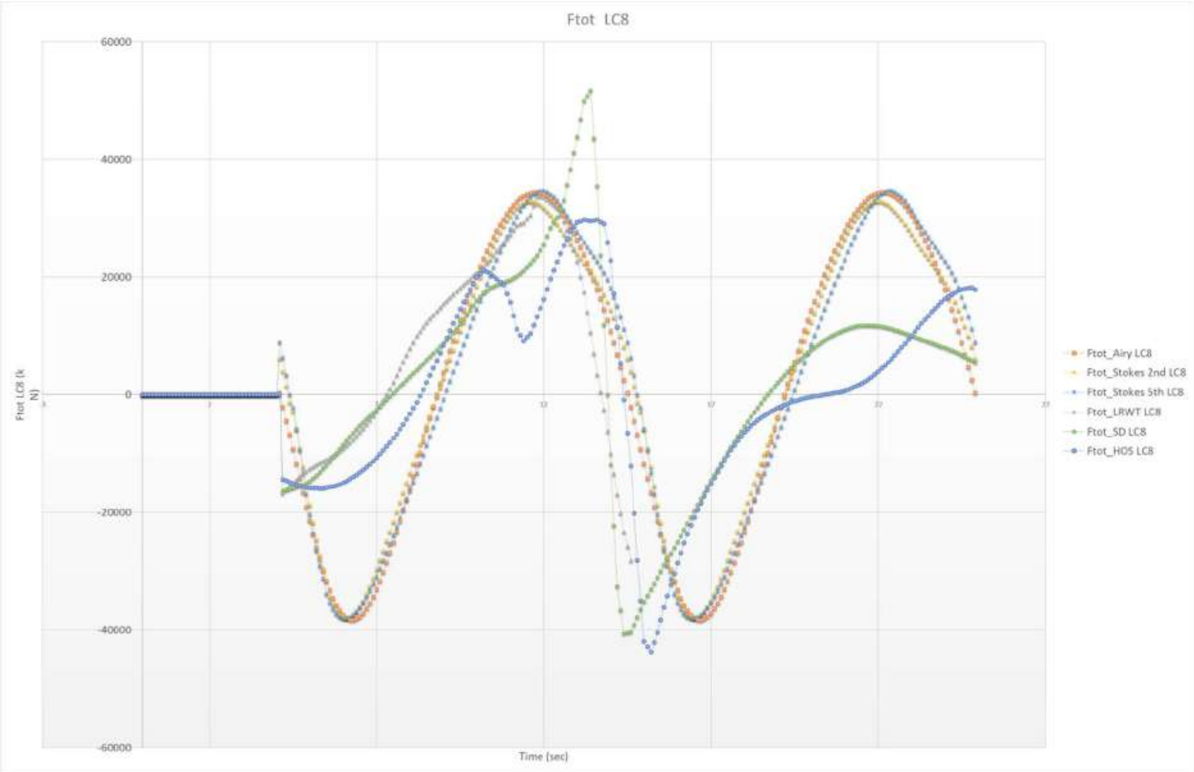

Figure 55: Total forces of wave modelling with the theories a) Airy, b) Stokes 2nd, c) Stokes 5th, d) LRWT, e) SD, f) HOS, for the load case LC8.

7. RESULTS OF WAVE – STRUCTURE INTERACTION ANALYSIS

This chapter provides the results of the semi-submersible OC4 platform mooring system simulation obtained from this study through MSC Marc software for the load combinations defined in Chapter 6 WAVE LOADING. Specifically, the chapter consists of three parts.

Part 1: LOAD CASE LC1

Part 2: LOAD CASE LC6

Part 3: LOAD CASE LC8

Part 4: HOS, SD, LWRT, STOKES 5^{TH} COMPARISON PER LOAD CASE

It is emphasized that the studied load cases concern environmental marine conditions to cover both operational and extreme sea states, as the wind speed gradually increases from load case 1 to 8, where the wave actions are extremely high, and the wind turbine is considered parked. According to [52], as we pass from the load case 1 to load cases 6 and 8, the wind speed increases from cut-in to cut-out wind speed with a bin size of 4 m/s. Also, the turbulent wind field is generated according to the Norwegian Petroleum Directorate (NPD) wind spectrum [52]. The results are presented for each load case, for all the wave theories simulations conducted, normalized in two ways. The first normalized diagrams category is normalized to the maximum resulted x displacement of the HOS wave theory for each load case, and the second one is to the maximum resulted x displacement of LC1 for each load case.

DYNAMIC RESPONSE RESULTS			
1st PART			
WAVE THEORY	MAX NORMALIZED FORCES/ NORMALIZATION TO MAX FORCE LC1		
	LC1	*LC6*	*LC8*
HOS	1.000	2.398	4.487
2nd PART			
WAVE THEORY	MAX NORMALIZED DISPLACEMENT/ NORMALIZATION TO max_x_disp_HOS_per_lc		
	LC1	*LC6*	*LC8*
AIRY	-0.771	-0.950	-0.876
STOKES 2ND	-0.768	-0.943	-0.868
STOKES 5TH	-0.760	-0.985	-0.870
LRWT	-1.090	-1.042	-0.838
SD	-1.093	-0.997	-0.925
HOS	-1.000	-1.000	-1.000
3nd PART			
WAVE THEORY	MAX NORMALIZED DISPLACEMENT/ NORMALIZATION TO max_x_disp_LC1		
	LC1	*LC6*	*LC8*
AIRY	-1.000	-3.058	-5.160
STOKES 2ND	-1.000	-3.052	-5.140
STOKES 5TH	-1.000	-3.220	-5.203
LRWT	-1.000	-2.373	-3.493
SD	-1.000	-2.264	-3.845
HOS	-1.000	-2.483	-4.544

Figure 56: Table of results – dynamic response of the offshore structure normalized.

7.1 WAVE – STRUCTURE INTERACTION LOAD CASE LC1

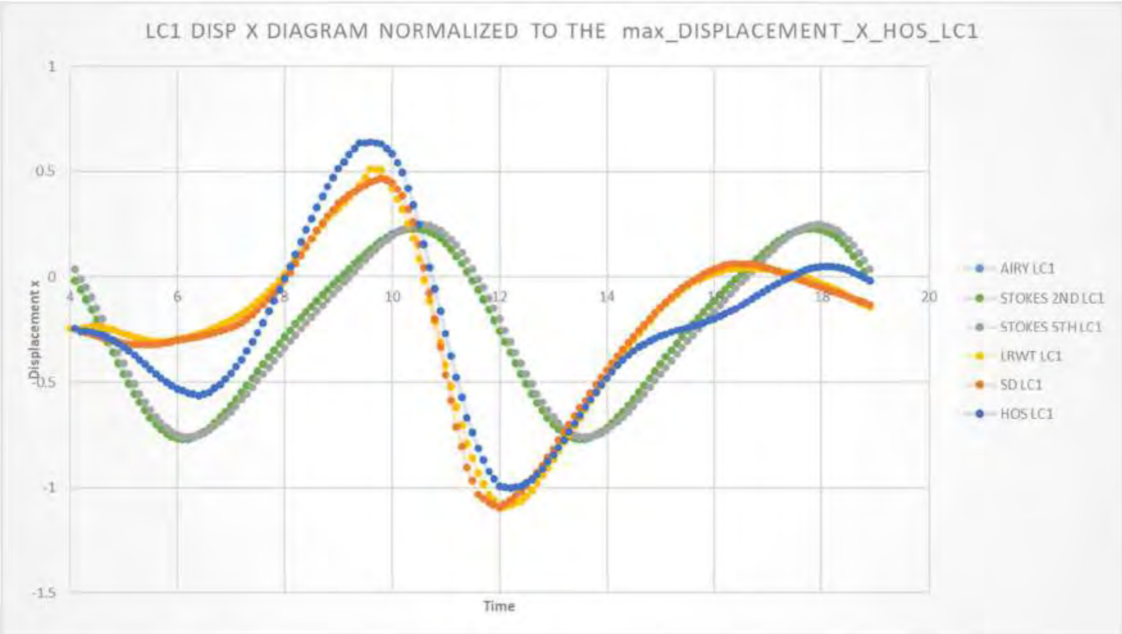

Figure 57: Displacement x – time normalized to the max_HOS_x_displacement_LC1, all wave theories.

7.2 WAVE – STRUCTURE INTERACTION LOAD CASE LC6

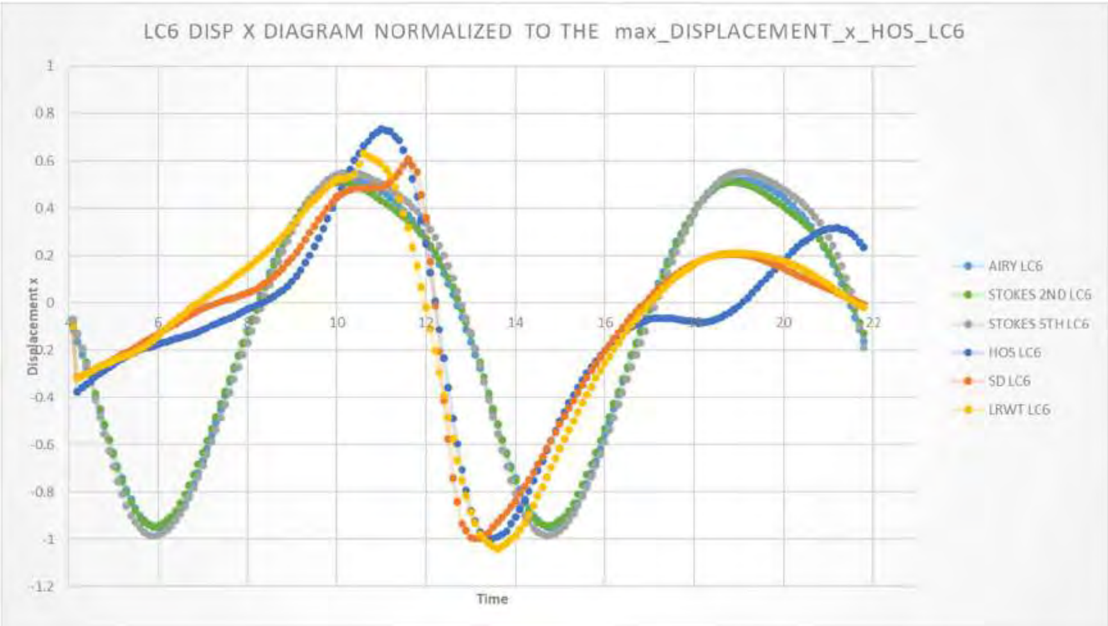

Figure 58: Displacement x – time normalized to the max_HOS_x_displacement_LC6, all wave theories.

7.3 WAVE – STRUCTURE INTERACTION LOAD CASE LC8

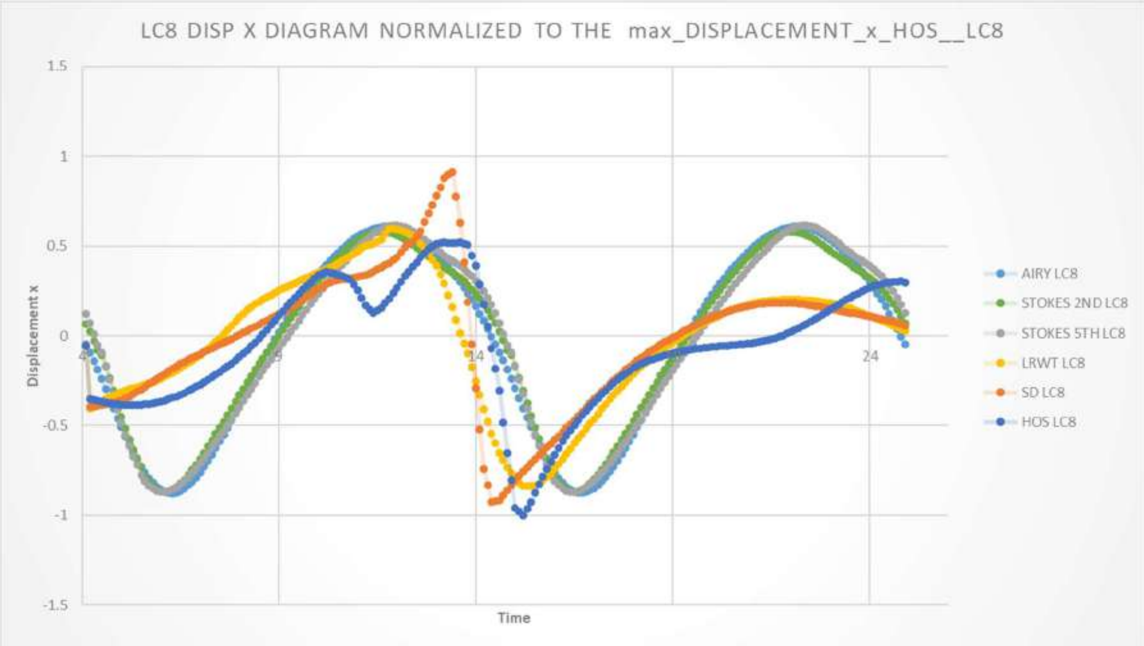

Figure 59: Displacement x – time normalized to max_HOS_x_displacement_LC8, all wave theories.

7.4 HOS, SD, LRWT, STOKES 5TH COMPARISON PER LOAD CASE

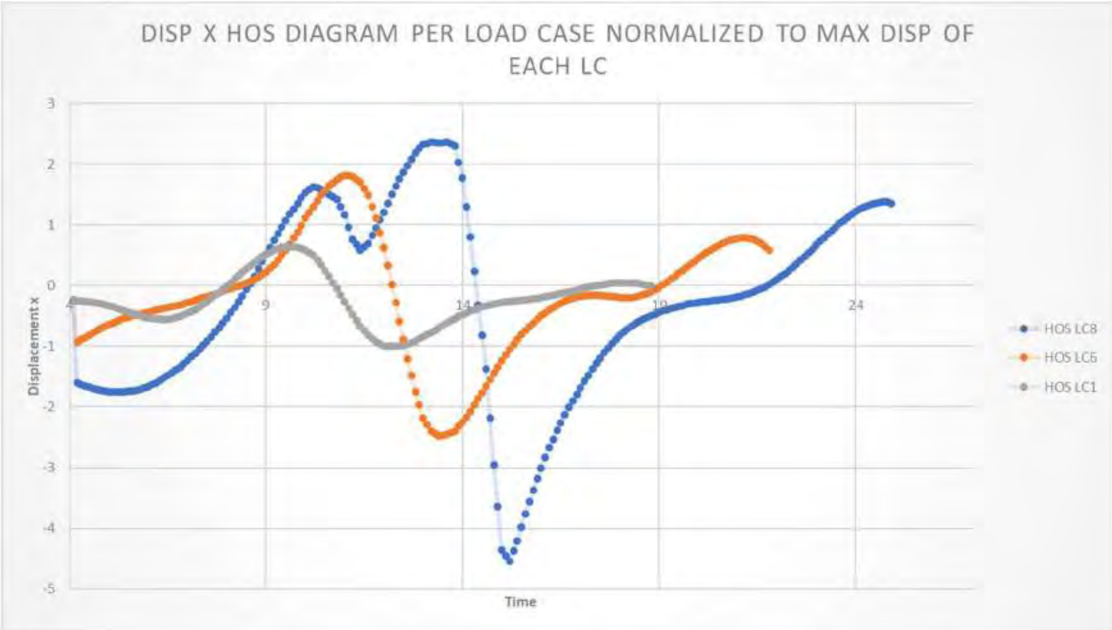

Figure 60: Displacement x – time HOS diagram, normalized to max_x_displacement_HOS per load case

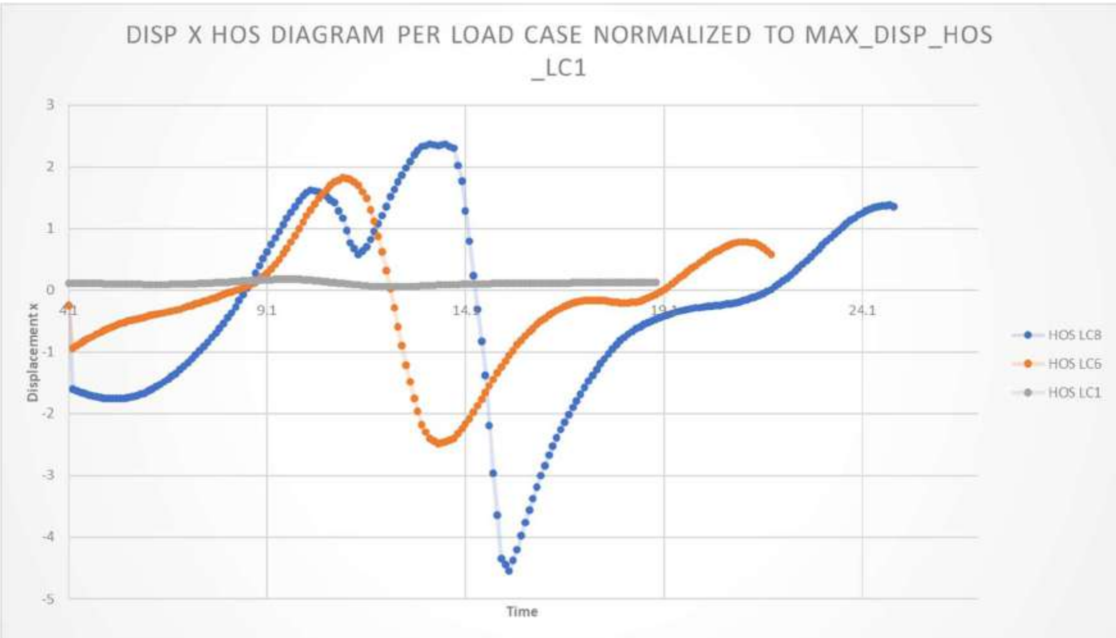

Figure 61: Displacement x – time HOS diagram, normalized to max_x_displacement_HOS _LC1

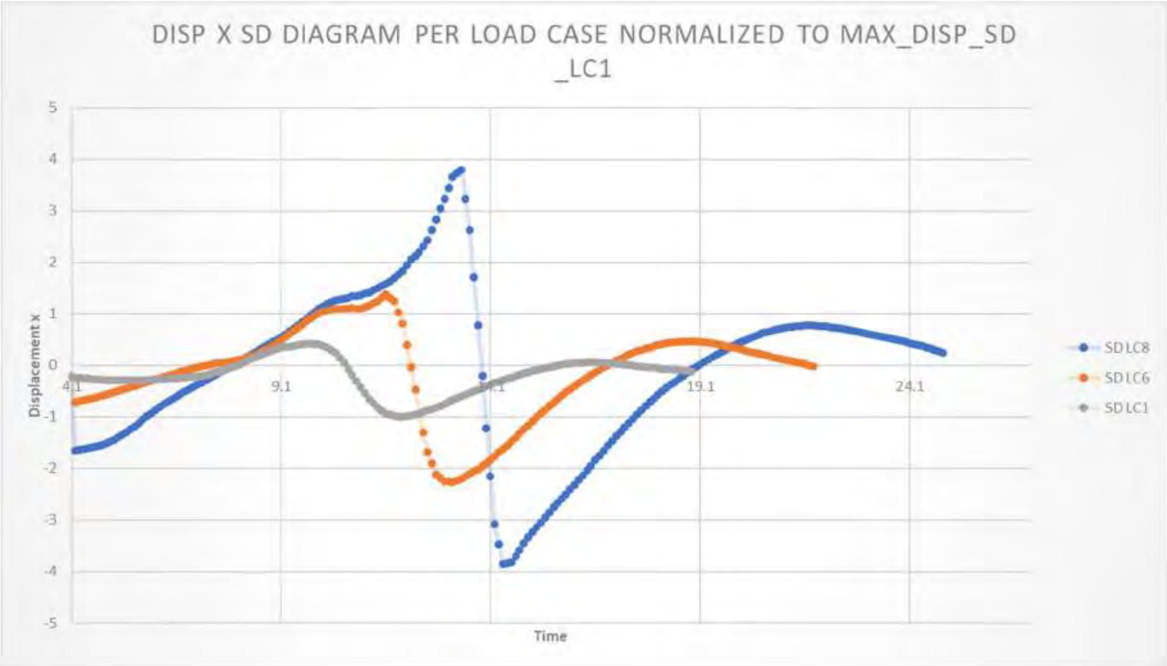

Figure 62: Displacement x – time SD diagram, normalized to max_x_displacement_SD_LC1

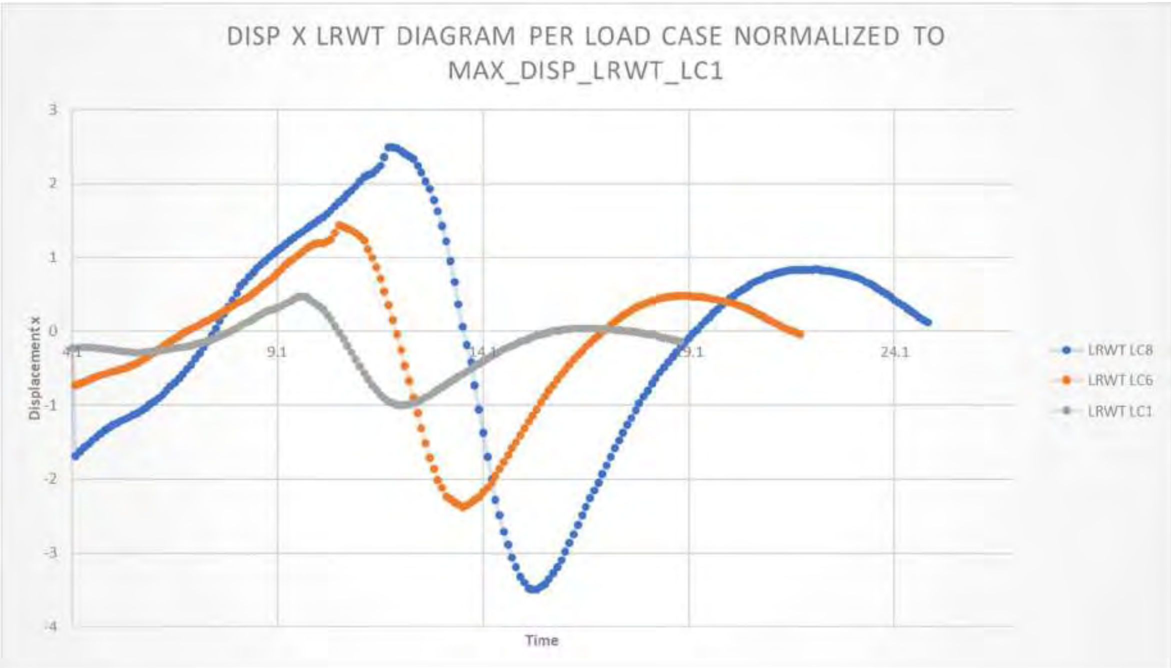

Figure 63: Displacement x – time LRWT diagram, normalized to max_x_displacement_LRWT_LC1

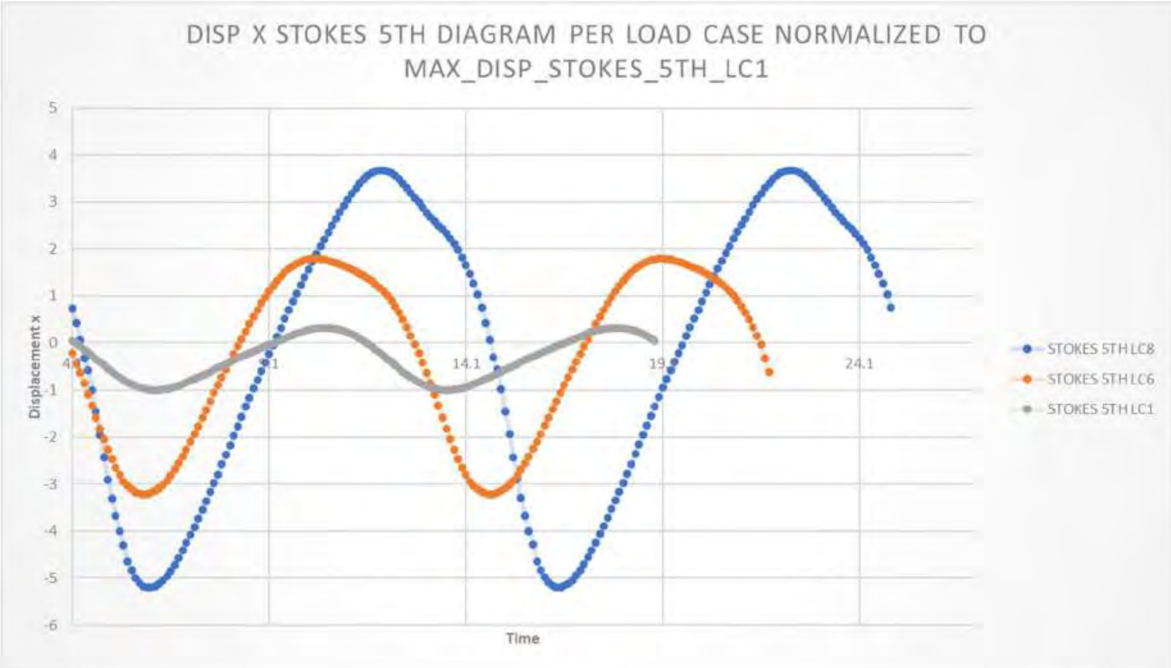

Figure 64: Displacement x – time Stokes 5^{th} diagram, normalized to max_x_displacement_ Stokes 5^{th} _LC1

It is noted that the methodology followed concerns small wave loads, 10^-3 orders of magnitude smaller than the forces calculated in the diploma thesis [25]. And this was chosen because the specific loads result in a much greater response of the structure. For this reason, the results are presented comparatively and not in absolute magnitude, so that the essence of the results and the approximation of the response estimate can be obtained.

The normalization was obtained in two ways: In the diagrams Figure 57, Figure 58, & Figure 59 & Figure 60, normalization was done with the maximum response resulting from the calculations with the HOS theory, for each load case. A second normalization was done with maximum response resulting from the calculations with the HOS theory of load case LC1, for each load case, and is shown in the diagrams Figure 61, Figure 62, Figure 63 & Figure 64.

Despite the difficulty in applying forces with buoyancy, self-weights and the large, calculated wave loads, the approach of the boundary condition of 50m z displacement from the bottom to the sea surface, led to a successful modeling of the chain and a well quantified estimation of response of the platform. Detailed modelling, with the direct application of forces without the use of displacement, is a challenge for subsequent students and researchers.

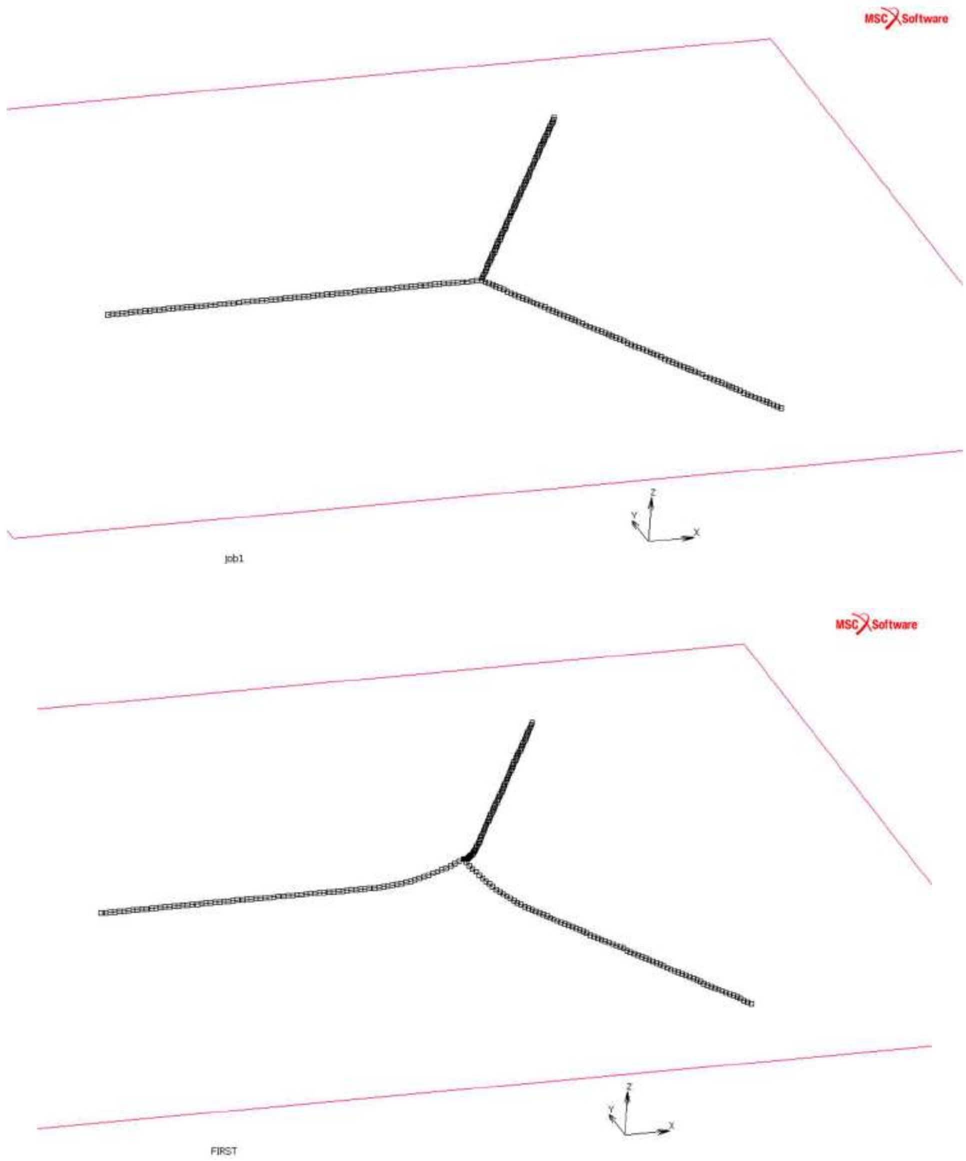

Figure 65: Platform simulation for z=-50m to the free surface, z=0m, in Marc Mentat

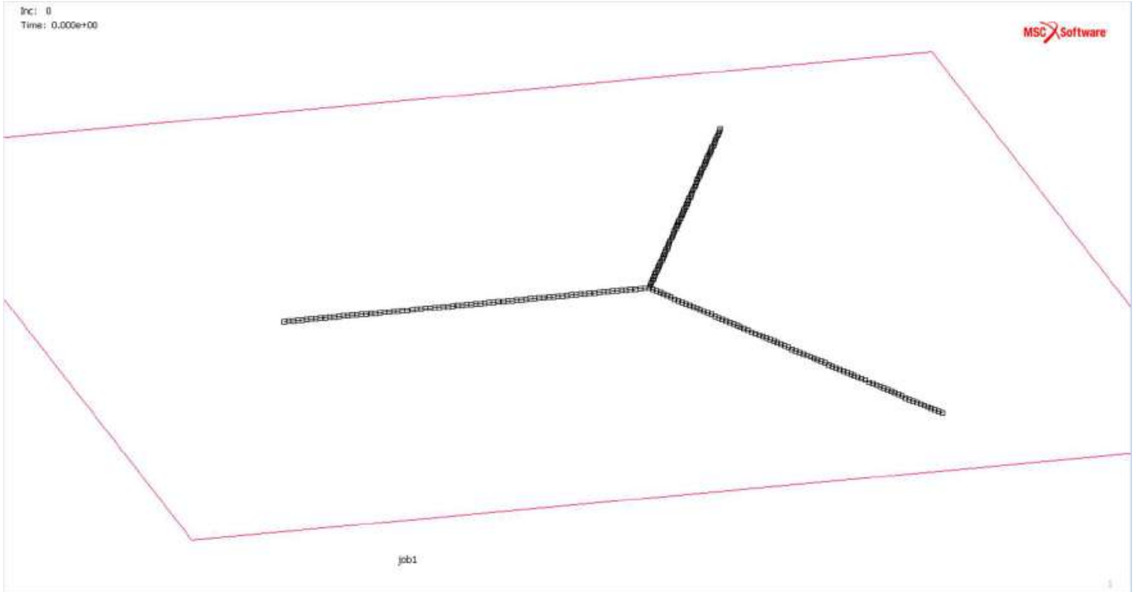

Figure 66: The mooring system movement for z=-50m to the free surface, z=0m, in Marc Mentat for LC6

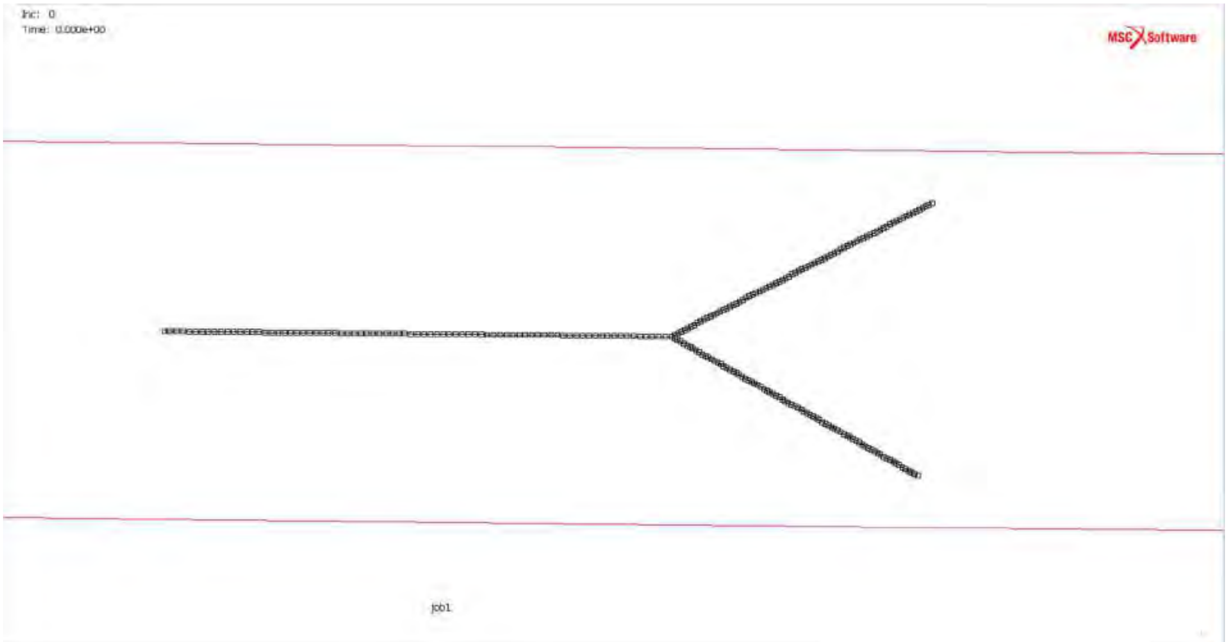

Figure 67: The mooring system movement for z=-50m to the free surface, z=0m, in Marc Mentat for LC6_real loading.

Below is presented the diagram for the load cases LC1, LC6 and LC8 calculated by [25] with the theory HOS .

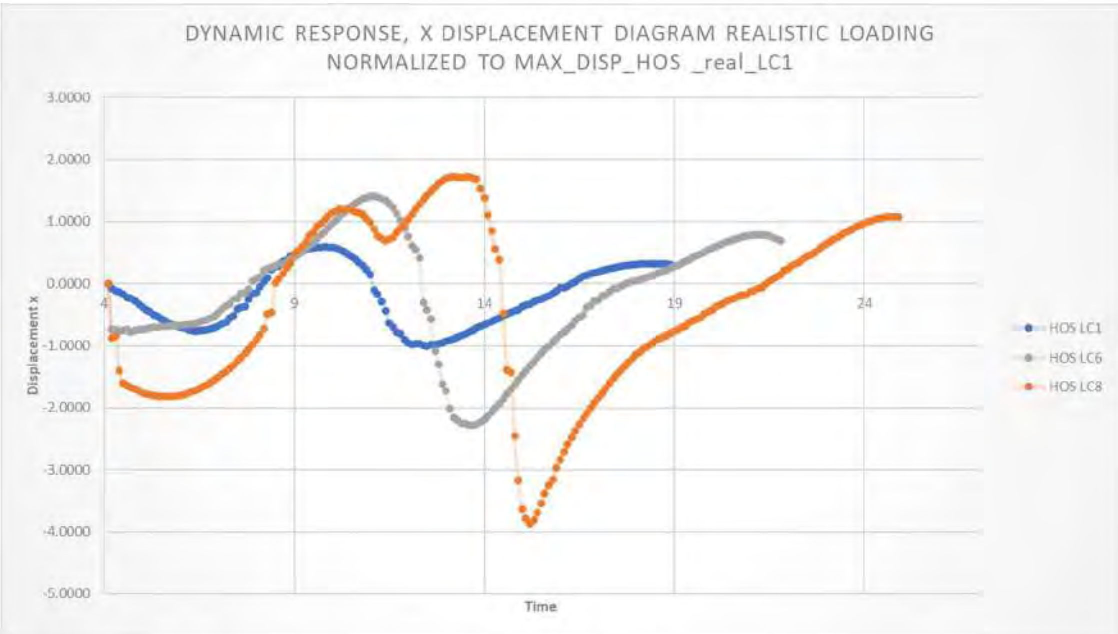

Figure 68: Displacement x – time, resulted from real loads calculated by HOS (up), dispplacement x – time, resulted from real loads calculated by HOS theory for normalized to max_x_displacement_HOS_LC1_real (down)

8. CONCLUSIONS

Before extracting the conclusions from the results described in Chapter 7: RESULTS OF WAVE – STRUCTURE INTERACTION ANALYSIS, it is underlined that he methodology followed concerns small wave loads, 10^-3 orders of magnitude smaller than the forces calculated in the diploma thesis [25], under the difficulties of simulating the problem in detail, the buoyancy of the platform and the cables, as well as the damping coefficient of the water through the Marc program. This consideration of downscaling of the loads also results in response under a scale, so the results were normalized to study the response behavior of the platform rather than the exact numerical results. It is the behavior that is of interest in the present work, to examine the theories and the effects on the mooring system in comparison.

According to the research process carried out to calculate the response in the construction we come to the following conclusions regarding the structure response.

For the first load case, LC1, which refers to smooth environmental conditions and wind speed, it is observed that both normalization to the maximum resulted x displacement of the HOS wave theory and to the maximum resulted x displacement of LC1 for each load case, give similar response. Examining the steady wave theories, the response is calculated close to 0.7, while in the case of the random ones, it is close to 1. Compared with the fully nonlinear model, the LRWT and SD theories result in an overestimated response, while the steady wave theories (Airy, Stokes 2^{nd} and Stokes 5^{th}) lead to underestimation.

The case LC6, refers to the average state between the three sea states and the same response behavior of the structure evolves compared to the first case. But this time the differences between steady and random wave theories are much smaller, as for the random theories we have values much closer to 1, while for the steady ones around 0.95. It is obvious that immediately after the HOS theory, the LRWT theory is the most effective, and the SD follows. Regarding the steady theories, as before, it is noticed that Stokes 5^{th}, has the best convergence, then Stokes 2^{nd}, and Airy, which is valid in all load cases.

The two abovementioned load cases refer to operational conditions, but the third case LC8 covers extreme sea states, where the wave actions are extremely high, and the wind turbine is considered parked. The platform response resulting from steady wave theories is close to 0.8, but this results also from the random wave theory LRWT. SD wave theory leads to better results of 0.9.

As discussed in chapter 4: WAVE THEORIES AND WAVE MODELLING, steady wave models assume that every and each wave component preserves its shape and its characteristics in each period, leading to analytical periodic wave solutions. Therefore, this assumption concludes to simple mathematical calculations, neglecting the real sea wave spectrum and, accordingly, wave directionality. So, considering all load cases results and all theories, underestimation of the horizontal displacement values of the platform is observed. In contrast, random wave theories lead to a better approach of the real sea, describing the wave field in three dimensions and therefore the directionality is considered.

This behavior of the forces is also reflected in the results of the horizontal displacement according to the results of this work. Steady wave theories do not lead to correct results as the effects of the maximum loads do not only come from the kinetic field but also from the free surface that it produces in time, influencing the final maximum force. On the other hand, random wave theories lead to more accurate results.

Discussing the results of the table in Figure 56 in more detail, 2^{nd} part shows a response and loading ratio behavior, which indicates linearity. This linear behavior may be observed since we are in the region of very small forces, 10^{-3} order below than realistic. As for the random wave theories for LC1, SD and LWRT give a slightly overestimated response, while the steady wave theories result in 23% reduced values, always compared to the reference method, HOS. In fact, while increasing nonlinearity from LC1 to LC8, LRWT and SD continue giving results close to realistic and steady wave theories give only 10-12% deviation (underestimation). Specifically, the extreme wave loading LC8 LRWT is associated with reduced displacement values by 15%, while losing its ability to properly describe the displacement, as LC8 is highly nonlinear loading and LRWT has no nonlinearity in it. As expected, the SD theory, which considers up to 2^{nd} order nonlinearity, is clearly improved. On the other hand, the steady wave theories are again moving away from the realistic solution, and this should draw our attention to the fact that the previous success in LC6 must be coincidental.

The 3rd part of the table is also indicative of a non-linear behavior of the response since as mentioned the loadings are non-linear.

Another conclusion from the results of the table is the fact that the displacement to the left is greater than the displacement to the right, as shown by the minus sign.

Finally, for the HOS theory, the change in displacement at LC1 becomes much steeper progressively and has a higher order effect by changing load case. It is obvious that there are non-linearity effects but, as the wave load is on a smaller scale, and the response will be on a different scale than the actual one and in proportion to the displacement.

This present study was a successful effort to simulate the semi-submersible offshore platform OC4 mooring system and to develop a dynamic model capable of accepting wave loads and masses of the structures, calculating the dynamic response. Successful modeling of the chain and a well quantified estimation of response of the platform was achieved.

9. SUGGESTIONS FOR FUTURE RESEARCH

This present work described the dynamic model capable of receiving the wave loads and the masses of the whole structure and extracting the platform response. Although, the difficulty in applying forces with buoyancy, self-weights, and the large forces, while the boundary condition of 50m z displacement from the bottom to the sea surface occurs is a demanding and challenging task. This research led to response effects an order of magnitude smaller than we would expect. Detailed modelling, with the direct application of forces without the use of displacement, is a challenge for subsequent students and researchers.

At a later stage, after the mooring system has been fully studied, a finite element modeling of the full geometry of the offshore platform will be extremely useful. A detailed platform model with discrete all the columns and cross braces of the structure, where the loads will be applied, will give more detailed numerical results of the structure's response.

A further proposed study concerns different depths and research in both wave loading calculations and wave-structure simulation and interaction. Investigating the different depths, dynamic response could provide results for any marine installation area we choose. The sea as a continuous dynamic phenomenon is of great interest from the engineer's aspect, and therefore the effort to understand and develop such a model will be an important step in strengthening Greece's participation in the promising and rapidly growing sector of marine and ocean technology.

BIBLIOGRAPHY

[1] Adcock, T. A. A., Taylor, P. H., Draper, S. (2015) "Nonlinear dynamics of wave-groups in random seas: unexpected walls of water in the open ocean". *Proceedings of the Royal Society* A 471: 20150660.

[2] Papaioannou, O., Misias D. (2018). *Nonlinear random waves: unexpected water walls creation in intermediate water depths*. Diploma Thesis, University of Thessaly Volos.

[3] Siontorou, A. (2019). *Nonlinear random waves: The effect of second order terms on the creation of unexpected walls of water in intermediate water depths*. Diploma Thesis, University of Thessaly Volos.

[4] Houtani, H., Waseda, T., Fujimoto, W., Kiyomatsu, K., Tanizawa, K. (2015). Freak wave generation in a wave basin with HOSM-WG method, OMAE2015-42284.

[5] Katsardi, V. & Swan, C. (2005). The effects of reduced water depth on the description of extreme waves and the prediction of the water particle kinematics, Proceedings of OMAE2005, 67110

[6] Katsardi V, de Lutio L, Swan C. (2013). An experimental study of large waves in intermediate and shallow water depths. PartI: wave height and crest height statistics, *Coastal Engineering* 73, 43–57.

[7] Chatziioannou, K., Katsardi, V., Koukouselis, A., Mistakidis, E. (2017). The effects of nonlinear wave-structure and soil-structure interactions in the design of an offshore structure, *Marine Structures* 52, 126-152.

[8] Mavrakos S.A. Study and design of floating structures. Athens: EMP University Press, 1999.

[9] https://www.usna.edu/NAOE/_files/documents/Courses/EN330/Random-Wave-Analysis.pdf

[10] Wang, S.R. & Parrish, Patrick & Dills, Patrick & Lee, Thomas. (2006). Multimedia Learning Materials for Marine Applications. 1 - 4. 10.1109/OCEANS.2006.306927.

[11] Kanaki, N. 2017. *Calculation of loads of Sleipner A, Statoil gravity platform, in intermediate water depths*. (bachelor's thesis)

[12] García-Mira, R., Real, J., Uzzell, D., San Juan, C., & Pol, E. (2006). *Coping with a threat to quality of life: the case of the Prestige disaster.* European Review of Applied Psychology, 56(1), 53–60. https://doi.org/10.1016/j.erap.2005.02.008

[13] Karabas, T., Krestenitis, I., & Koutitas, X. (2015). Coastal engineering – coastal protection projects [Undergraduate textbook]. *Kallipos, Open Academic Publications*. https://hdl.handle.net/11419/2095

[14] Katsardi V. Lecture notes " Coastal Engineering – Coastal Protection Works". Department Civil Engineering. Hydraulic and Environmental Engineering Sector. University of Thessaly, 2015

[15] Tsoukala V. K., Lecture notes " Wave Trasformations ". Department Civil Engineering. National Technical University of Athens, 2015. (http://mycourses.ntua.gr/courses/CIVIL1026/document/Ak_Etos_2014-2015/%CC%E5%F4%E1%F3%F7%E7%EC%E1%F4%E9%F3%EC%EF%DF_%CA%F5%EC%E1%F4%E9%F3%EC%FE%ED.pdf).

[16] http://www.coastalwiki.org/wiki/Diffraction

[17] https://adventure.howstuffworks.com/outdoor-activities/water-sports/surfing6.htm

[18] https://www.eoas.ubc.ca/courses/atsc113/sailing/met_concepts/08-met-waves/8c-breaking-waves/index.html

[19] Bay, İbrahim. (2005). Measurement and Analysis of Wave Overtopping.

[20] Stockdon, H. F., Holman, R. A., Howd, P. A., & Sallenger, A. H. (2006). Empirical parameterization of setup, swash, and runup. Coastal Engineering, 53(7), 573–588. https://doi.org/10.1016/j.coastaleng.2005.12.005

[21] https://dspace.lib.ntua.gr/xmlui/bitstream/handle/123456789/41510/Christodoulou%20Christos.pdf?sequence=1&isAllowed=y

[22] https://www.weather.gov/bro/ripcurrentdefinition

[23] https://www.weather.gov/mlb/ripcurrent_rules

[24] Clauss, G. F., & Klein, M. (2011). The New Year Wave in a seakeeping basin: Generation, propagation, kinematics and dynamics. Ocean Engineering, 38(14–15), 1624–1639. https://doi.org/10.1016/j.oceaneng.2011.07.022

[25] Papadomichelakis, E. 2022. Realistic wave load analysis on an offshore floating wind turbine. (bachelor's thesis).

[26] GWEC-offshore-wind-2021-updated-1.pdf

[27] Kaynia, A. M. (2019). Seismic considerations in design of offshore wind turbines. *Soil Dynamics and Earthquake Engineering*, *124*, 399–407. https://doi.org/10.1016/j.soildyn.2018.04.038

[28] https://www.irena.org/publications/2022/Jul/Renewable-Energy-Statistics-2022

[29] Thanh Trung, Nguyen. (2020). EEMD-HT transform for identifying modal parameters of fixed offshore jacket platforms using vibration response measurement. Journal of Civil Structural Health Monitoring. 10. 10.1007/s13349-020-00422-3.

[30] http://www.mie.uth.gr/labs/mex-lab/FigureB2-8.html

[31] Gaidai, O., Cao, Y., Xing, Y., & Balakrishna, R. (2023). Extreme springing response statistics of a tethered platform by deconvolution. International Journal of Naval Architecture and Ocean Engineering, 15, 100515. https://doi.org/10.1016/j.ijnaoe.2023.100515

[32] Eren, Tuna. (2019). Conversion of Surface Systems into Subsea Wellhead Systems.

[33] Sharma, R. (2019). An introduction to offshore platforms. 10.13140/RG.2.2.31319.21925.

[34] Leimeister, Mareike & Kolios, A & Collu, Maurizio. (2018). Critical review of floating support structures for offshore wind farm deployment. Journal of Physics: Conference Series. 1104. 012007. 10.1088/1742-6596/1104/1/012007.

[35] Halkyard, John & Sirnivas, Senu & Constantinides, Yiannis & Oakley, Owen. (2005). Benchmarking of Truss Spar Vortex Induced Motions Derived from CFD With Experiments. 10.1115/OMAE2005-67252

[36] Le Méhauté, B. (1976) An Introduction to Hydrodynamics and Water Waves. Springer, Berlin. https://doi.org/10.1007/978-3-642-85567-2

[37] http://web.mit.edu/fluids-modules/www/potential_flows/LecturesHTML/lec19bu/node3.html

[38] Wang, Liguo & Isberg, Jan. (2015). Nonlinear Passive Control of a Wave Energy Converter Subject to Constraints in Irregular Waves. Energies. 8. 6528. 10.3390/en8076528.

[39] United States. Army. Corps of Engineers. (1984, January 1). Shore Protection Manual (1984 edition). Open Library. Retrieved December 30, 2022, from https://openlibrary.org/books/OL3001149M/Shore_protection_manual.

[40] Ahmed, Hany. (2011). Wave interaction with vertical slotted walls as a permeable breakwater.

[41] Fenton, J.D. (1985). A fifth order Stokes' theory for steady waves. Journal of Waterway, Port, Coastal and Ocean Engineering, Vol. 111, pp. 216-234.

[42] Wheeler, J.D. (1970). Method for calculating forces produced by irregular waves. Journal of Petroleum Technology, Vol. 22, pp. 359–367.

[43] Longuet-Higgins, M.S. & R.W. Stewart (1960). Changes in the form of short gravity waves on long waves and tidal currents. Journal of Fluid Mechanics, Vol. 8, pp. 565–583.

[44] Sharma, J.N. & R.G. Dean (1981). Second-Order directional seas and associated wave forces. Society of Petroleum Engineers Journal, Vol. 21, pp. 129–140.

[45] Ducrozet, G., Bonnefoy, F., Touzé, D. L., & Ferrant, P. (2016). HOS-ocean: Open-source solver for nonlinear waves in open ocean based on High-Order Spectral method. Computer Physics Communications, 203, 245–254. https://doi.org/10.1016/j.cpc.2016.02.017

[46] West, B. J., Brueckner, K. A., Janda, R., Milder, D. M., & Milton, R. A. (1987). A new numerical method for surface hydrodynamics. Journal of Geophysical Research, 92(C11), 11803. https://doi.org/10.1029/jc092ic11p11803

[47] Robertson, A., Jonkman, J., Masciola, M., Song, H., Goupee, A. J., Coulling, A. J., & Luan, C. (2014). Definition of the semisubmersible floating system for Phase II of OC4. https://doi.org/10.2172/1155123

[48] Altosole, M., Benvenuto, G. B., Figari, M., & Campora, U. (2008). Real-time simulation of a COGAG naval ship propulsion system. *Proceedings of the Institution of Mechanical Engineers, Part M: Journal of Engineering for the Maritime Environment*. https://doi.org/10.1243/14750902jeme121

[49] DNVGL, 2018a. DNVGL-OS-E301 Position Mooring.

[50] Liu, Y., Xiao, Q., & Incecik, A. (2017). A Coupled CFD/Multibody Dynamics Analysis Tool for Offshore Wind Turbines with Aeroelastic Blades. *Volume 10: Ocean Renewable Energy*. https://doi.org/10.1115/omae2017-61062

[51] A. Öchsner and M. Öchsner, The Finite Element Analysis Program MSC Marc/Mentat, DOI 10.1007/978-981-10-0821-4_1

[52] Xhu, K., Larsen, K., Shao, Y., Zhang, M., Gao, Z., & Moan, T. (2021). Design and comparative analysis of alternative mooring systems for floating wind turbines in shallow water with emphasis on ultimate limit state design. *Ocean Engineering*, *219*, 108377. https://doi.org/10.1016/j.oceaneng.2020.108377

FRONTPAGE PICTURE: Robertson, A., Jonkman, J., Masciola, M., Song, H., Goupee, A. J., Coulling, A. J., & Luan, C. (2014). Definition of the semisubmersible floating system for Phase II of OC4. https://doi.org/10.2172/1155123